Petrology and Metamorphic Pressure-Temperature Evolution for the Trans-Saharan Orogenic Belt in Nigeria

January 2018

UGWUONAH Emmanuel Nwachukwu

Petrology and Metamorphic Pressure-Temperature Evolution for the Trans-Saharan Orogenic Belt in Nigeria

A Dissertation Submitted to

the Graduate School of Life and Environmental Sciences,

the University of Tsukuba

in Partial Fulfillment of the Requirements

for the Degree of Doctor of Philosophy in Science

(Doctoral Program in Earth Evolution Sciences)

UGWUONAH Emmanuel Nwachukwu

Contents

Abstract

Understanding the Rodinia-Gondwana-recent transition story of the 3000 km long Trans-Saharan Orogenic Belt is daunting due to the size of the orogenic belt, the complexity of the events of tectonism, the rock types involved, and the time laps of the history. It demands a painstaking regional approach to the study of the tectonic-metamorphic signatures of the orogeny. Three case-study localities within latitudes 07°00'N and 09°10'N and longitudes 005°40'E and 009°10'E were studied in this research for the purposes of (1) examining possible terrain-scale differences in crustal evolution across a major tectonic block like the Benin Nigeria Shield, (2) making comparisons between tectonic blocks like the eastern and western Nigerian Basement and (3) using the results to attempt a reconstruction of the tectonic and metamorphic history of the orogenic belt within Nigerian basement complex areas.

In Keffi and environs in north-central Nigeria, detailed petrological and pressure-temperature data from the pelitic schists and amphibolites were obtained. All pelitic samples contain garnet + biotite + plagioclase + quartz + chlorite + ilmenite, but the staurolite-bearing assemblage contains staurolites and subordinate retrograde chlorites in addition. *P–T* pseudosection analyses calculated using THERMOCALC software for the suitable rock types, constrain garnet + staurolite equilibration within the range of 6.4-7.7 kbar and 610-630°C with a clockwise *P-T* path which is the highest *P-T* value recorded in literature for the Nigerian Schist Belt. In Obudu area, migmatite gneiss stabilized in granulite-facies metamorphism at equilibrium *P-T* condition of 785-805 ºC and 6.72-6.75 kbar as constrained from cross-matching of THERMOCALC pseudosection and a combination of conventional thermobarometric methods. The stable mineral assemblage of the rocks includes garnet + biotite + sillimanite + cordierite + plagioclase + rutile + quartz + liquid. Mineral inclusions study, conventional thermobarometry and *P-T* pseudosection analysis were used to constrain the prograde, peak and retrograde conditions of the migmatites defining a clockwise *P-T* path and a magmatic-arc setting. Akoko area of Ondo state in southwestern Nigeria has been characterized as a granulite facies terrane with a dominant (early Pan-African) E-W foliation and lineation directions and stable mineral assemblage of garnet + biotite + sillimanite + cordierite + plagioclase + K-feldspar + quartz + ilmenite + magnetite + liquid. A *P-T* condition of 790-830 ºC and 5.6-6.6 kbar is constrained for this area using THERMOCALC pseudosection.

The results of this study show that the eastern and western parts of the Nigerian basement were equally affected by granulite facies metamorphism as recorded in the migmatite gneisses of this study. The central Nigerian region represented by Keffi Schist Belt, however, presents a higher-pressure and lower-temperature metamorphic facies. This suggests amalgamation at the center, of two opposing subduction systems.

List of Figures

List of Tables

Chapter 1: General Introduction

1.1 Research background

The Pan-African orogeny consists of a series of major Neoproterozoic orogenic events related to the formation of the supercontinents Gondwana and Pannotia about 600 million years ago. It is an orogenic cycle that included the opening and closing of several large oceans and the collisions of several continental blocks. The term Pan-African was coined by Kennedy (1964) for a tectono-thermal event at about 500 Ma when a series of mobile belts in Africa formed between much older cratons. Pan-African contemporaneous orogenic events on other continents include; Brasiliano in South America, Adelaidean in Australia, Beardmore in Antarctica, Cadomian in Europe and the Baikalian orogeny in Asia.

The closure of sedimentary basin gaps between cratonic fragments during the Pan-African orogeny led to the creation of several orogenic belts (Fritz et al. 2013; Kursky et al. 2003; Westerhof et al. 2014). Eleven notable Pan-African orogenic belts within African continent alone include (1) The Arabian-Nubian Shield, extending from Ethiopia to the southern Levant, (2) The Mozambique Belt, extending from east Antarctica through East Africa up to the Arabian-Nubian Shield, (3) The Zambezi Belt which branches off the Mozambique Belt in northern Zimbabwe and extends into Zambia, (4) The Damara Belt which is exposed in Namibia between the Congo and Kalahari Cratons and continues southwards into the coastal Gariep and Saldania Belts and northwards into the Kaoko Belt, (5) The Gariep and Saldania belts which run along the western and southern edge of the Kalahari Craton, (6) The Kaoko Belt which branches north-west from the Damara Belt into Angola, (7) The West Congo Belt, (8) The Central African belts between the Congo and Nigerian shields which continues eastwards as the Oubanguide Belt with which they form the Central African Shear Zone, (9) The Saharan Metacraton between the Hoggar Mountains and the Nile river consists of an Archaean-Palaeoproterozoic basement overprinted by Pan-African granitoids, (10) The Rokelide Belt which passes along the western margin of the Archaean Man Shield in the southern West African Craton and (11) The 3000 km-long Trans–Saharan Belt (see Fig. 1) which runs north and east of the more than >2 Ga West African Craton covering the Tuareg and Nigerian Shields (Kröner and Stern 2004). Attempts have been made to correlate the African Pan-African belts with the South American Brasiliano belts on the other side of the Atlantic.

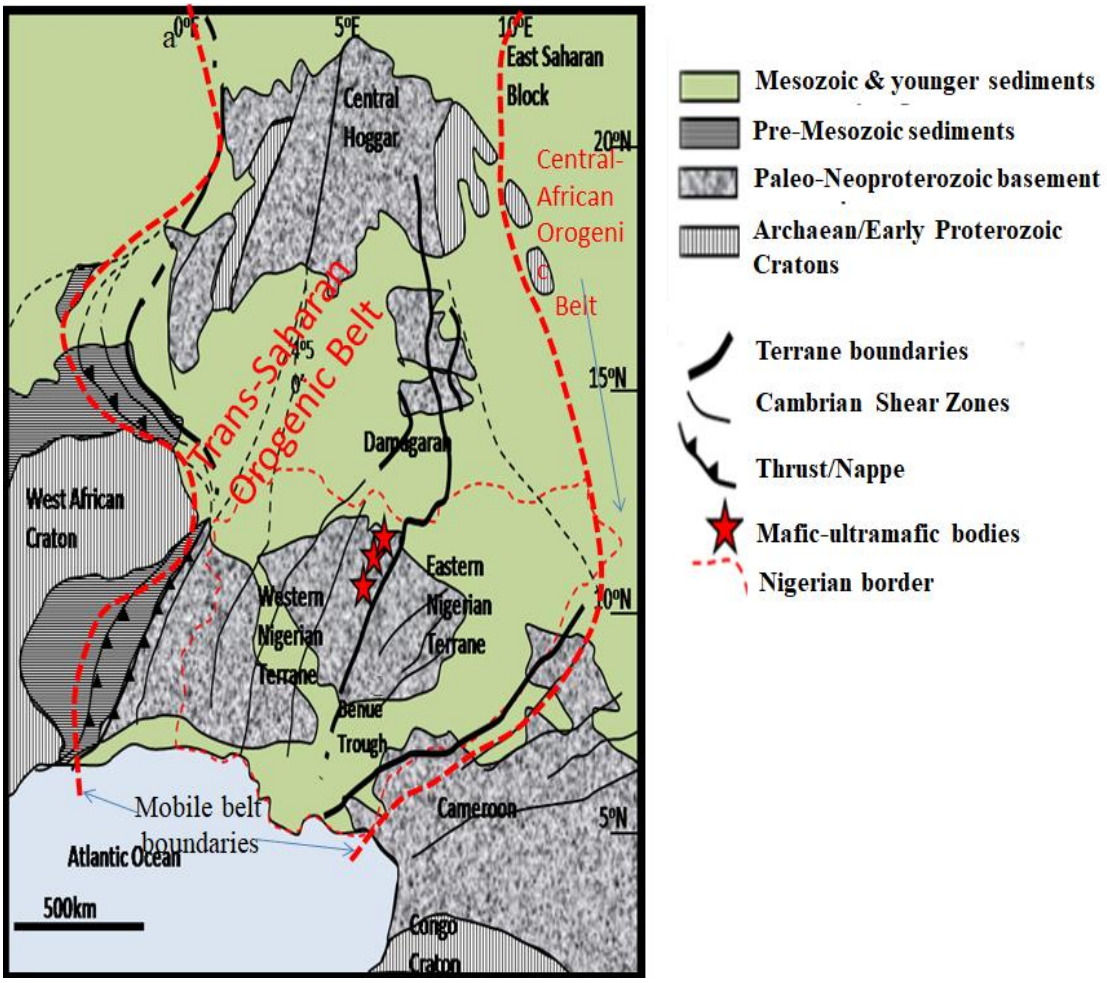

Fig. 1-1 Regional geologic map of the Hoggar–Aïr–Nigeria province of the Neoproterozoic Trans-Saharan Belt resulting from terrane amalgamation between the cratons of West Africa and Congo and the East Saharan block. Redrawn from Ferré and Caby (2006). Mobile belt boundaries as adapted from Cordani et al. (2013).

The Trans-Saharan Belt is a complex assemblage of N-S trending geological domains which have undergone different evolutions (Bouller 1991). Even the Pan-African belt of central northwest Africa is part of the Trans-Saharan Belt (Cahen et al. 1984) and it stretches also into Brazil (Ferre et al. 1996). It consists of Pre-Neoproterozoic basement strongly reworked during the Pan-African event and of Neoproterozoic ocean assemblages. Black et al. (1994) and Liegeois et al. (1994) showed that this belt consists of continental terranes amalgamated during oblique collision between the West African Craton and the Tuareg Shield (Caby 1989; Affaton et al. 1991; Castaing et al. 1993).

The Nigerian basement has been collectively designated as part of the Trans-Saharan Orogenic Belt according to Kennedy (1964) who observed that all crystalline shield areas in Nigeria have been reactivated by the last episode of metamorphism - the Pan-African (950 – 450 Ma). He postulated that all other pre-Pan-African ages obtainable from parts of the basement complex are protolith ages.

Pan-African orogeny has different structural imprints on different parts of the Trans-Saharan Orogenic Belt. By far the most dominant foliation and lineation directions recorded are the N-S to NNE-SSW directions which represent E-W to NNW - SSE compressional regimes. However, some parts of the orogenic belt are dominated by E-W trending foliation and lineation directions which unequivocally represent a different stress regime – specifically, a N-S compressional force. Many researchers agree that the sequence of the compressive/amalgamating forces which led to the closure of the sedimentary basin and subsequent formation of the Gondwana supercontinent followed an initial northward movement of the African and south American plates leading to the creation of East-west trending shears, foliations and lineations encountered in all orogens affected by this tectonism. The northward movement of plates changed direction to N-E and finally to E and S-E, consequently, creating the NW-SE through N-S to NE-SW foliation, lineation and shear directions.

According to da Silva et al. (2005) in their study of the Mantiqueira Province of south America, the Pan-African orogenic stresses were absorbed into early E-W to WNW-ESE or NW-SE syn-collisional tectonics, followed by development of NE-SW, NNE-SSW transpressional (dextral) shear zones, precisely dated at ca. 790 Ma and 730–700 Ma (Brasiliano I); ca. 640–620 Ma and ca. 600 Ma (Brasiliano II) and, ca. 595–560 Ma and 520–500 Ma (Brasiliano III), respectively. Caby (1998) presented a threefold subdivision for the Pan-African tectono-metamorphic events in northern Africa: an Early Pan-African tectonic-metamorphic ‘Event’ (750–700 Ma); a Main Pan-African ‘Episode’ (630–580 Ma); and a Late Pan-African ‘Episode’ (580–520 Ma). Egbuniwe (1982) suggested 3 phases of metamorphism (M1, M2 and M3) to be associated with 3 phases of deformation (D1, D2 and D3) within the crystalline rocks of the basement complex in northern Nigeria. In southwest Nigeria, Boesse and Ocan (1988) recognized 3 phases of metamorphism but only 2 phases of deformation. Goodenough et al. (2014) measured the timing of magmatism within the Minna Batholith in Minna, West-Central Nigeria. The result showed that the earliest magmatism was 790–760 Ma, which was followed by 600–650 Ma, 590 Ma and 560–450 Ma episodes. All these show synchronous episodes of

both magmatism and deformation across the entire Trans-Saharan Orogen. Hence, according to da Silva et al. (2005), 'the evolution of the distinct orogens is a response to continental collision processes, responsible for the development of extended deep shear systems. In most cases, the systems are the limits of distinct terranes and separate distinct records of orogenic magmatism, deformation and metamorphism'.

This research was undertaking to elucidate the Rodinia-Gondwana-recent transition story of the Trans-Saharan Orogenic Belt, using the Benin-Nigerian Shield as laboratory through the perspectives of petrology, mineralogy and tectono-metamorphic studies. The need to fully dwell on the domains of the geological, mineralogical and tectono-metamorphic characteristics of the different parts of the Trans-Saharan Orogenic Belt and beam such perspectives on the Rodinia-Gondwana transition story cannot be over-emphasized. Aspects of such study include to determine if the early to syn-tectonic metamorphic episodes (usually associated with E-W to NW-SE shear and foliation directions) produced granulite facies terranes. Such terranes may be the lost micro-continental units in the hitherto Goiás-Pharusian Ocean, trapped within the orogenic belt during the final ocean closures. On the other hand, minerals potential assessment of the basement areas of Nigeria still demands attention because most mineral exploration models require an understanding of the geological evolution of the crust in the area of interest; critical information includes the timing of magmatic events, the types and sources of the magmas, identification and definition of ancient plate boundaries.

A regional study of the minerals paragenesis and metamorphic *P-T* responses (particularly of the metasediments) to Pan-African orogeny is the way we must go to begin to proffer solutions to these problems. Since the foliations, lineations and Landsat-delineated suture zones of the Trans-Sahara are dominantly N-S to NNE-SSW in orientation, an East-West cross-sectional approach within latitudes 07°00'N and 09°10'N in the Benin-Nigerian Shield areas is chosen for the start. Within this chosen region, three case-study localities lying within longitudes 005°40'E and 009°10'E have been identified for more detailed sampling including Keffi and environs in north-central Nigerian basement (Lat. 08°30'N - 09°07'N and Long. 007°37'E - 008°18'E), Obudu area in southeastern Nigeria (Lat. 06°35'N - 06°50'N and Long. 009°00'E - 009°10'E) and Akoko areas of Ondo State, southwestern Nigeria (Lat. 07°30'N - 07°40'N and Long. 005°40'E - 005°50'E).

This study presents the first petrological, mineralogical and metamorphic *P-T* data of three localities namely; Keffi (north-central Nigeria), Obudu (southeast Nigeria) and Ikare-Erusu-Arigidi-Ogbagi areas (Ondo State, southwestern Nigeria) and the first attempt to study the metamorphic evolution of metasediments of these localities using mineral equilibrium modeling in a complex system $Na_2O–CaO–K_2O–FeO–Fe_2O_3–MgO–Al_2O_3–SiO_2–H_2O–TiO_2$ (NCKFMASHTO) with THERMOCALC 3.33 (Powell and Holland, 1988) software. This study also presents new mineralogical and petrological data of the metamorphic suite of the study areas and discusses the evidences of metamorphic grades, qualitative timing of metamorphism and *P-T* path. The result of this research will go a long way to re-writing the story of the Nigerian metamorphic basement and embolden the investigation of the Rodinia-Gondwana-recent transition story and the variations in metamorphic response to orogenesis.

1.2 Objectives of the research

1. To examine possible terrain-scale differences in crustal evolution across a major tectonic block like the Benin Nigeria Shield and across tectonic blocks like the eastern and western Nigerian Basement.

2. To attempt a comparison of the Eastern and Western Nigerian Precambrian Basement in terms of tectonic settings, rock compositions and geotectonic evolutional histories.

3. To reconstruct the tectonic and metamorphic history of the Nigerian basement complex.

Chapter 2: Regional geology

The Pan-African Tran-Saharan Belt is a Neoproterozoic orogen stretching from North Africa to Brazil (Caby 1989; Boullier 1991). It spreads through Morocco, covering the Sirwa-Bou-Azzer ophiolitic mélange and the Saghro arc, to the Tuareg shield of Algeria, Mali and Niger. Farther south, it encompasses the Laouni, Azrou-n-Fad, Tefedest, and Egere Aleskod – parts of a single passive margin in central Hoggar. The southern part of the Trans-Saharan Belt in Africa is exposed in Benin, Togo and Ghana where it is known as the Dahomeyan Belt. The western part of this belt consists of a passive margin sedimentary sequence in the Volta basin which was overthrusted from the east along a well delineated suture zone by an ophiolitic melange and by a 613 Ma high-pressure metamorphic assemblage (up to 14 kbar, ~700 °C) including granulites and eclogites. The eastern part of the belt consists of a high-grade granitoid-gneiss terrane of the Nigerian province, partly consisting of Palaeoproterozoic rocks which were migmatized at ~600 Ma (Kroner and Stern 2004). In Nigeria and in Togo-Benin, the width of the belt and a range of ages, spanning 750-500 Ma, suggest multiple collisions (Ajibade and Wright 1989).

The metasediments of the Trans-Saharan Orogenic Belt are believed to have been deposited within the Goiás-Pharusian Ocean basin which formed between two major blocks; the Laurentian-Amazonian-West African Block (now the North-America, Brazilian and West-African Cratons) to the west of the ocean, and the Central African Block (now the Tuareg Shield and Congo-Gabon Cratons) to the east during the breakage of the Rodinia supercontinent into the two major blocks in a process that started around 900 Ma (Li et al. 2008; Cordani et al. 2013). The tectonic process was extremely complex, leading to the formation of several sutures. However, evidence is mounting of the possibility of multiple collision zones within the orogenic belt due to the assembly of other micro-cratonic units which existed between the three major cratons stated above and surrounded by the Goiás-Pharusian Ocean in a process which Kröner and Stern (2004) described as a trend of oceanic opening, followed by a subduction and collision-related evolution between 900 and 520 Ma. According to Cordani et al. (2013), as a consequence of the subduction of oceanic lithosphere related to the closure of the Goiás-Pharusian Ocean, several accretionary complexes and possible micro-continents were trapped within orogenic belts formed during the Neoproterozoic collisional events.

In Nigeria however, the basement geology of East and West are different. Obviously, the schist belt of Nigeria is restricted in their occurrence to the Western Nigerian basement separated

from the eastern side approximately along longitude 8°. These schist belts are also closely associated with gold mineralization (especially in the north-west basement) which is not found in the eastern Nigerian basement. According to Pidgeon et al. (1976), Rahaman (1988) and Bruguier et al. (1994), the western Nigeria is characterized by (i) Archean basement comprising tonalite-trondhjemite granodiorite (TTG) type orthogneisses and amphibolites corresponding to a gold metallogenic province and banded-iron formations (Woakes et al. 1987) in which amphibolites display greenstone affinities (Klem et al. 1984). (ii) A cover of synformal schist belts (Grant 1978; Fitches et al. 1985; Ajibade et al. 1987) ranging from greenschist to amphibolites facies (Caby 1989; Ugwuonah and Obiora 2011). While the eastern Nigerian basement is characterized by higher grade gneisses and migmatites relative to the western Nigerian basement (Onyeagocha and Ekwueme 1990), pervasive migmatization and granite plutonism (Wright 1971) and a uranium and tin metalogenic province (Woakes et al. 1987). The boundary between these two provinces is marked by a major lineament on the Landsat imagery (Ananaba and Ajakaye 1987). The eastern domain stretches from the Cameroon line to the area between Kaduna and Jos (approximately at Longitude 8° east).

2.1 Keffi

According to Ugwuonah and Obiora (2011), Keffi area in north-central Nigeria is dominantly underlain by gneisses including; augen gneiss unit and a banded gneiss unit, while the schists encircled by gneisses occur within the central and low-lying areas. The augen gneiss covers the northern and southwestern parts while the banded gneiss underlies the central and the southeastern parts. The schists occupy the central parts of the study area and are second most dominant rocks in the area. This gneiss-migmatite and schist arrangement as in other parts of the basement, has also been intruded by a granitic batholith (Gudi batholith).

2.2 Obudu

Giant spurs continuous with the Cameroon Mountain to the east, protrude into Nigerian eastern margin to the west to form the metamorphic basement of the rim of eastern Nigeria and the eastern boundary of the Trans-Saharan Orogenic Belt within the Benin-Nigeria Shield area.

These spurs ranging from the Hawal massif to the north, through the Obudu (location of the study area) to the Oban massifs to the south, are underlain by rock units including migmatitic gneisses and schists, granitic gneisses, meta-ultramafics, charnockites and amphibolites of varied ages. The metamorphic basement of the southeastern part of Nigeria has been recorded to be composed of a high-grade granitoid-gneiss terrane, partly consisting of Palaeoproterozoic rocks which were migmatized at ~600 Ma (Onyeagocha and Ekwueme 1990; Kröner and Stern 2004). In Obudu area, the migmatites (host rock) were intruded by large north-south aligned granite gneiss plutons which were later intruded by meta-ultramafic units.

2.3 Akoko

The western province is particularly dominated by narrow, N-S trending, low-grade schists of greenschist to amphibolite facies (Grant 1978; Fitches et al. 1985; Ajibade et al. 1987; Caby 1989; Ugwuonah and Obiora 2011). The schistose rocks are intercalated with migmatite-gneiss 'older' basement, which together with the schists is intruded by Pan-African granitic plutons (Rahaman 1988; Bruguier et al. 1994).

Akoko area forms part of the southern bloc of the western province. In this area however, schistose outcrops are lacking, and the dominant metasedimentary unit is the migmatite-gneiss. This migmatite host rock, together with two intruding large plutons of granite gneiss and charnockite, are aligned in the east-west direction with a dominant E-W to NW-SE trending foliations and lineations.

Chapter 3: Metamorphic *P–T* evolution of garnet-staurolite-biotite pelitic schist and amphibolite from Keffi, north-central Nigeria: Geothermobarometry, mineral equilibrium modeling and *P-T* path

3.1 Introduction

The Pan-African Trans-Saharan Belt is an orogenic belt that is more than 3000 km long and occurs to the north and east of the >2 Ga West-African craton within the Anti-Atlas and covering the Tuareg and Nigerian Shields (Kröner and Stern 2004). Even the Pan-African belt of central northwest Africa is part of the Trans-Saharan Belt (Cahen et al. 1984) and it stretches also into Brazil (Ferre et al. 1996). It consists of Pre-Neoproterozoic basement strongly reworked during the Pan-African event and of Neoproterozoic intra-oceanic magmatic rocks (Umberto et al. 2013). Black et al. (1994) and Liégeois et al. (1994) showed that this belt consists of continental terranes amalgamated during oblique collision between the West African Craton and the Tuareg Shield (Caby 1989; Affaton et al. 1991; Castaing et al. 1993). The Precambrian Basement Complex of Nigeria lies within the internal region of the reactivated part of the Trans-Saharan Belt, east of the West African craton and northwest of the Congo craton. Reactivation at this plate margin is believed to be due to the collision of these two cratons. Lithologically, the Precambrian basement rocks of Nigeria have been subdivided into; Gneiss-migmatite complex (including the Older Metasediments), the Younger Metasediments (the schist belt) and the Older Granite suit (see Fig. 3-1). They were later intruded by the Younger Granites in the Jurassic time (Obiora 2005; Dada 2006).

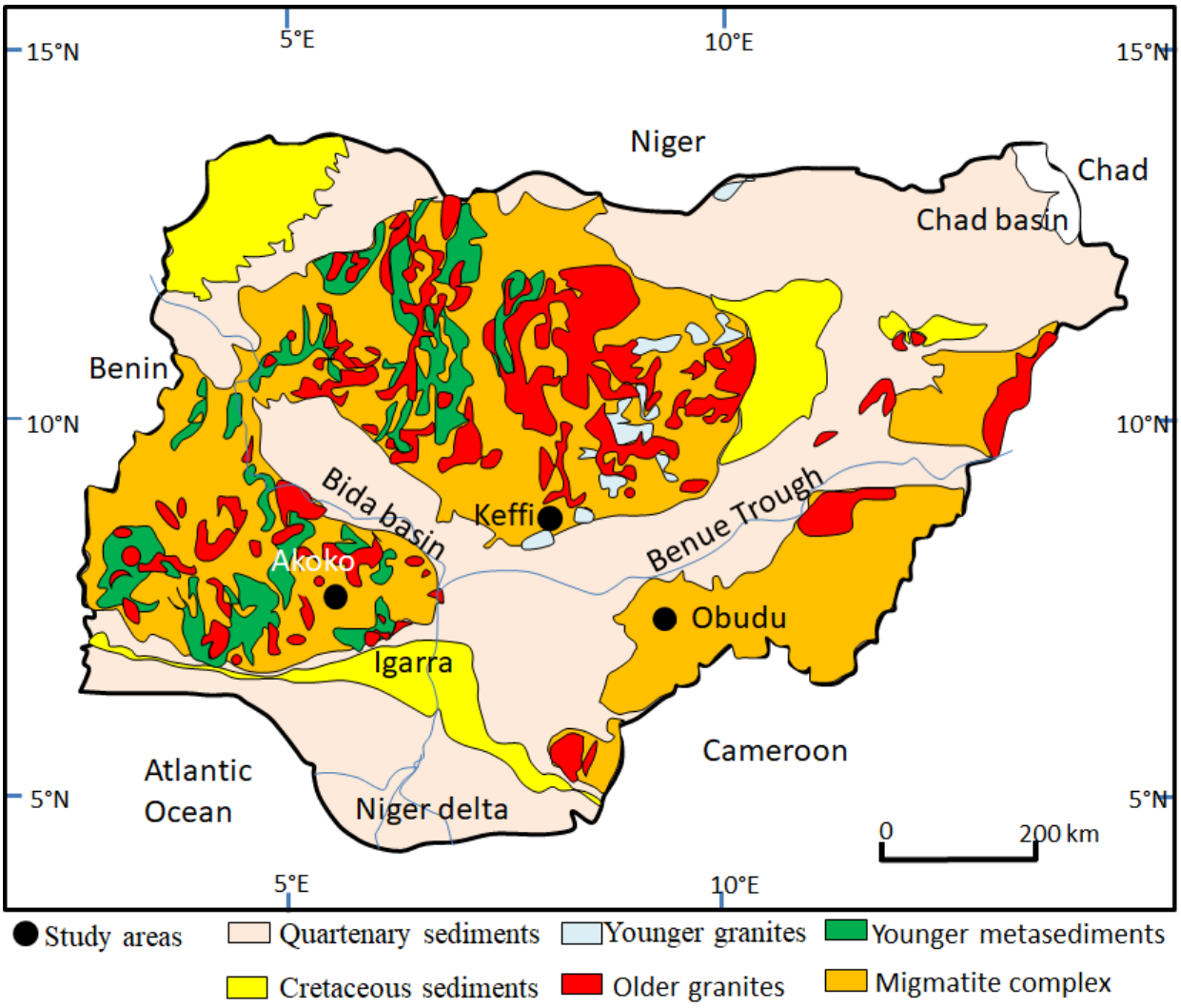

Fig. 3-1 Geological map of Nigeria showing study area. Redrawn from Okezie (1974).

McCurry (1976) used the term "Older Metasediments" to refer to the metasedimentary remnants within the gneisses and migmatites, which was deposited perhaps 2,500 m.y. ago, and the term "Younger Metasediments" for all low to medium-grade metasedimentary belts which she considered to have been deposited 1,000-800 m.y. ago. Using structural distinctions, Grant (1978) distinguished two units of the Nigerian Schist Belt (Younger Metasediments) as; (1) a simple and monocyclic type and (2) a complex and polycyclic type. Grant (1978) identified these two structurally diverse signatures imprinted on two schist belts side by side within the northwest Nigerian basement. He described the first type at Birnin Gwari area as having the simple linear style with uniform north-south structural trends. This belt was called the Birnin Gwari Schist formation. The second – the Kushaka Schist formation, is the complex type with great variability in structural trends. The complex style appears in the mixture of north-south and east-west

structural trends and in the presence of refolded major folds. But all other occurrences of the Younger Metasediments preserve only the NNE-SSW Pan-African imprints of foliation (McCurry 1976; Grant 1978; Rahaman 1988; Bruguier et al. 1994). We can therefore assume for now, with a high degree of accuracy, without further chronological analysis that all such rock units (schist) with the simple linear structural styles, within the Nigerian Schist Belt belong to the Younger Metasediments group. Though geographically they are restricted to the western half of Nigeria from north to south, some units of schistose rocks, contemporaneous with the Younger Metasediments have been mapped in the far eastern Nigerian basement by Ekwueme (1991), Ekwueme (2003), Ephraim (2005) and Ephraim et al. (2008) and some parts of Cameroun by Mvondo et al. (2003). However, according to these researchers, the schist belts in Eastern Nigeria (Eastern Nigerian Schist Belt; ENSB) are more closely related to the Central African Fold Belt group than with the schist belts in western Nigerian province (Western Nigerian Schist Belt; WNSB).

This study reports the first detailed petrographical and mineralogical data on the various samples from the Keffi Schist Belt (Lat. 8° 30$^{'}$ - 9° 07$^{'}$ N and Long. 7° 37$^{'}$ - 8° 18$^{'}$) in Nassarawa state of Nigeria – a location lacking a clear definition of its terrane affiliation either to the eastern or the western Nigerian basement terranes. This study also applied geothermobarometers and the pseudo-section approach to the *P–T* evolutionary discussion of the schist unit. The study area was chosen firstly because it is an area that is hitherto unresearched and secondly because of its position at the center of Nigeria and the border between the eastern and the western Nigerian geological terranes. It becomes important thus to characterize this area fully with a view to defining its terrane affiliation. Lastly, this area was chosen because it belongs to the simple linear style schist belt.

This study is the first among a planned research on characterization of orogens within the Trans-Saharan Belt (including also the definition of the tectonic settings of the different tectonic blocs). It is centered on the investigation of the limits of the Pan-African Belt and the variations in metamorphic response to orogenesis beginning with the study of the youngest and most unique members of metasediments within the Trans-Saharan Belt in Nigeria. The results of this study will provide useful information for understanding the tectono-thermal evolution of the Great Nigerian Schist Belt within the Trans-Saharan Orogen.

3.2 Description of lithologic characteristics

3.2.1 Garnet-biotite schist

This unit is exposed at locations K1 (08º 52.5’ N, 007º 60.15’ E), K2 (08º 54.75’ N, 007º 49.35’ E), K4 (08º 54.30’ N, 007º 63.30’ E), K11 (08º 39’ N, 007º 42.60’ E) and K17 (08º 58.80’ N, 007º 55.65’ E) (see Fig. 3-2). The rock unit is the most dominant facies of the schistose rocks in the study area. It is medium grained with a characteristic schistose fabric and consists mainly of micas (biotite and muscovite), quartz and garnet. It weathers deeply in many locations making dip and strike measurements difficult. At location K1, the rock is greenish-grey in color, indurated and irregularly impregnated with leucocratic quartzo-feldspathic materials and revealing the foliation trend which is observed everywhere in the rock. The foliation has high-angle dips of 45˚-75˚ and strikes 10˚ (NNE-SSW). This green colored variety of the unit becomes less indurated downstream where it is gradational into the staurolite schist. A whitish colored variety of the unit occurs at the boundary between the green variety and the staurolite-bearing schist facies (location K10). The rock is mesocratic to leucocratic, containing mainly white feldspar, biotite, muscovite and quartz. It occurs in a layer exposed under a bridge with thickness varying from 10-15 m. The foliation is striking 10˚ NNE-SSW with dip of 35˚ to the ESE direction.

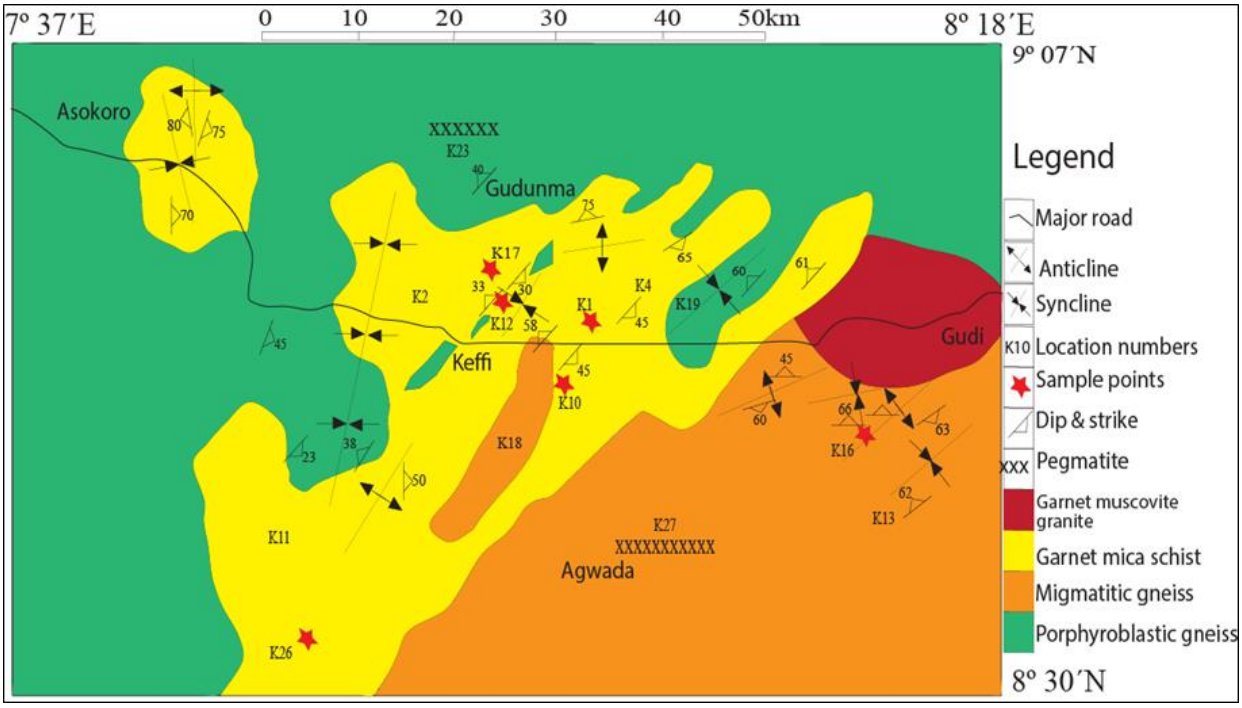

Fig. 3-2 Geologic map of Keffi area (after Ugwuonah and Obiora, 2011).

3.2.2 Staurolite-garnet-biotite schist

Exposures of this unit are most prominent at location K10 (08º 50.086’ N, 007º 57.082’ E). It is exposed over a distance of 1 km in a river valley. The surface of the long outcrop is dotted with long and slender, euhedral, staurolite crystals (Figs. 3-3a, b). The staurolite crystals have an average length of 2.5 cm with width of 0.3 cm. The rock weathers into silty-sand, with specks of shiny mica flakes. The foliation is striking 7° NNE-SSW with dip of 45° to the ESE direction.

3.2.3 Garnet -chlorite-biotite schist

The schist occurs at location K26 (08º 32.25’ N, 007º 42.60’ E). It is melanocratic to mesocratic and more indurated than the staurolite-garnet-biotite schist. The rock is fine-grained, and rich in quartz. It is easily weathered to form very loose silty sand.

3.2.4 Metabasite

This unit is exposed in a porphyroblastic gneiss quarry site at location K12 (08º 54.75’ N, 007º 55.65’ E) where the exposure reveals a sharp boundary between the schist and augen gneiss (Figs. 3-3c, d). This dominantly micaceous schist is medium to coarse-grained and unusually melanocratic with a greenish-blue black color. It consists dominantly of dark-greenish-blue micaceous minerals and biotite, with minor amounts of feldspar and quartz. It is occasionally cross-cut by veins of clear subhedral quartz crystals. The amphibolite is found at location K16 (08º 49.30’ N, 008º 11.25’ E) where it is in-folded within the migmatite gneiss unit. It is coarse-grained, melanocratic and clearly banded with alternation of dominant mafic layer and subordinate feldspathic layers.

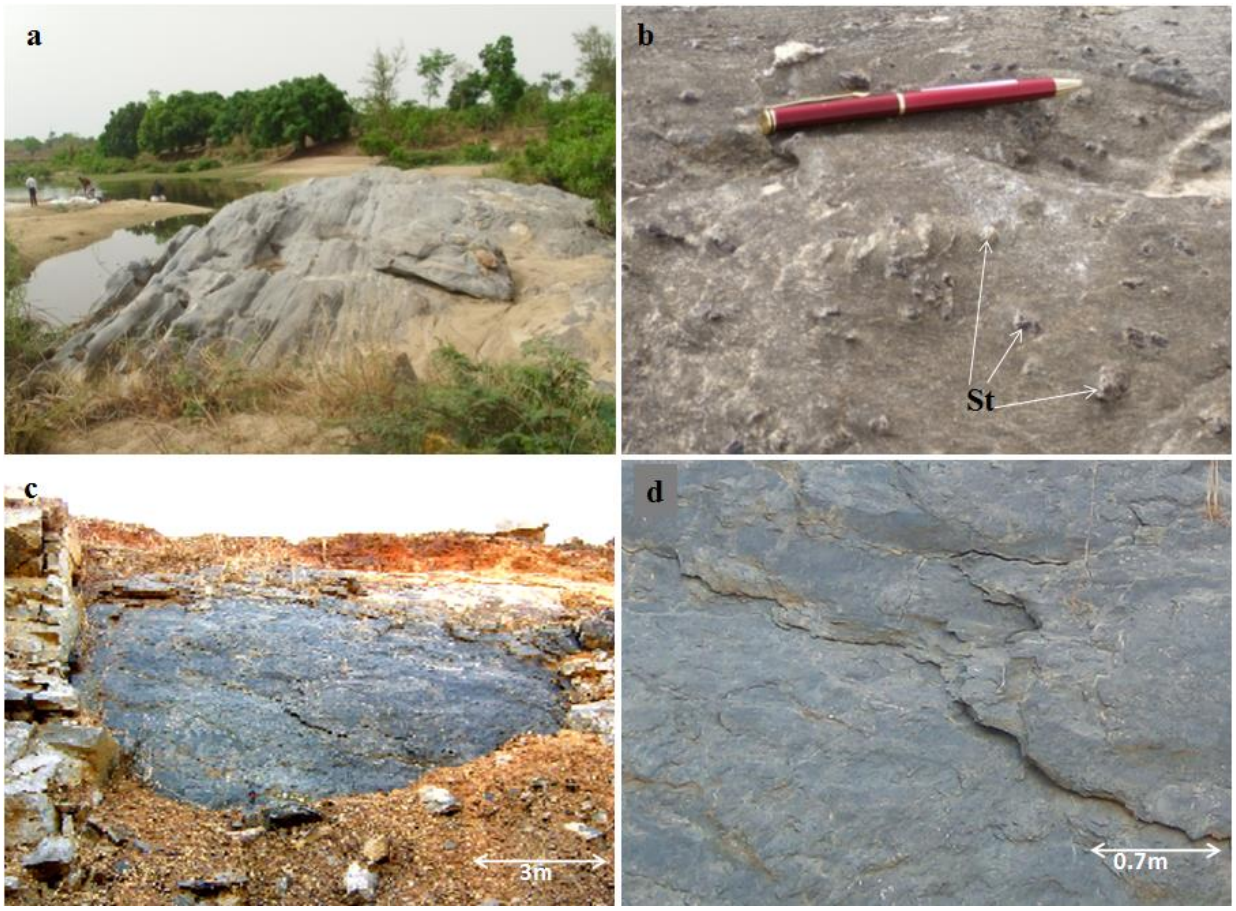

Fig. 3-3 Field photographs of the rock under study. (a) Staurolite-mica schist outcrop on the River channel. (b) Staurolite-mica schist showing the rough surface created by the presence of the staurolite porphyroblasts (location K10). **(**c**)** The sharp contact between the metabasite schist and porphyroblastic gneiss (location K12). **(**d**)** A closer view of the metabasite schistose texture. Mineral abbreviations are as suggested by Kretz (1983).

3.3 Petrography

The petrographic features of the representative units are briefly summarized below. Two samples of the staurolite-garnet mica schist, three samples of garnet-biotite schist and two metabasites, which have the assemblages suitable for geothermobarometric calculations were selected and analyzed. The staurolite-garnet mica schist was further subjected to pseudosection analysis. The textural characteristics of these rocks are shown in Fig. 3-4, while the approximate modal abundances of the minerals are listed in Table 3-1. Pelitic schists and amphibolites discussed in this study were collected from the area about 60 × 60 km² around area north-central Nigeria. The main target lithology is the pelitic schist which has unique characteristics and shows slight variations in metamorphic response to tectonism. Five best fresh samples were

hence selected from the schist. However, due to the low - medium-grade nature of these pelitic schist samples, it became necessary to employ also the instrument of the associated and nearby metabasites which were thus selected for hornblende-plagioclase geothermometry. Two samples of the metabasites were analyzed.

3.3.1 Staurolite-garnet-biotite schist

This lithology exposed at location K10 (see Fig. 3-2) is characterized by the occurrence of equilibrium garnet + staurolite + biotite + quartz + muscovite + plagioclase + ilmenite and retrograde chlorite. It is porphyroblastic and strongly to moderately foliated as defined by the micaceous minerals in the matrix. The uniform foliation is characterized by the alignment of biotite and quartz mixed with slender lats of muscovite. This unit is represented by sample K10a. The mineralogy of the sample is biotite (30-35%), quartz (25-30%), muscovite (15-20%), staurolite (2-5%), garnet (5-7%), plagioclase (10%) and chlorite (<2%) with accessory tourmaline, zircon, and ilmenite (Figs. 3-4a-c). The porphyroblast population is made up by poikiloblastic staurolite and garnet. Inclusions in garnet are quartz, biotite, muscovite and ilmenite, while staurolite has all the inclusions that are present in garnet plus some garnet and plagioclase. The occurrence of biotite, muscovite, quartz, plagioclase and ilmenite both within and outside the porphyroblasts confirm that they belong to both the prograde and peak assemblages. Biotite inclusions in garnet contain higher SiO_2, MnO, and MgO and less FeO than those outside of garnet. Biotite is the most dominant mineral and is medium grained (~0.4×0.2 mm) with brownish to dark brownish color and subidioblastic to xenoblastic in shape. Quartz measures ~0.3×0.2 mm, while muscovite measures ~0.3×0.05 mm, ilmenite measures 0.01–0.20 mm, and rare tourmaline 0.01–0.10 mm. Poikiloblastic staurolite and garnet make up the porphyroblast population with staurolite size approximating 3×2 mm, while subidioblastic garnets measure approximately 0.4×0.3 mm and idioblastic garnets have a radius of ~0.4 mm. The sparsely distributed and disoriented retrograde chlorites are mostly subidioblastic in shape and measure ~0.4×0.2 mm.

3.3.2 Garnet-biotite schist

This lithology has mineral constituents which includes garnet + biotite + quartz and accessories. It is represented by samples K10b, K1 and K17. Sample K10b is mineralogically similar to K10a (staurolite-garnet-biotite schist), with equilibrium garnet + biotite + quartz + muscovite + plagioclase + ilmenite and retrograde chlorite, but lacks modal staurolite. Even

though chlorite cannot form directly from alteration of staurolite, there seems to be a correlation between the lack of staurolite in this sample and corresponding increase in size and quantity of secondary chlorite. In few spots, chlorite has formed prismatic pseudomorphs of staurolite in association with white mica and considerable clusters of opaques. This sample is also more lepidoblastic than porphyroblastic as defined by a dominance of the platy micaceous minerals (biotite) over prismatic minerals in the coarse-grained mode. Furthermore, the biotites are more poikiloblastic as they are riddled with more inclusions of quartz, tourmaline and ilmenite than in sample K10a (see Fig. 3-4d). The largest and most dominant mineral in this subunit is poikiloblastic biotite with some measuring up to 1×0.5 mm. Biotite makes up about 30-35% of the rock. Quartz measures ~0.3×0.2 mm and makes up ~25-30%. Muscovite (0.3×0.2 – 0.3×0.02 mm) makes up ~10-15%. Garnet which measures about 0.4 mm in diameter makes up ~4%. Chlorite which measures 0.5×0.4 mm, constitutes ~5%. Opaque minerals (mostly ilmenite) constitute ~10%.

In sample K1 (Fig. 3-4e), the lithology is shown to be medium to fine grained with good uniform distribution of the planner and linear minerals which define the foliation. It is porphyroblastic with sparsely distributed porphyroblasts of garnet dotting the equigranular matrix. The garnet porphyroblasts range in sizes between 0.5 and 1 mm in diameter and they make up about 6% of the rock. The matrix is dominated by more polycrystalline than monocrystalline fragments of mostly undulose extinction quartz which range in size between 0.03×0.05 – 0.2×0.3 mm. Quartz constitutes ~55-60% of the rock. The next most dominant mineral in the rock is uniformly brownish biotite whose only inclusions are few opaque minerals. Some of the opaque inclusions are surrounded by pleochroic haloes. They are mostly subhedral in shape and their slender lat-like forms range in sizes between 0.02×0.4 mm and 0.2×0.4 mm. Biotite constitutes about 30-35% of the rock. Muscovite makes up less than 2% of the rock. They are mostly euhedral to subhedral and needle sized. Actual size measurement is about 0.01×0.4 mm. Ilmenite makes up the opaque mineral population which constitutes about 6-10% of the rock. K-feldspar with sizes of about 0.02×0.04 mm makes up less than 3% of the rock.

In sample K17 (Figs. 3-4f and g), the lithology is shown to be finer-grained with the same uniformly brownish but now two generations of biotite which includes; the more dominant, anhedral and skeletal biotite and the fewer euhedral ones. They range in size between 0.5×0.1 mm and 0.02×0.03 mm and make up about 35% of the rock. Quartz is the most abundant mineral

in the rock. Its sizes range between 0.03×0.05 – 0.2×0.3 mm and it constitutes ~55-60% of the rock. Tourmaline appears in this subunit. It is mostly idioblastic in shape with approximate size of about 0.2×0.1 mm and constitutes less than 3% of the rock. Opaque minerals include graphite and ilmenite. They constitute about 5% of the rock. Garnet is very rare both in size and occurrence. Its size is about 0.2×0.2 mm and it makes up less than 2% of the rock. Plagioclase of oligoclase composition makes up less than 5% of the rock.

3.3.3 Garnet-chlorite-biotite schist

This lithology is represented by sample K26 (Fig. 3-4h). It is fine- to medium-grained heterogeneous rock with good alignment of minerals in a preferred direction. It shows a gradational boundary between the biotite-dominated and chlorite-dominated sections. Skeletal garnet porphyroblasts occur within the biotite-dominated area and constitutes less than 3% of the rock. Needles and laths of biotite range in size between 0.05×0.2 – 0.1×0.4 mm. Biotite makes up about 25 – 30 % of the rock. Chlorites are remarkably greenish in color and smaller in size ranging between 0.01×0.2 – 0.05×0.3 mm. They make up about 15 – 20% of the rock and show characteristic berlin-blue interference colors. Quartz is the dominant mineral in the rock, with size range average of 0.2×0.3 mm, and they make up about 55% of the rock. Tiny lats of plagioclase make up less than 5% of the rock. The opaque constituent is ilmenite which makes up about 5% of the rock.

3.3.4 Metabasites

This lithology is represented by samples K12 and K16. In sample K12, the rock is melanocratic, coarse-grained and equigranular, with minerals aligned in a preferred direction. The mineral constituents include biotite, hornblende, plagioclase ($An_{35.9\text{-}43.1}$), clinopyroxene (see Fig. 3-4i), quartz and ilmenite. Clinopyroxenes are the largest minerals in size and abundance, measuring about 3.2×1.2 mm in some crystals but some are in ophitic relationship with hornblende. Clinopyroxenes make up about 30-35% of the rock. Biotites are uniformly brownish and bladed in form but characteristically subhedral in shape. They measure about 2×1 mm in size and constitute about 20% of the rock.

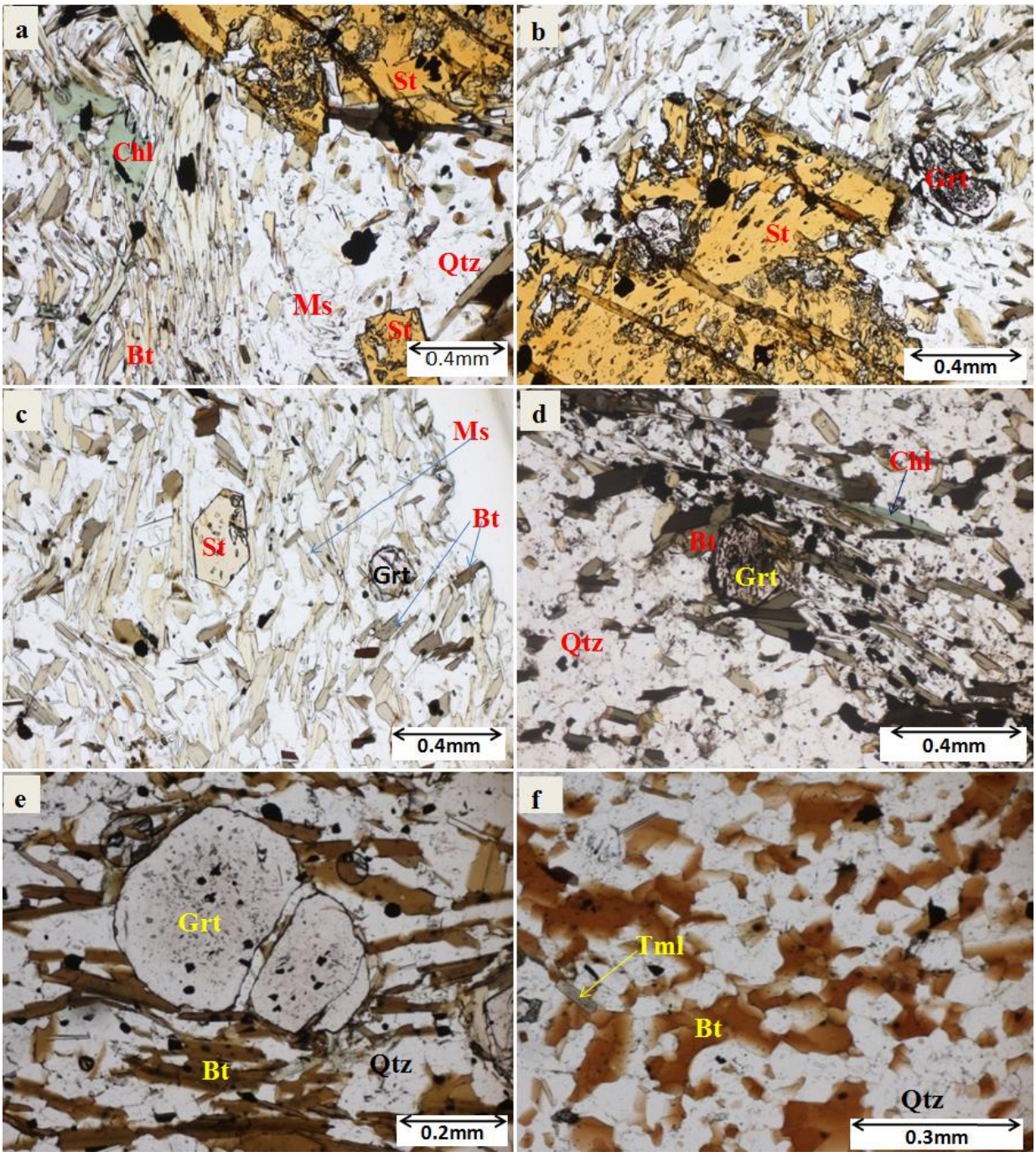

Fig. 3-4 Photomicrographs of rock thin sections. (a-c) Showing the quartz, biotite, garnet, staurolite, chlorite, association in sample K10a. (d) Showing the quartz, biotite, garnet, chlorite, association in sample K10b. (e) Showing the quartz, biotite, garnet, association in sample K1.

Andesine plagioclase (An_{35-41}), is the dominant leucocratic mineral. They measure in size between 2×2 - 2×1 mm and constitute about 15% of the rock. Hornblende also measure 2×1 mm on the average and constitute about 12% of the rock. Quartz is fine grained in size and is sporadically distributed in rounded to semi-rounded drops, measuring about 0.2×0.2 mm. They

constitute about 5% of the rock. The opaque minerals are few relatively coarse crystals of ilmenite measuring 1.2×1.5 mm on average. They together make up about 2% of the rock.

In sample K16 (Fig. 3-4j), the lithology is medium to coarse grained. The minerals are aligned in a preferred direction and segregated into bands of quartzo-feldspathic and mafic layers.

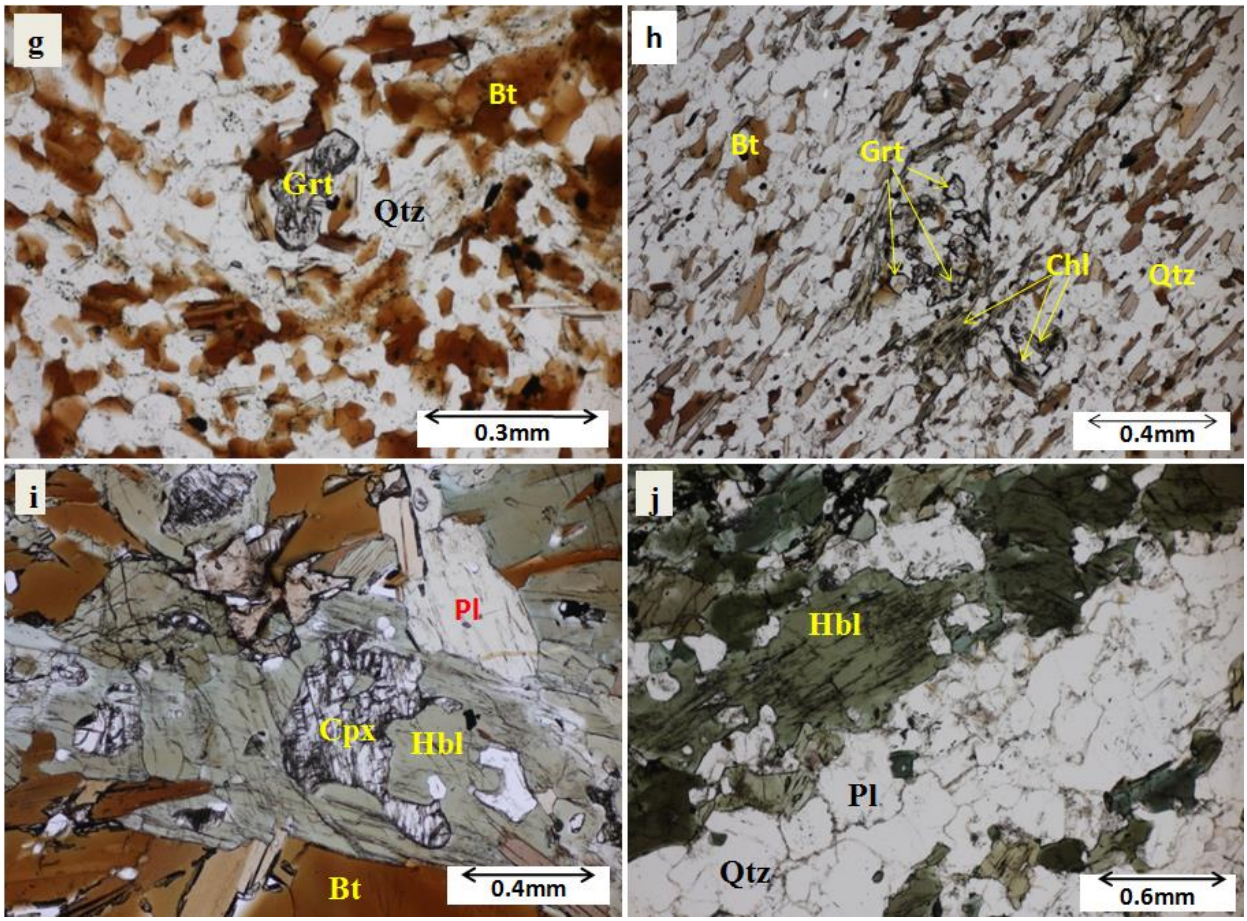

Fig. 3-4 (f and g) Showing the quartz, biotite, garnet, tourmaline association in sample K17. (h) Showing the quartz, biotite, chlorite association in sample K26. (i) Showing hornblende, clinopyroxene, plagioclase, biotite association in K12. (j) Showing hornblende, plagioclase, quartz association in sample K16. Mineral abbreviations after Kretz (1983).

The mineral constituents include; hornblende, plagioclase (An_{34-38}), quartz, and ilmenite. Hornblende is by far the most dominant mineral in this rock, though a little less coarse grained than in sample K12, it measures between 1.5×1.5 – 1.5×0.8 – 0.3×0.3 mm sizes and makes up about 60-70% of the rock. Plagioclase in this rock is andesine (An_{34-38}) only. Its sizes vary between 1×0.4 and 0.2×0.2 mm and it makes up about 10% of the rock. Quartz, like in sample

K12 has small sizes (e.g. 0.2×0.2 mm) but is more in abundance in this sample, making up about 7-10% of the rock. Unlike in sample K12, opaques (ilmenite) are fine-grained and disseminated throughout the rock. They make up less than 3% of the rock.

3.4 Mineral Chemistry

The mineral chemistry data of the examined rocks are described below. Representative compositions of minerals in the analyzed samples are given in Tables 3-2, 3, 4, 5, 6.

3.4.1 Garnet

Garnet in the schist samples is essentially a solid solution of almandine - spessartine - pyrope and subordinate grossular. The garnet chemistry is mostly homogeneous from core to rim with little or no clear evidence of chemical zoning. Garnet analyses show the mole % distribution of almandine, spessartine, pyrope and grossularite as ranges of 71.6-72.7, 13.0-14.0, 9.5-11.1 and 3.1-4.8 respectively. The garnet chemistry and the calculated values are shown in Table 3-2.

3.4.2 Plagioclase

Plagioclase in sample K10a is albite-rich ($An_{16.3\text{-}19.5}$; oligoclase) with minor (less than 0.8 mol%) orthoclase content. Sample K1 also registers plagioclase of oligoclase composition ($An_{17.3\text{-}17.6}$), while sample K17 has slightly anorthite-rich composition of $An_{28.1}$. In the metabasite (sample K12), plagioclase analysis of six cores and five rims reveal a nearly homogeneous andesine composition of the range of $An_{35.9\text{-}37.2}$ and $An_{36.0\text{-}43.1,}$ respectively, while in the amphibolite, plagioclase core compositions gave $An_{34.0\text{-}36.8}$ and the rim gave $An_{37.3\text{-}38.0}$ (see Table 3-3).

3.4.3 Biotite

Biotite in the examined samples have varied Mg content in moles with the ratio of X_{Mg} (Mg/(Mg + Fe)) = 0.50 in sample K10a through X_{Mg} = 0.49 in samples K1 and K26 to X_{Mg} = 0.46 in sample K17 and their titanium contents per formula unit (pfu) fall within 0.24 and 0.17 pfu (see Table 3-4). These values fall within the ranges X_{Mg} = 0.28 - 1.00 and Ti =0.04-0.60 pfu, that are needed for empirical calculation of biotite geothermometry for the rocks (Henry et al. 2005).

3.4.4 Staurolite

Staurolite occurs only in sample K10a. The analyses show from core to rim a consistent Fe-rich composition (X_{Mg} = 0.18) with ~0.5 wt. % TiO_2. ZnO content is generally low ranging between 0.8 and 1.1 (wt. %) in measured crystals (Table 3-4).

3.4.5 Clinopyroxene

Clinopyroxene in sample K12 is diopside with high X_{Mg} of 0.77 to 0.75 without any compositional zoning (see Table 4). The calcium content of the clinopyroxene ranges between 0.94-0.95 pfu, while sodium content ranges between 0.022-0.028 pfu (see Table 3-4). Classification was done using the pyroxene classification triangle of Morimoto et al. (1998).

3.4.6 Calcic amphibole

Calcic-amphibole in sample K12 shows slight decrease of X_{Mg} from core (0.68) to rim (0.65) with Ti and Na+K content ranges of 0.06-0.10 and 0.33-0.38 pfu, respectively (see Table 3-4), while in sample K16, two groups of calcic-amphiboles were detected. The most dominant group is slightly higher in Fe-content than that in sample K12, with X_{Mg} = 0.56-0.53 and higher Ti and Na+K content ranges of 0.11-0.12 and 0.42-0.46 pfu, while the second and subordinate group has similar X_{Mg} value of 0.67 and less Ti and Na+K content ranges of 0.01-0.02 and 0.14-0.15 pfu than those found in K12. Application of hornblende classification of Leake et al. (1997) on both K12 and K16 amphibole compositions shows their plots within magnesio-hornblende field for sample K12 and magnesio-hornblende and actinolite fields for the dominant and subordinate groups in sample K16 (see Fig. 3-5). The hornblende classification of Locock (2014) which is based on the tables of Deer et al. (1966) and Joy and Evans (2014) also confirmed all the calcic-amphiboles in K12 and the dominant group of K16 as magnesio-hornblende and gave their formulae as $(Na_{0.24}K_{0.13})(Ca_{1.92}Mn_{0.05}Fe_{0.02}Na_{0.01})(Mg_{2.95}Fe^{2+}_{1.56}Al_{0.38}Ti_{0.10}Cr_{0.02})(Si_{7.03}Al_{0.97})O_{22}(OH)_2$ for K12, and $(Na_{0.26}K_{0.18})(Ca_{1.97}Na_{0.02}Mn_{0.02})(Mg_{2.39}Fe^{2+}_{1.89}Al_{0.42}Fe^{3+}_{0.15}Ti_{0.12}Mn_{0.03})(Si_{6.76}Al_{1.24})O_{22}(OH)_2$ for K16, while the subordinate group in K16 is confirmed as actinolite with the formula as $(Na_{0.11}K_{0.034})(Ca_{1.92}Mn_{0.04}Fe_{0.03}Na_{0.006})(Mg_{3.2}Fe^{2+}_{1.58}Al_{0.21}Ti_{0.01}Cr_{0.003})(Si_{7.65}Al_{0.35})O_{22}((OH)_{1.98}O_{0.019})$. Magnesio-hornblende is known to be common in many amphibolites, schists and pegmatitic alkali gabbros (Leake 1968) while actinolite is very common in contact and regional

metamorphosed limestone and dolomite but also found in metamorphosed mafic (greenschist facies) and ultramafic rocks. It is a common fine-grained alteration product of pyroxenes (Kerr 1977).

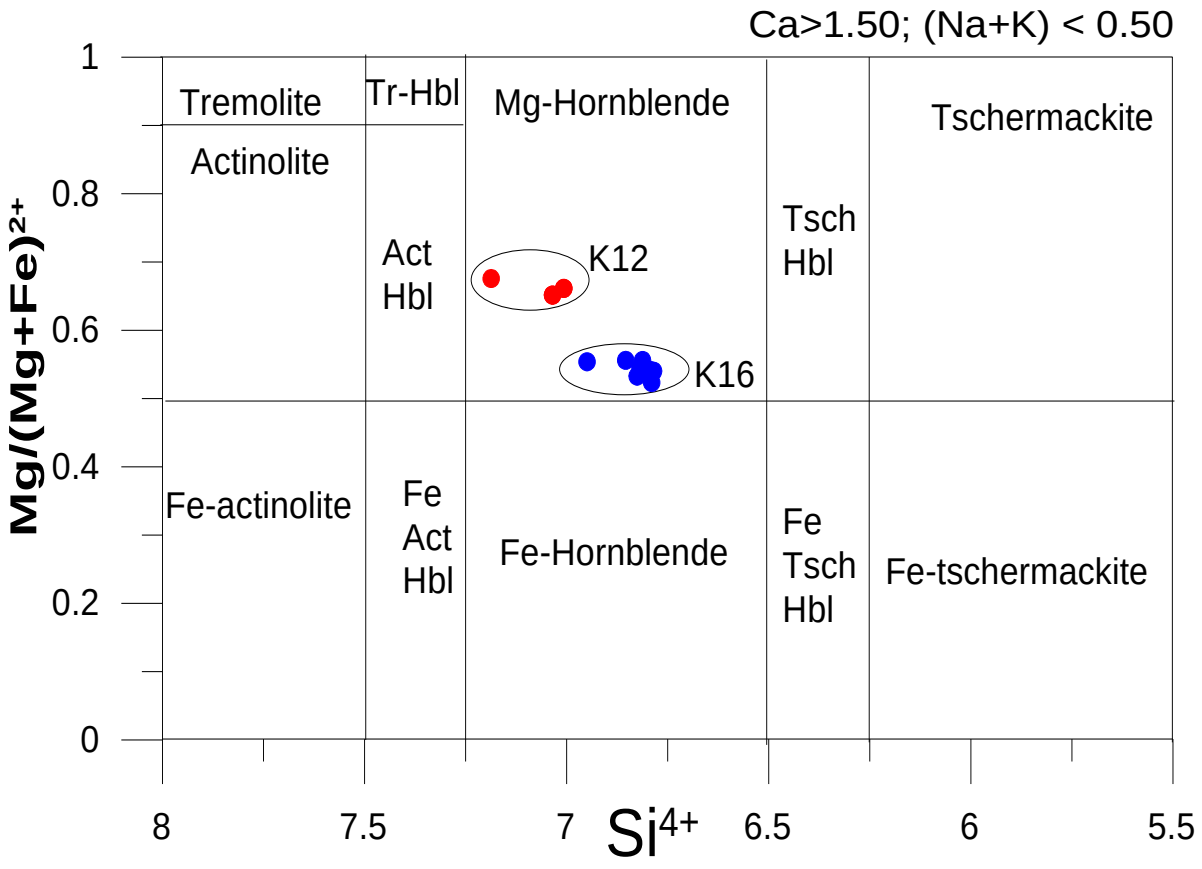

Fig. 3-5 Amphibole classification diagram after Leak et al. (1997), showing the magnesio- hornblende and actinolite ompositions of the measured amphiboles in samples K12 and K16.

3.5 Metamorphic *P–T* conditions

Available geothermobarometers and phase equilibria analysis techniques were applied to determine peak metamorphic conditions of the pelitic schists and amphibolites. The bulk composition of sample K10a is SiO_2 = 65.22, Al_2O_3 = 14.66, TiO_2 = 0.92, FeO = 6.89, MnO = 0.214, MgO = 3.11, CaO = 1.23, Na_2O = 2.13, K_2O = 3.14, LOI = 1.69, while that of sample K10b is SiO_2= 63.56, Al_2O_3 = 16.80, TiO_2 = 0.88, FeO = 6.27, MnO = 0.105, MgO = 2.94, CaO = 1.12, Na_2O = 2.58, K_2O = 3.55, LOI = 1.55. The results of *P–T* calculations are briefly summarized below.

3.5.1 Garnet–biotite geothermometer

Fe–Mg exchange between coexisting garnet and biotite was used to estimate peak temperatures of metamorphism for the pelitic schist samples (samples K1, K17, K26 and K10a). Three methods were adopted including; (a) Kaneko and Miyano (2004) - a refined garnet-biotite Fe−Mg exchange geothermometer with application in amphibolites and granulites that consider the effect of Fe^{3+} and Al^{3+} contents in biotite, (b) Kleemann and Reinhardt (1994) - a calibration which uses the garnet activity model of Berman (1990) and a newer activity model for biotite. This biotite activity model includes non-ideality of Mg, Fe-Al mixing whereas Mg-Fe mixing was assumed to be ideal and (c) Dasgupta et al. (1991) for which the input parameters include available thermo-chemical data for quaternary Fe–Mg–Ca–Mn garnet solid solution and excess free energy terms, associated with mixing of Al and Ti, in octahedral sites, in biotite solid solution. Application of the thermometers to cores of garnets and biotites was used to obtain the temperatures of the rocks at pressure of 7 kbar. The reference pressure of 7 kbar was chosen because it falls within the staurolite-garnet-biotite stability field of sample K10a as constrained using pseudo-section analysis (see Figs. 3-6a and b).

The result of garnet-biotite geothermometry after Kaneko and Miyano (2004), Kleemann and Reinhardt (1994) and Dasgupta et al. (1991) gave temperature ranges of 610-615 °C, 550-560 °C and 510-515 °C for sample K10; 620-630 °C, 550-560 °C and 520-530 °C for sample K1; 590-600°C, 510-520 °C and 470-480 °C for sample K17 and 590-595 °C, 530-535 °C, 460-465 °C for sample K26, respectively. Of the three methods applied here, Kaneko and Miyano (2004) gives the most accurate result here (all its result being consistent with the *P-T* pseudo-section result) and this can be attributed to the Fe^{3+} correction factor inbuilt in the formula.

3.5.2 Garnet–biotite–muscovite–plagioclase geobarometer

The garnet–biotite–muscovite–plagioclase (GBMP) barometer after Wu (2015) which was empirically revised for *P–T* conditions of 1–14 kbar and 450–840 °C, using 263 metapelitic rock samples from all over the world, was applied. This barometer is based on activity models for garnet, biotite and plagioclase identical to those of the well-calibrated garnet–biotite thermometer and the garnet–aluminosilicate–plagioclase–quartz (GASP) barometer. The GBMP barometer is less temperature dependent than the GASP barometer and can be applied to either Al_2SiO_5-absent or Al_2SiO_5-bearing metapelites.

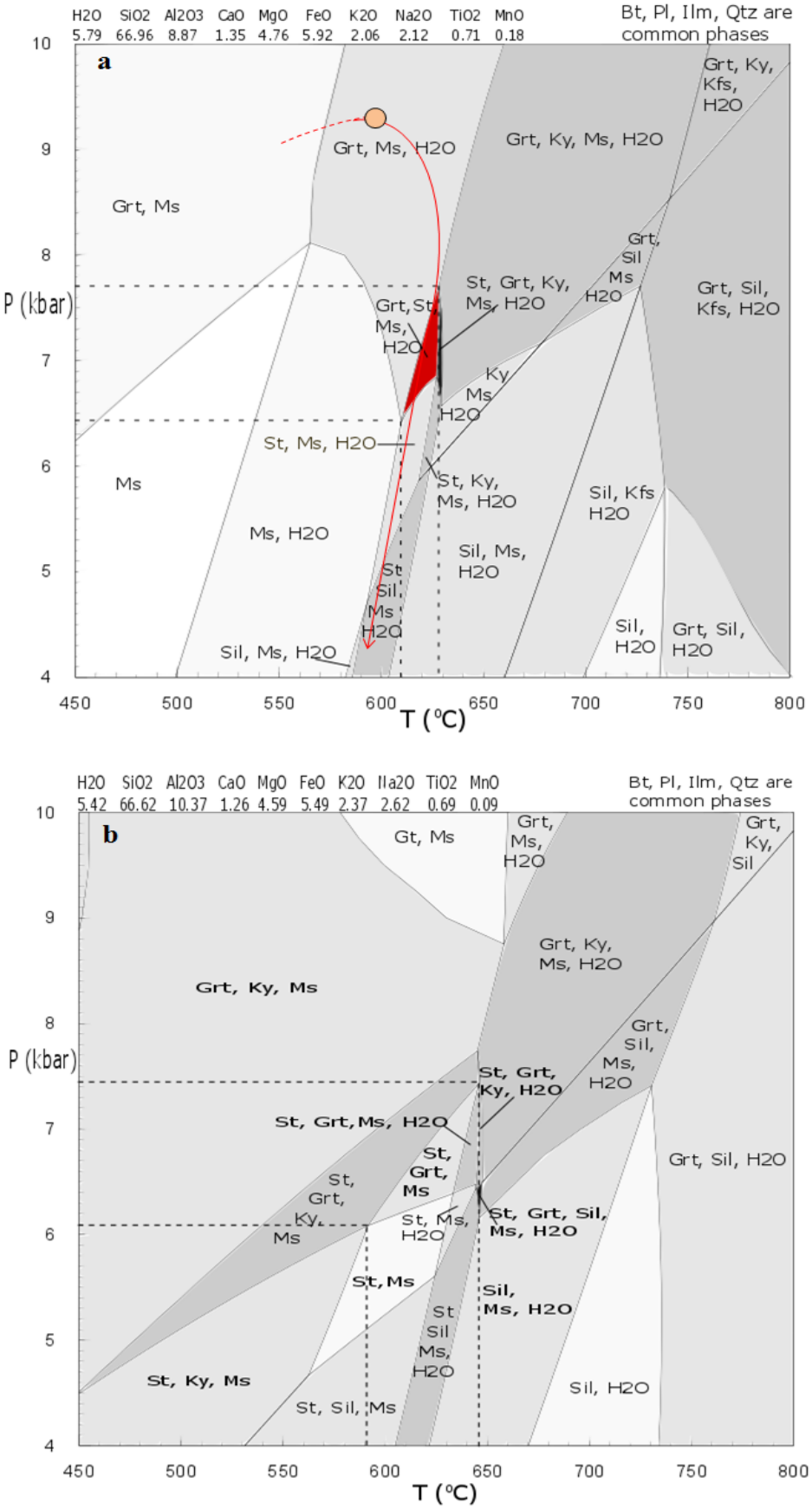

Fig. 3-6 (a) Pseudo-section plot of sample K10a in MnNCKFMASHT system, showing the peak *P–T* condition (the red color field) which is the stability field of the stable mineral phases in our rock sample. Other fields are in different tones of grey. The lightest grey fields are fields where only one uncommon mineral phase is stable while the darkest color depicts field where five uncommon mineral phases are stable, other fields are variations between these two ends. Mineral abbreviations are as suggested by Kretz (1983).

(b) Pseudo-section plot of sample K10b using the same method as for (a).

The total error of the GBMP barometer is estimated to be about ±1.2 kbar on considering input temperature error and analytical errors of chemical compositions of the phases involved. The random error of the GBMP barometer is evenly distributed with respect to pressure, temperature and mineral composition. For the schist samples, the GBMP barometer gave the following results; sample K1 = 6.41±1.2 kbar, sample K10a = 5.29±1.2 kbar, sample K17 = 3.18±1.2 kbar. Other samples lacked the EPMA analysis of one or more of the four minerals - mostly muscovite (see Table 3-5).

3.5.3 Optimal thermobarometry

Optimal thermobarometry or "Average *P-T (avPT)"* calculation for sample K10a was carried out using the method of Powell and Holland (1994). This three-stage process begins with the raw data generated from EPMA analysis of minerals which is fed into software called the AX-program (an activity-composition calculation program) of the same authors. The AX-program recalculates the analysis to a mineral formula and then determines the activities of mineral end-members. These end-members activities of the minerals are now applied to the *avPT* script files (RP13 and RP13ax) and run by THERMOCALC to generate the average *P-T* of the rock. THERMOCALC does this by combining the information for the several independent reactions in a least squares sense to calculate the conditions of formation. The equations for the independent sets of reactions and their corresponding calculations are presented in Table 3-6. Optimal *P-T* result as calculated for sample K10a, however, gave a condition of 9.3 kbar and 597 °C.

3.5.4 Hornblende-plagioclase geothermometer

Hornblende-plagioclase geothermometer as put forward by Holland and Blundy (1994) was applied in the calculation of the peak temperatures of the metabasites (samples K12 and K16) which contained assemblages including associated hornblende and plagioclase. This calculation is based on the reaction edenite + albite = richterite + anorthite – a quartz independent thermometry at 7 kbar. This quartz independent thermometry was chosen because it is more reliable at medium to high temperatures and because plagioclase in the rock samples have appreciable anorthite contents ($An_{34.0\text{-}43.1}$). The calculated results gave the temperatures of the metabasites as 665-695 °C (sample K12) and 650-700 °C (sample K16) at 7 kbar. A summary of the calculated temperatures and pressures are presented in Table 3-5 and a

corresponding *P-T* graph is used to show a pictorial representation of the *P-T* distribution for the rocks of the study area (see Fig. 3-7).

3.5.5 Mineral equilibria modeling

The peak *P–T* condition of the rocks was constrained in pseudo-section using THERMOCALC version 3.33, with the October 2009 updated version of the Holland and Powell (1998) data set (file tcds55.txt). Based on the mineral assemblages and compositions obtained in this study, a model system MnO–Na_2O–CaO–K_2O–FeO–MgO–Al_2O_3–SiO_2–H_2O–TiO_2 (MnNCKFMASHT) was selected to calculate the pseudo-section (see Figs. 3-6a and b). Fe_2O_3 was not considered because magnetite and hematite are not observed in the examined samples, suggesting that peak metamorphism was relatively in reduced condition. The pseudo-section analyses have been done for pelitic schist samples K10a (staurolite-garnet-biotite schist) and K10b (garnet-biotite schist). They were collected from the same locality within a distance of 5-10m but sample K10b is now classed as garnet-biotite schist member because it lacks staurolite in its mode. AFM diagram was also employed for sample K10a to confirm stability of the measured mineral species. The AFM diagram contains plots of all samples and the garnet-biotite pairs of the different samples show consistent tie-line behavior which confirms similar distribution coefficients implying both complete equilibration of the sample set and that the garnet-biotite solid solutions are suitable for the samples (see Fig. 3-8).

The petrographical observations discussed earlier indicate that the peak assemblage for sample K10a is garnet + biotite + staurolite + muscovite + plagioclase + quartz + ilmenite. The bulk composition in molar percentages of the oxides in the sample is SiO_2 = 67.84, TiO_2 = 0.72, Al_2O_3 = 8.98, CaO =1.37, MgO = 4.82, FeO = 5.99, K_2O = 2.08, Na_2O = 2.15, MnO = 0.19, H_2O = 5.87 (H_2O is obtained from LOI for pseudo-section modeling). Water was obtained from LOI after applying different degrees of water content (from excess water to low water) to the calculation methods of both THERMOCALC and THERIAK-DOMINO software but could not get a *P-T* space for the mineral assemblage. The calculated equilibrium phase diagram displays the stability field for the assemblage at 610-630 °C /6.4 - 7.7 kbar (Fig. 3-6a), which compares approximately to the peak metamorphic conditions (570-610 °C/7 kbar) of the sample as obtained from garnet-biotite geothermometry.

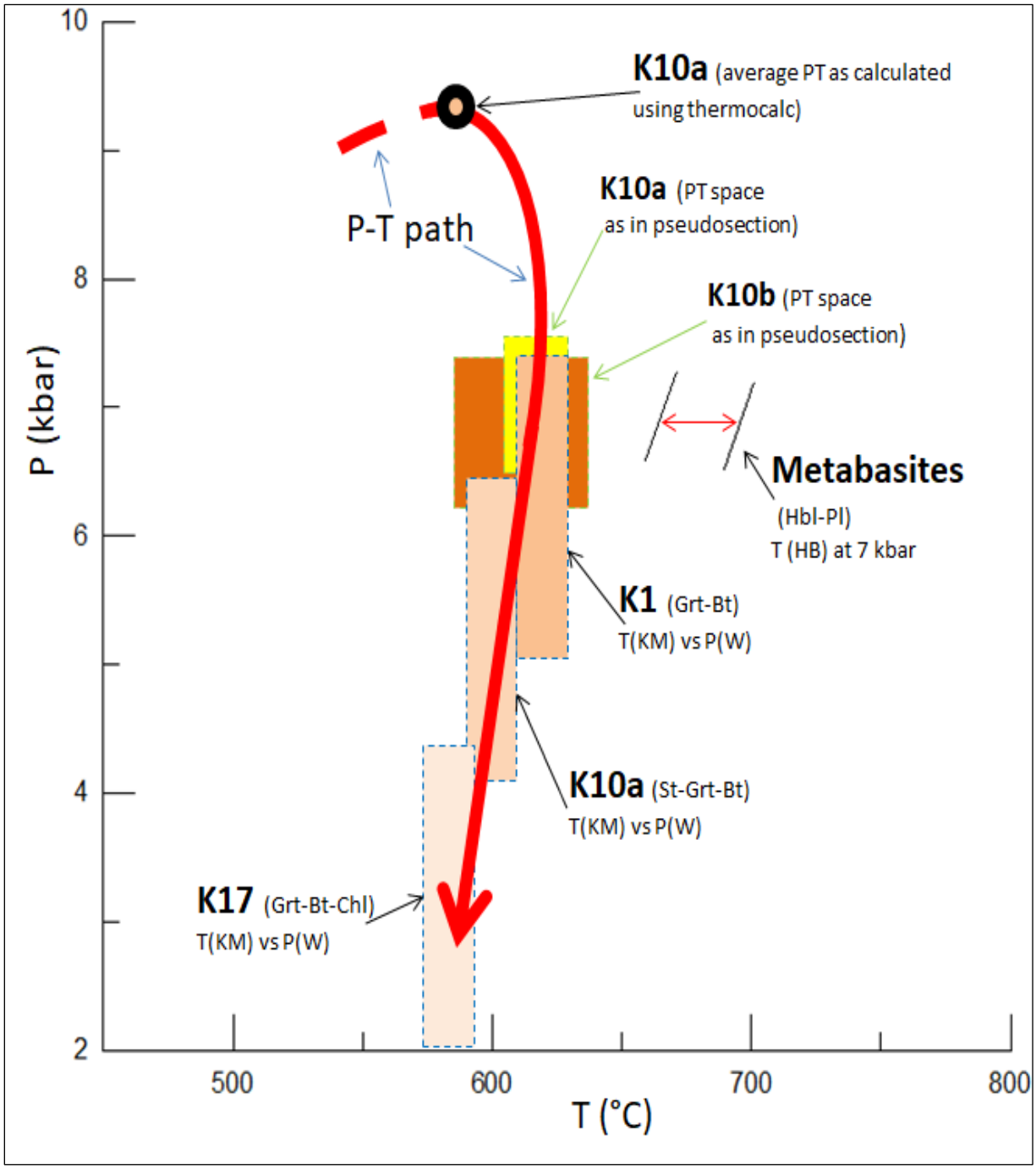

Fig. 3-7 *P-T* diagram displaying the calculated *P-T* conditions of different samples of schist in the study area and the inferred *P-T* path. Insets (in dashed green boundaries) are the pseudo-section *P-T* spaces of samples K10a and K10b for comparison with the calculated results (dashed-blue boundries). Where P (W): garnet-biotite-muscovite-plagioclase barometry of Wu (2015), T (KM): garnet-biotite thermometry of Kaneko and Miyano (2004), T (HB): hornblende-biotite thermometry of Holland and Blundy (1994). The red line (dashed and continuous) represents the inferred *P-T* path.

The major difference between samples K10a and K10b is that sample K10a shows modal staurolite with very subordinate secondary chlorite, while sample K10b shows no modal staurolite but appreciable secondary chlorite. For sample K10b, the peak assemblage is quartz + biotite + garnet + plagioclase + muscovite + ilmenite. The bulk composition in molar percentages of the oxides in the sample is SiO_2 = 66.92, TiO_2 = 0.69, Al_2O_3 = 10.47, CaO =1.26, MgO = 4.59, FeO = 5.49, K_2O = 2.37, Na_2O = 2.62, MnO = 0.09, H_2O = 5.42. The calculated equilibrium phase diagram

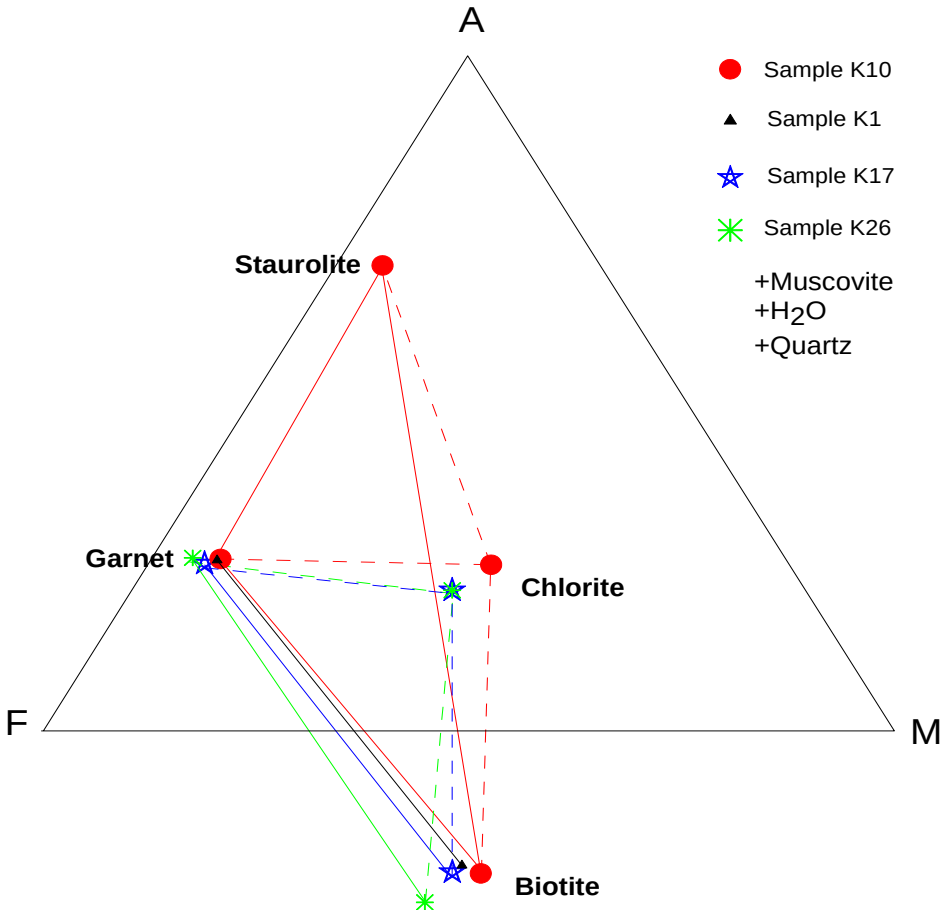

Fig. 3-8 AFM diagram of sample K10a as projected from muscovite, H_2O and quartz confirming stability of measured minerals.

displays a broader and more complex stability field than sample K10a, spanning the temperature range of 590-650 °C at 6.1-7.5 kbar with the water line passing up through the field at 630 ºC separating the field into water-absent (590-650 ºC/6.1-7.5 kbar) and water containing (630-650 ºC/6.4-7.5 kbar) fields (see Fig. 3-6b). It is important to state here that even though chlorite

appears in sample K10b as secondary, it is not stable on any part of the *P-T* space, which may suggest that staurolite was present in the immediate past as part of the peak assemblage for this sample but was only used up in a retrograde reaction while secondary chlorite grew in the sample. At 630-650 °C /6.4 - 7.5 kbar, sample K10b has the same stable phases as sample K10a though at slightly increased temperature. Other samples were not prepared for pseudo-sections because some occurred near sample K10 and most importantly that they did not contain the garnet-biotite-staurolite association or other higher metamorphic grade associations which we needed to constrain the maximum *P-T* of the rocks.

3.6 Discussion

This is the first detailed report of petrology, mineral chemistry, geothermobarometry, and mineral equilibria modeling on pelitic schists and amphibolites from the Keffi area which until now is geographically regarded as part of the Western Nigerian Schist Belt. The study area is underlain by extensive, moderately deformed pelitic schist bounded on four sides by gneisses and granitoid rocks. The examined samples contain peak mineral assemblages common in amphibolite-facies metamorphic terranes. Application of conventional garnet-biotite geothermometers based on garnet-biotite geothermometry of Kaneko and Miyano (2004), which considers the effect of Fe^{3+} and Al^{3+} contents in biotite, gave peak metamorphic conditions of 590 °C to 625 °C at 7 kbar from staurolite-garnet-biotite schist sample K10a. This result compares closely with the *P–T* range of 610-630 °C/6.4-7.7 kbar obtained by mineral equilibrium modeling of the same sample using pseudo-section. Sample K10b (garnet-biotite schist) shows a wider spread for what is considered the stability field (a *P–T* range of 590-650 °C/ 6.1-7.5 kbar). However, since staurolite is not found in the mode of sample K10b, the peak *P–T* conditions of the pelitic schist is therefore inferred to be 610-630 °C/6.4-7.7 kbar as obtained in sample K10a. Consistent garnet-biotite temperatures within the range of 590-630°C at 7 kbar were calculated for other pelitic samples K1, K17 and K26. Hornblende-plagioclase geothermometry of metabasites (samples K12 and K16), however, gave a slightly higher temperature range of 645-700 °C at 7 kbar.

From the optimal *P-T* analysis, it is noted that out of the nine independent sets of reactions constrained and considered by the calculation process, four reactions occurred between 7-8 kbars, another four reactions occurred between 9-10 kbars but one reaction (the chlorite forming reaction) occurs at 2 kbar. These findings help to confirm not only that the chlorite

crystals found in the mode of the rock are secondary and retrograde as reported in the petrography, but also that the *P-T* path passed up through 7 kbar, peaked in pressure above 9 kbar, returned through 7 kbar and ended below 2 kbar (see Table 3-6).

The possible *P-T* path, however, can be deciphered from the mineral inclusions in garnet through the inclusions in staurolite to the observed stable mineral assemblages. The mineral inclusions in garnet (quartz, biotite, muscovite and ilmenite) represents the original rock composition at the upper greenschist facies which most probably included plagioclase. The pseudo-section shows that at such lower temperatures, garnet cannot be a stable mineral because it is only stable at higher pressures (>8 kbar). Thus, the growth of garnet must have started at about 8 kbar. This is consistent with the result of the average *P-T* calculations (597 ºC /9.3 kbar) as obtained using THERMOCALC software which also gave the *P-T* values of individual garnet forming reactions between 7.1-9.3 kbar/597 ºC. The inclusions in staurolite include all the inclusions that are in garnet plus garnet itself and plagioclase. This confirms firstly that plagioclase was in the prograde assemblage and secondly that staurolite formed after garnet. But staurolite stands at lower pressure relative to garnet. The *P-T* window where both garnet and staurolite coexist for sample K10a is at higher temperature but lower pressure as constrained in the pseudo-section (610-630 ºC/6.4-7.7 kbar). The combination of GBMP barometer of Wu (2015) and garnet-biotite thermometer of Kaneko and Miyano (2004) gave final *P-T* values of 610-611 ºC/5.3±1.2 kbar for sample K10a, 622-627 ºC/6.4±1.2 kbar for sample K1 and 593-597 ºC/3.2 kbar for sample K17. These analyses when connected show a clockwise *P-T* path for the rocks of the study area (see Fig. 3-8).

The inferred peak *P–T* conditions of Keffi Schist Belt (610-630 °C and 6.4-7.7 kbar) are nearly consistent with those obtained from adjacent regions. Previous petrological studies of the western Nigerian Schist Belt (WNSB) and schist occurrences in the eastern Nigerian basement and their environs mostly lacked detailed petrography and mineral chemistry. Most studies have constrained low to intermediate semi-quantitative *P-T* conditions based on mineral assemblages. The Zuru, Karaukarau and Wonaka Schist Belts (in northwestern Nigeria) and the Ilesha Schist Belt (in southwestern Nigeria) were reported to have attained the greenschist-facies metamorphism (Turner 1983). However, Zeh and Holness (2003) specifically constrained the *P–T* conditions of 590±20 °C at 5±0.5 kbar for the Ilesha Schist Belt. Ige et al. (1998) constrained a

temperature range of 570-625 °C from the metamorphosed mafic-ultramafic complex of Mokuro and llesha Schist Belts in the southwestern Nigeria.

The mineral assemblage, including muscovite + garnet + quartz + chlorite + biotite + epidote + tourmaline which was reported for the Maru Schist Belt in northwestern Nigeria by Aliyu (2012) corresponds to the epidote-amphibolite facies. Perhaps the Schist Belt which is most similar lithologically (see introduction) and mineralogically to the Schist Belt under study (Keffi Schist Belt) is the Zungeru-Birnin-Gwari Schist Belt in northwestern Nigeria. Muscovite + biotite + garnet + staurolite association, which corresponds to the middle-amphibolite facies, was reported for this Schist Belt by Elueze (1981) as is found for the rocks under study. The addition of sillimanite to the assemblage above in Iseyin-Oyan River Schist Belt in the southwestern Nigeria was reported by Rahaman (1976b).

In the eastern Nigerian to the Cameroon basement, however, higher pressure assemblages are recorded in the schistose rocks. Ephraim et al. (2008) reported a *P*–*T* condition of 600-650 °C and ~8 kbar for the migmatitic schists of the eastern Nigeria, while Yonta-Ngoune et al. (2010) reported a metamorphic peak of ~650 °C at 9.5 kbar for the Boumnyebel talc-schists of Cameroon in the Pan-African Belt of Central-Africa. The Poli Schist Belt in Cameroon was reported to show amphibolite-facies at the base and greenschist-facies at the top (Turner 1983).

Strictly, in consideration of all the results of this research, especially the optimal *P*-*T* results, it will be untrue to say that our findings are far from the *P*-*T* signatures of the eastern Nigerian to the Cameroon basement. As a matter of fact, the results of this study are more reminiscent of the signatures of the eastern than of the western Nigerian metamorphic basement. It is hard, however, not to feel at this point the need for more data especially from the western Nigerian basement in this regard to be able to make a good conclusion regarding the terrane affiliation of the study area. So far, however, the grades of the metamorphic *P*-*T* conditions presented can be simplified as WNSB < study area ≤ ENSB.

Variations in metamorphic style have been recorded along the northern margin of the Damara Orogen, Namibia, by Goscombe et al. (2003). Evidences are therefore rife for the variations in metamorphic response to tectonism regionally as found within Trans-Saharan, Central-African and Western-south African orogens (Rahaman 1976b; Elueze 1981; Turner 1983; Zeh and Holness 2003; Goscombe et al. 2003; Ephraim et al. 2008; Yonta-Ngoune et al. 2010; Aliyu 2012). Such variations are here observed even within a single rock unit (samples

K10a and b) and down to single hand specimen (sample K26) as found in the study area. According to Dada (2008), "variations in the metamorphic imprints on the rocks of the Nigeria – Boborema province are observed in the mineral assemblages associated with penetrative fabrics in the older rock units and, to a lesser extent in the granitoids, and reflect the heterogeneity of the metamorphism".

From the structural analysis and field evidence (see Fig. 3-2), rocks of the study area are compressed into a parallel NNE-SSW alignment with many anticlines and synclines defining the lithostratigraphic arrangement in which a larger number of the axial planes aligned in the NNE-SSW direction. This confirms that a WNW-ESE compressive regime was important in the overall metamorphism of the rocks leading to crustal shortening. But the low-medium pressure constrained for these rocks of this study (6.4-7.7 kbar from pseudo-section and 9.3 kbar from optimal *P-T*) is not suggestive of frontline or accretionary wedge tectonic setting but rather of moderate depth of about 21-34 km (perhaps the base of accretional sediments) far removed from the accretionary wedge. The medium and sustained temperature range of about 610-630 °C when divided by average depth of 27.5 km gives a geothermal gradient of about 23°C/km. This plus other factors including; simple linear structural style and geochemistry of the intruding batholiths (calc-alkaline) (Umeji and Caen-Vachette 1991), absence of rock types such as greenstones, ophiolites, meta-pelagic sediments including meta-cherts and metacarbonates are all supportive of withdrawal from wedge setting or frontline accretionary margin. Even the preservation of simple, uniform foliation directions resembling bedding planes is not the characteristic of rocks that have undergone high pressure experiences of the accretionary wedge setting but are rather typical of magmatic-arc to near back-arc settings (Cawood et al. 2009). However, within the study area and its surroundings, there are granitic intrusions (the Gudi batholith) on the eastern portion of the study area (see Fig. 3-2) and the Nassarawa-Eggon granite which is about 15-20 km east of the study area. These granitic intrusions are late Precambrian, calc-alkaline granites (Umeji and Caen-Vachette 1991). Calc-alkaline granites are not characteristics of a back-arc setting but rather of a magmatic arc.

Ferré et al. (2002) suggests that the transpressive tectonics and terrane accretion model proposed by Black et al. (1994) for Hoggar in North Africa may also apply to Nigeria while Turner (1983) on the other hand suggested that the younger Nigerian Schist Belts are due to back-arc extension related to subduction associated with that accretion. The results of this work

however differ from both theories, supporting neither an accretionary wedge nor a back-arc setting but rather a magmatic arc setting for the study area. From this study, therefore, the positioning of the study area within the magmatic arc setting is implied, and expectations are that a continued research into the geology of Nigeria will increase our understanding of tectonic processes and crustal evolution of the Trans-Saharan Orogenic Belt.

3.7 Conclusions

The peak metamorphic conditions attained by the Keffi Schist Belt in north-central Nigeria during the Pan-African tectonic episode, did not exceed middle-amphibolites facies and the magnitude of this metamorphic grade determined by empirical calculations and pseudo-sections combined is a *P–T* range of 610-630 °C/6.4-7.7 kbar. This range of values is higher than all the values of metamorphism obtained so far for the rocks of the WNSB. The study area presents evidence for slight variations of metamorphic response to tectonism as seen in various samples from different parts of the Keffi Schist Belt and even to the outcrop and hand specimen units. It is therefore important to bear in mind this (most times intricate) heterogeneity in the character of a tectono-metamorphic terrane so that an average value or a range of values seems more appropriate in describing the metamorphic signatures of any tectono-metamorphic terrane. The *P-T* path as observed in this study is a clockwise path that is consistent with a scenario of considerable crustal thickening. A sequence of burial of supra-crustal rocks to depths of about 32-34 km accompanied by temperature of about 597 ºC, followed by exhumation to 20-25 km with simultaneous increase in temperature to 610-645 ºC would have been the trend before final surfacing of the metamorphosed rocks. The calculated *P-T* conditions and other litho-tectonic evidences all confirm a magmatic arc tectonic setting (not back-arc) for this part of the Nigerian Basement, and many such areas within the Trans-Saharan belt at large. With regards to the terrane affiliation of the study area, the results of this research are at best inconclusive yet, but by these results also the inclination is to class Keffi and its environs as part and parcel of the Eastern Nigerian basement.

Chapter 4: Metamorphic *P-T* evolution of medium-pressure pelitic granulites of Obudu area, Southeastern Nigeria: geothermobarometry and mineral equilibrium modeling

4.1 Introduction

Trans-Saharan Orogenic Belt was part of a large sedimentary basin which received detritus during the breakage of the Rodinia supercontinent at the early Pan-African and later became part of Gondwana hinterland after the amalgamation at late Pan-African. Studies by different researchers (Rahaman 1976b; Elueze 1981; Turner 1983; Zeh and Holness 2003; Goscombe et al. 2003; Ephraim et al. 2008; Yonta-Ngoune et al. 2010; Aliyu 2012) have shown variations in metamorphic response to the orogenesis on the same units of rocks recorded as different *P-T* values, different mineralogical and textural signatures constrained in different parts of the orogenic belt especially within the Benin-Nigeria Shield areas. Black (1978) developed the concept of amalgamation of micro-continents and Cordani et al. (2013) has suggested the trapping of several accretionary complexes and possible micro-continents within the orogenic belt during the ocean closures. Landsat imagery and aerial photography have also suggested the occurrence of north-south running suture zones through the length of the orogenic belt including the Benin-Nigerian Shield areas.

The need to fully understand the geological, mineralogical and tectono-metamorphic characteristics of the different parts of the Trans-Saharan Orogenic Belt and be able to discuss accurately, the Rodinia-Gondwana transition story drives the quest for this research. A sustained regional study on the characterization of the minerals paragenesis and metamorphic *P-T* responses (particularly of the metasediments) to Pan-African orogeny of the different parts of the Trans-Saharan Orogenic Belt within the Benin-Nigerian Shield is the way to begin to proffer solutions to these problems. Since the foliations, lineations and Landsat-delineated suture zones of the Trans-Sahara are dominantly N-S to NNE-SSW in orientation, an W-W cross-sectional approach within latitudes 07°00’N and 09°10’N in the Benin-Nigerian Shield areas is chosen for the start. Within this chosen region, four case-study localities lying within longitudes 005°40’E and 009°10’E have been identified for more detailed sampling in an on-going research. In the on-going study, Keffi and environs in north-central Nigerian basement (Lat. 08°30’N - 09°07’N and Long. 007°37’E - 008°18’E) have been characterized as a subduction-influenced magmatic-arc

tectonic setting with a clockwise *P-T* path which reveals a metamorphic history that was initially dominated by heightened pressure at low temperature and peaked at medium temperature and pressure (610-630°C and 6.4-7.7 kbar).

In this chapter, attention is focused on the metamorphic suite of Obudu area in the south-eastern flank of the Nigerian basement (see Fig. 3-1) especially the metasediments with a view to characterizing the minerals paragenesis, the tectono-metamorphic signatures and *P-T* path. The study area was chosen firstly because it is an area that has received little to no previous detailed research attention and secondly because of its position not only at the center of south-eastern Nigerian basement but also the eastern margin of the Benin-Nigerian Shield and the border between the Trans-Saharan and Central-African Orogenic Belts. This is the first attempt to study the granulite-facies metamorphic evolution of south-eastern Nigerian metasediments using mineral equilibrium modeling in a complex system Na_2O–CaO–K_2O–FeO–Fe_2O_3–MgO–Al_2O_3–SiO_2–H_2O–TiO_2 (NCKFMASHTO) with THERMOCALC 3.33 (Powell and Holland, 1988). New mineralogical and petrological data of the metamorphic suite of Obudu areas are presented and discussion is made of the evidences of granulite-facies metamorphism and *P-T* path. The result of this research will go a long way to expose the special characteristics which are peculiar to the easternmost parts of the Benin-Nigerian Shield, embolden the investigation of the limits of the Pan-African orogeny and the variations in metamorphic response to orogenesis.

4.2 Description of lithologic characteristics

In the study area (see Fig. 4-1), migmatites are the host rocks and they were intruded by very large volumes of granitic magma now referred to as the granite gneiss unit which was further intruded by smaller volumes of dioritic and ultramafic magmas. The granite gneiss is emplaced concordantly to the foliation direction of the migmatites while the meta-dioritic and meta-ultramafic units are discordantly placed. The granite gneiss is much more metamorphosed relative to the now meta-dioritic and the meta-ultramafic rocks as evidenced by the much weaker to absent foliations of the later (see Figs. 4-2a, b, c, d, e and f).

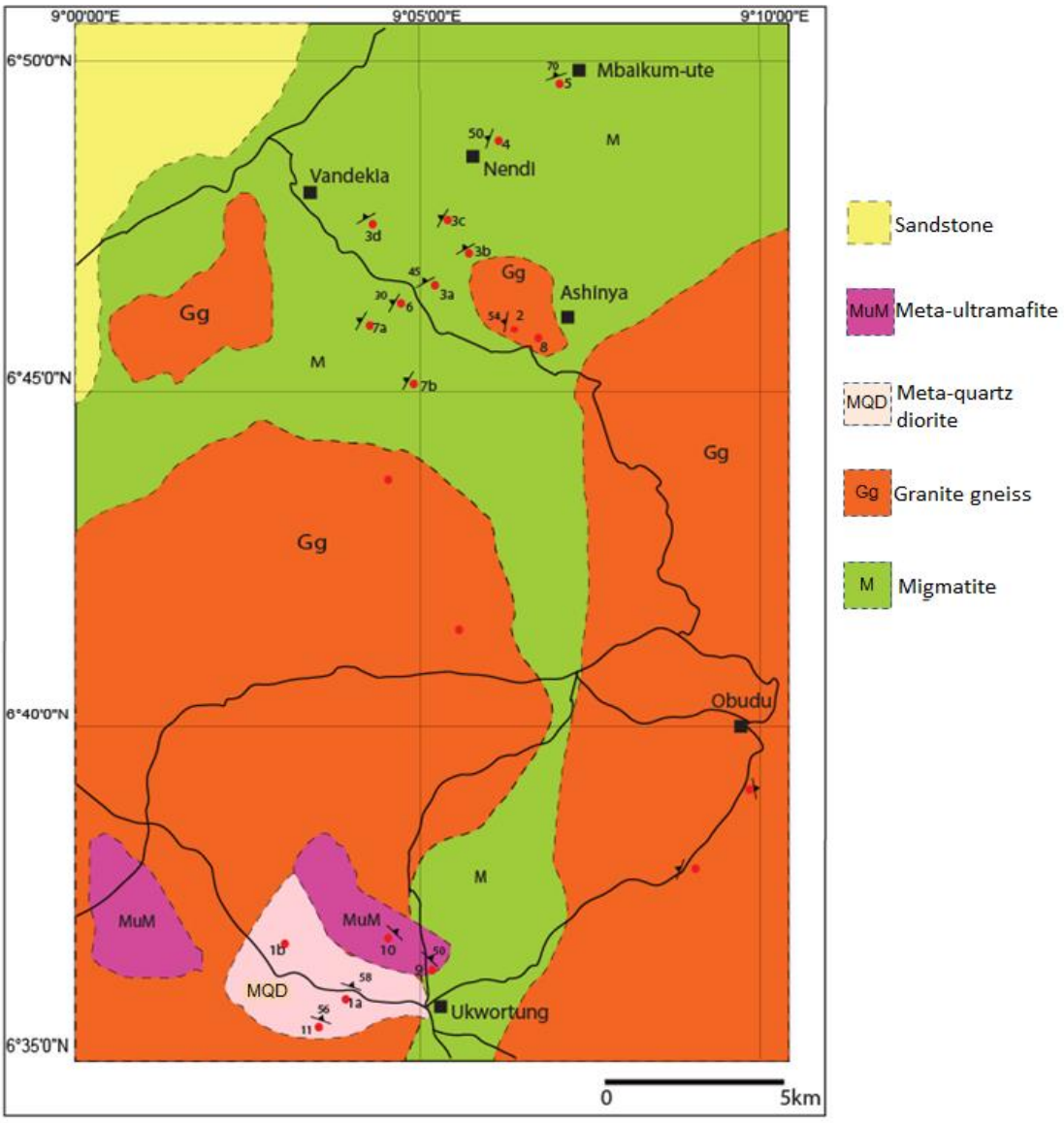

Fig. 4-1. The geological map of the study area (Obudu west) as modified from Malomo (2008).

The structural arrangement of rocks and foliations are dominantly N-S in orientation as indicated by the trend of the granite gneiss which is the most dominant rock unit in the study area and by the trend of foliation of both the granite gneiss and the migmatite schist host rock. This structure is of regional significance as it concurs with the general trend of foliations and lineations of the Trans-Saharan Orogenic Belt. Two minor lithologies (meta-quartz diorite and amphibolite) in sharp contact with each other, trend orthogonally to that of the two dominant lithologies and occur at the southern end of the study area.

The migmatite schist (host rock) is obviously less resistant to erosion. It underlies the low-lands and valleys in the southern part where it meanders between large bodies of the

dominant and more resistant granite gneiss. It, however, spreads out to dominate the northern region where the granite intrusive only occasionally occurs. The foliations on the migmatite schist unit tend to change directions closer to the granite gneiss bodies. However, the unit gradually grades into a more resistant migmatitic gneiss at Nendi village in the north as observed in a pit where it is quarried for construction works. Migmatites are the second most dominant rocks in the study area. At locations 3a, 3b, 3c, 3d, 6, 7a and 7b (Vandekya village) (see Fig. 4-1), the rock is mesocratic, coarse-grained with lit-per-lit injections of quartzo-feldspathic materials. The rock also reveals micro-folding of foliations and the boudinaging of quartzo-feldspathic materials. The rock is migmatitic but with a high percentage of biotite and coarse garnet forming the dark colored bands separated by leucocratic quartzo-feldspathic injections. The strike of the foliation is; NNE/SSW to ENE/WSW. Dip direction is westward and dip amount is 30-50º. At locations 4 and 5 (Nendi and Mbaikum villages (north to north-east of Vandekya village)), however, the foliation of the migmatite becomes more strongly aligned with higher values of dips (50-70º). The rock is more banded with greater levels of migmatization and the presence of prominent blocks and globes of pre-tectonic mafic intrusives. These mafic intrusives are melanocratic and dominantly biotitic. Typical exposures of the rock are found in a quarry site at Nendi village (see Figs. 4-2b-d).

Granite gneiss outcrops are hilly exposures showing a mesocratic coarse-grained rock with alignment of minerals in a preferred direction and relicts of older materials (paleosome) with irregular folding of foliation trends. At Ashinya village, the height of the hill is about 300m with length of about 400m in the NNE/SSW direction. The strike of the foliation is N/S to NNE/SSW. The dip direction is WNW and dip amount is 54º (see Fig. 4-2a). The mineralogy is dominated by quartz and subordinate feldspar interlaced with tiny specks of biotite that occasionally coagulate to define the foliation. Some portions of the rock show domains of higher biotite content defining wavy local foliation which may be concordant or discordant to the general foliation trend.

Meta-quartz diorite occurs within Ukwortung village and was encountered at locations 1a, 1b and 11. It is medium to coarse grained and shows weak foliation. The rock is bluish grey in color as defined by a mixture of diffused grey-black background color of mafic minerals slightly overshadowed by more dominant light greenish feldspar and colorless quartz matrix. The strike of the foliation is ESE/WNW with a dip direction of ENE and dip amount of about 58º

(see Fig. 4-2e). The foliation direction is almost orthogonal to the foliations on the granite gneiss unit which it intrudes.

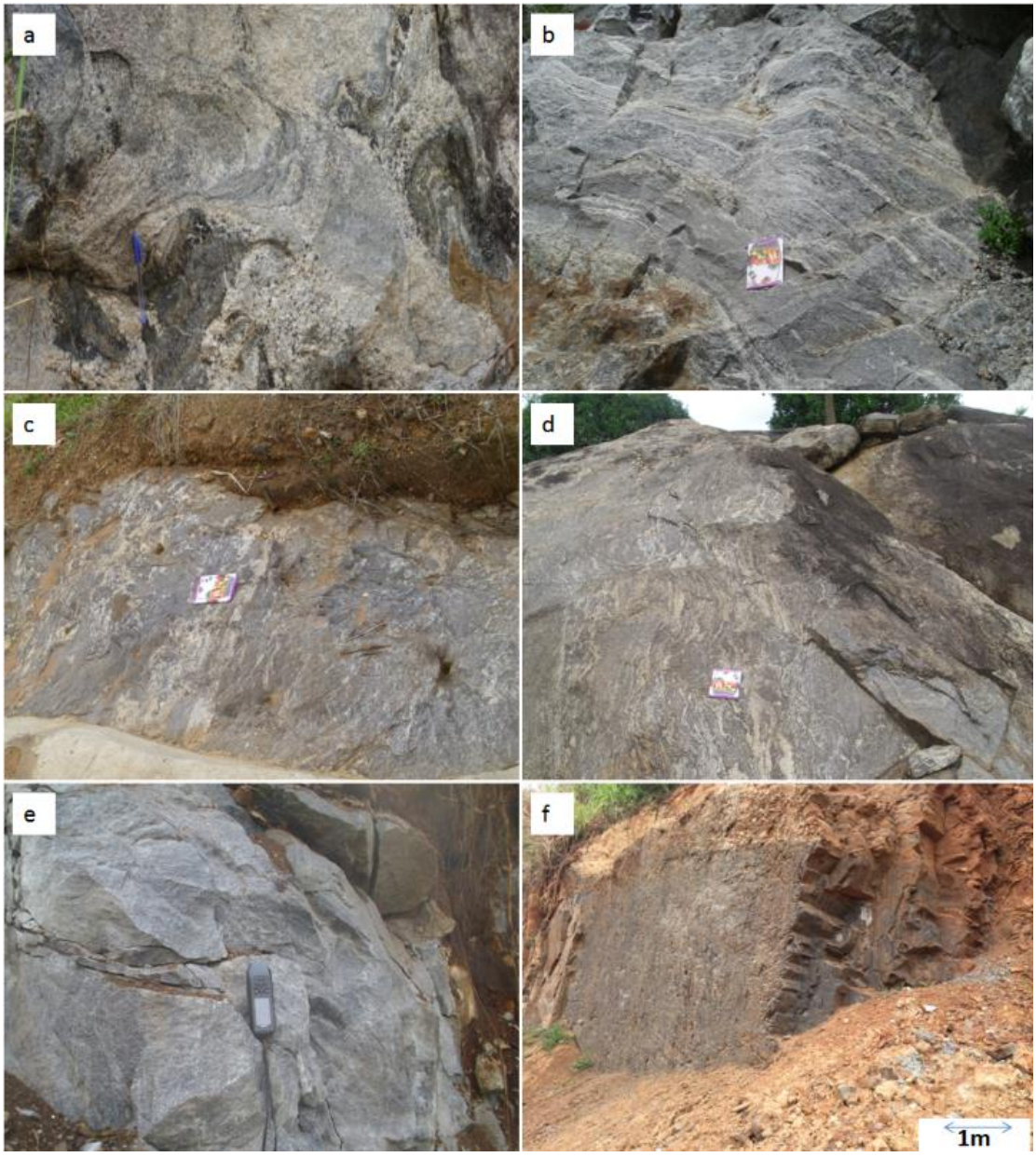

Fig. 4-2. Field photographs of representative samples discussed in this study. (a) Exposure of the gneissic granite unit at Ashinya village (sample 2). (b) The migmatite exposure in a quarry pit in Nendi village (sample 4). (c and d) A road side exposure of the migmatite at Vandeikya village (samples 3 and 6). (e) Exposure of the gneissic quartz diorite unit at a quarry pit in Ukwurtong village (sample 1). (f) Exposure of the metabasite unit in a dimension stone quarry site at Ogoja road, Ukwurtong village (sample 10).

Amphibolite also occurs in Ukwortung village and sampled at locations 9 and 10. The rock is melanocratic and coarse grained. At location 9, the rock shows strong alignment of minerals in a preferred direction. The minerals are lepidoblastic and bladed with their long axes in the direction of foliation. At location 10, however, the minerals are rather nematoblastic and less foliated. Typical characteristics are shown in a quarry site where the rock is cut into slabs for polishing (see Fig. 4-2f).

4.3 Petrography

The major focus of petrographic analysis is on the metasedimentary unit while other rock units were analyzed for supportive data. In view of this, fresh samples of all rock units were collected mostly from quarry pits. This ensured that there are no alterations by percolating meteoritic waters as observed in all thin sections (see Figs. 4-3a-i). Minerals abbreviations (Bt = biotite, Grt = garnet, Qz = quartz, Kfs = K-feldspar, Pl = plagioclase, Crd = cordierite, Sil = sillimanite, Hbl = hornblende, Rt = rutile, Ol = olivine, Spl = spinel, Ilm = ilmenite, Opx = orthopyroxene, Cpx = clinopyroxene) are after Whitney and Evans (2010).

4.3.1 Garnet-sillimanite-biotite (migmatitic) schist (samples 3a and 6)

This sample is coarse-grained and mesocratic with strong alignment of minerals in a preferred direction. The mineral constituents include biotite, garnet, plagioclase, sillimanite, cordierite and quartz (see Table 4-1). Cordierite belongs to the equilibrium assemblages of the rock occurring as coronae around garnet and in symplectites with biotite and spinel. The microstructures and texture are very interesting in this unit with the occurrence of two stages of inclusions; i.e. inclusions of mainly K-feldspar, quartz and sillimanite within plagioclase inclusions in garnet (see Figs. 4-3(a – h)) plus the abundance of mainly quartz-cordierite and quartz-biotite symplectites around garnets. Plagioclase, sillimanite and rutile occur both as inclusions in garnet and in the matrix while most garnet porphyroblasts have cordierite coronae around them (see Fig. 4-3d). Most of the coronae around garnets have varied thicknesses with pure cordierite at the immediate rim of the garnets. This cordierite ring is sometimes truncated by quartz and plagioclase, while behind the cordierite rings, varied thicknesses of a mixture of microcrystalline biotite, sillimanite, plagioclase, quartz and cordierite occur.

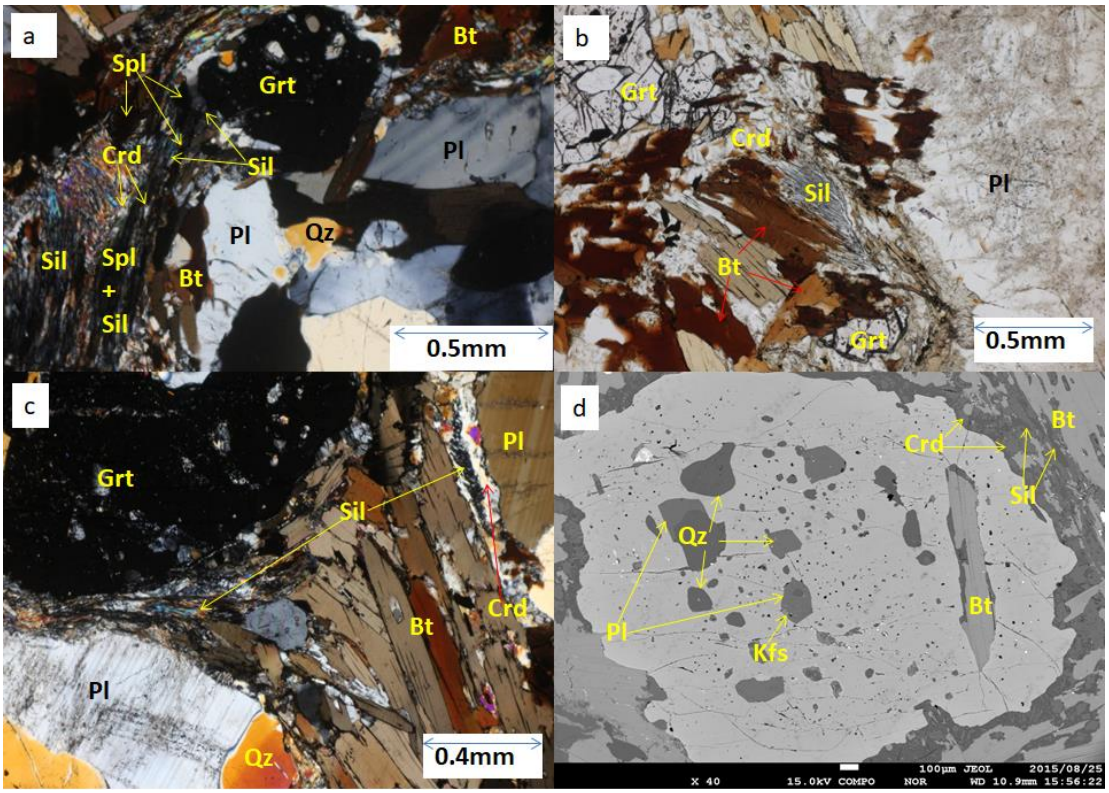

Fig. 4-3 Photomicrographs showing textures of samples discussed in this study. (a) Garnet porphyroblast in sample 3a is shown with inclusions of quartz in plagioclase and biotite (XPL). (b) The peak assemblage of garnet-biotite-sillimanite-quartz-cordierite-plagioclase in sample 3a (PPL). (c) The peak assemblage of garnet-biotite-sillimanite-quartz-cordierite-plagioclase in sample 6 (XPL). (d) BSE image garnet porphyroblast in sample 7a with inclusions of the prograde assemblage of (quartz, biotite, plagioclase, orthoclase) and peak assemblage of cordierite, sillimanite and biotite.

Such new biotites or quartz-biotite or quartz-cordierite symplectites could form at the expense of garnet (with or without K-feldspar) (at high *T* and low *P*) according to the following reaction (4-1) (e.g. Brown 1998)

Grt + Ilm ± Kfs + melt = Bt + Crd + Qz …….. (4-1).

Biotite of the less brownish color and more euhedral shapes (which may be regarded as the younger generation), where they have contact with plagioclase, are separated from the latter by bands of cordierite measuring about 0.2 mm thick and running along the entire biotite-plagioclase boundaries (see Figs. 4-3b and c). The biotites measure between 0.1×0.25 mm to about 0.25×1.8 mm. They make up about 35% of the rock.

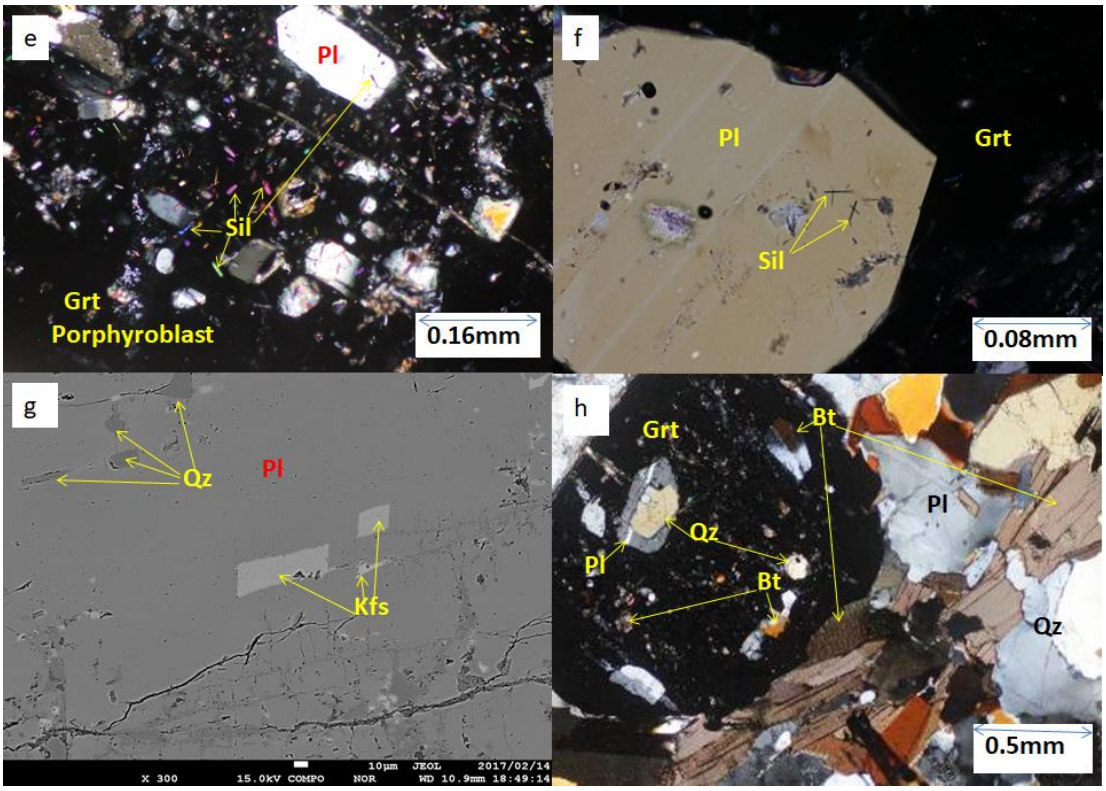

Fig. 4-3(e) and (f) Higher magnifications reveal that sillimanite is also part of the prograde assemblage preserved as inclusions in garnets of samples 3a, 6 and 7a. (g) BSE image of plagioclase porphyroblast showing inclusions of orthoclase and quartz as part of the prograde assemblage in sample 7a. (h) Rutile-plagioclase-quartz-biotite inclusions in garnet (sample 6) (XPL).

Plagioclase, with grey to white interference color has been affected by alteration. Their sizes range between 0.25×0.5 mm to as large as 1.5×1.5 mm and they make up about 15% of the rock. Some large plagioclase porphyroblasts contain inclusions of quartz and orthoclase. Plagioclase inclusions in garnet and within the cordierite-biotite-quartz-plagioclase-sillimanite coronae have anorthite content of 38.8–40.0 mol. %, while porphyroblastic plagioclase crystals in the matrix have anorthite content of 28.9–29.3 mol. %.

Quartz is also an important mineral in this rock, occurring both as inclusions in garnet and in the matrix. The matrix quartz sizes measure between 0.1×0.01 mm to about 1×2.2 mm although they are mostly anhedral in shape. They make up about 20% of the rock.

Cordierite is colorless with low relief and first order interference colors. They mostly occur around garnet and biotite, and between biotite-biotite and biotite-plagioclase boundaries

(see Figs. 4-3b and c). They also surround all garnets, forming coronae around them (see Fig. 4-3d). Most sillimanite needles occur within cordierite. These textures as found in sample 6 suggest the formation of cordierite from biotite and garnet through the retrograde reactions (4-2) (e.g. Pereira and Bea 1994) and (4-3) e.g. (Santosh 1987; Morimoto et al. 2004)

$Bt_{(Ti\text{-}rich)} + Grt_1 + Sil + Qz + Pl_{(An\text{-}rich)} + water \Rightarrow Crd + Bt_{(Ti\text{-}free)} + Grt_2 + Ilm + Pl_{(Ab\text{-}rich)}$ …. (4-2)

$Grt + Sil + Qz + water \Rightarrow Crd$…… (4-3)

which are common decompression reactions. Brown (1998) however noted that these reactions take place after the removal of the partial granitic melt and then the composition of the residue becomes appropriate for the formation of cordierite. Cordierite makes up about 5 - 10% of the rock.

Garnets are colorless with high relief and characteristically isotropic with many inclusions of plagioclase, quartz, biotite, rutile and sillimanite. They are mostly pseudo-hexagonal and subhedral in shape and measure about 0.6-1.2 mm in radius on the average. Many are partially replaced with coronae of cordierite, sillimanite and biotite. Garnet makes up about 10 - 15% of the rock.

Sillimanite, which is characteristically needle-shaped, colorless, euhedral and with moderate relief and upper first order interference colors occur mostly within cordierite, within garnet-biotite boundaries and as inclusions in plagioclase and garnet. Sillimanite makes up about 5% of the rock.

In sample 3, green spinel occurs in addition to the other assemblages. Some sillimanite needles closely associated with garnet appear to be surrounded by spinel in the presence of cordierite (see Fig. 4-3a). This relationship may be explained by the reaction (4-4) (e.g. Korikovsky et al. 2008)

$Grt + Sil \Rightarrow Crd + Spl$…… (4-4).

Spinel makes up less than 1% of the rock. Spinel is however not found in sample 6 which is the same unit as sample 3 but from a different location.

Ilmenite constitutes the opaque population while accessory minerals include spinel, titanite, apatite, rutile and zircon.

4.3.2 Granite gneiss (sample 66)

This unit which is the most dominant rock unit in the study area incidentally shows a simple textural display of mineralogy dominated by quartz and feldspar. This rock is leucocratic, coarse-grained, equigranular and weakly foliated. The mineral constituents include; quartz, plagioclase, biotite and K-feldspar. Most K-feldspars characterized mainly by their cross-hatched twinning seem to be late stage as they are all anhedral in shape, filling spaces and forming partial replacement on plagioclases. K-feldspars form mostly at quartz-quartz and quartz-plagioclase boundaries.

Biotite occurs in about two to three generations, though they are characteristically small sized measuring mostly about 0.05×0.25 mm to less. The oldest generation of biotite are dark brown in color and very weakly pleochroic. This group is mostly anhedral in shape with no traces of cleavage and seems to have been eaten up and left as relicts or skeletons of original biotite blades. The newer generations however are lighter brown to greenish brown biotite specks which are mostly euhedral to subhedral in shape with clear cleavage traces. They mostly occur along coarse quartz-plagioclase boundaries like the K-feldspars and, though they constitute about 5% of the rock, help to define the foliation direction.

Quartz is anhedral with low relief. Some crystals are very coarse with clear surfaces and characteristic first order interference colors of grey to white. Many of the crystals undergo parallel extinction but almost equal number undergoes undulose extinction. Some large crystals measure about 4×3 mm while some small crystals measure as small as 0.01×0.01 mm (inclusion sizes). Quartz makes up about 50-55% of the rock.

Plagioclase feldspar has characteristic albite twinning observable even under the clouded surface. They are mostly cloudy-surfaced and washed out with very faint traces of the cleavages and twinning. Many crystals are undergoing incipient alteration or sericitization. They mostly measure about 1.2×1.8 mm on the average and constitute about 15-20% of the rock.

Accessory minerals include apatite and zircon which make up less than 1% of the rock.

4.3.3 Meta-quartz diorite (samples 1a, 1b and 11)

This sample is a leucocratic to mesocratic rock which is coarse-grained with weak alignment of minerals in a preferred direction. The mineral constituents include; andesine (in dominant mode), quartz, biotite, orthopyroxene, hornblende and opaques (ilmenite and magnetite). In the domain of the mafic minerals, original orthopyroxenes, most of which are in contact relationships with plagioclases, are being replaced by anhedral amphiboles which in turn are being replaced by anhedral biotites. Hornblende-plagioclase intergrowths are common occurrence in the rock (see Figs. 4-3i and j). Droplets of apatite and anhedral skeletons of ilmenite dot the scene of the replacement reactions. Some coarse-grained amphiboles have been almost completely replaced by cloud-like mesh/networks of newly forming biotites and original plagioclase crystals surrounded by orthopyroxene corona have been replaced by biotite-quartz symplectites.

Many of the plagioclase crystals have cloudy surfaces but from the clear-surfaced crystals, the extinction angle measurement was obtained as 22.3º which corresponds to the andesine composition. They are mostly euhedral to subhedral and most of the crystals measure approximately 1×1.3 mm. Plagioclase makes up about 55-60% of the rock.

Quartz is the next most abundant mineral in the rock. The crystals are all anhedral in shape and more widely varied in sizes. Some crystals measure about 0.02×0.03 mm while some are as large as 3×2.5 mm. Others range in between these values. Quartz constitutes about 15% of the rock.

Orthopyroxene occurs in this rock and show uncoordinated fractures, and some have their surfaces grooved by erosion channels. They have high relief and undergo parallel extinction. They are mostly subhedral to anhedral in shape and are disseminated in the rock along some defined directions. The crystals measure between 0.05×0.3 mm to as large as 2.0×3 mm. Orthopyroxene constitutes about 12-15% of the rock.

Biotite is light brown to dark brown and greenish brown in color with very clear cleavage traces in well-formed sections. However, cloudy condensates and webs of newly forming biotites can be seen in replacement reaction textures with amphiboles. They are mostly slender and lath-shaped measuring about 0.01×0.25 mm to as large as 0.4×3 mm and constitutes about 10-15% of the rock.

Hornblende crystals measuring about 0.2×0.25 mm are restricted to an isolated domain in the rock and constitute less than 1% of the rock.

Opaque population is dominated by magnetite. They are mostly euhedral and cubic in shape, but some are subhedral, and they constitute less than 5% of the rock. Ilmenite also occurs to a lesser extent. Other accessories include apatite and zircon.

4.3.4 Meta-ultramafite (sample 10)

This is a melanocratic coarse-grained rock with alignment of minerals along a direction which is orthogonal to the direction of foliation in the migmatite host rock. Mineral constituents include olivine, edenite, hornblende, orthopyroxene, spinel and ilmenite. This rock is also fairly porphyroblastic with two generations of crystal sizes making it porphyroblastic and coarse-grained. The larger grains occur in bladed shapes which defined the schistose fabric and their population is dominated by amphiboles which measure between 0.7×0.5 mm to as large as 4.8×2.0 mm. Some amphibole porphyroblasts measuring about 3.4×3.4 mm show inclusions of olivine which measure up to 0.2×0.25 mm. Some amphibole crystals have continuous cleavage traces running through sub-ophitic and ophitic medium-sized orthopyroxenes which continues again in the amphibole after emerging from the pyroxenes indicating partial pseudomorphism of the pyroxenes by the amphiboles. Olivine crystals are also pseudomorphed by amphiboles which seem to be replacement products of retrograde metamorphism of olivine. Amphiboles make up about 55 – 60 % of the rock but olivine remains the most authentic primary mineral in the rock.

Olivine, which is colorless with high relief, lacks visible cleavage traces but fractures concoidally and shows a range of second order interference colors. They are mostly subhedral to anhedral in shape. Olivine is restricted to the phaneritic background and as inclusions in pyroxenes and amphiboles. Its size ranges between 0.25×0.25 mm to 0.25×1 mm. They make up about 10% of the rock.

Orthopyroxene, which is colorless in thin section with parallel extinction angles, makes up about 10 to 15% of the rock. Large porphyroblasts of orthopyroxene measuring about 5×4 mm occur with many inclusions of olivine, while a larger population of the pyroxenes occur in the phaneritic background where some also form pseudomorphs of olivine.

Spinel in this rock is brownish in color, occurring with olivine (see Figs. 4-3k - l). It makes up about 8% of the rock, while magnetite and ilmenite constitute the opaque population and make up about 6-7% of the rock.

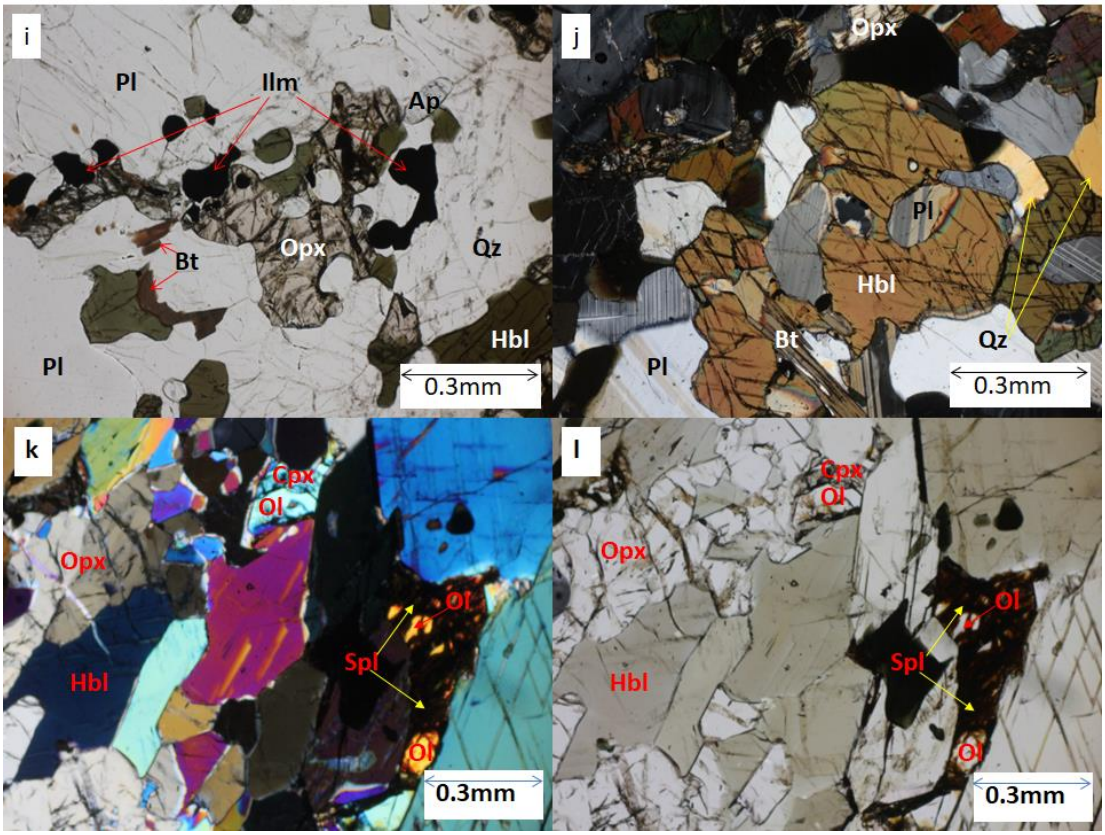

Fig. 4-3(i) Hornblende-plagioclase-biotite-orthopyroxene-quartz-ilmenite association in sample 1a (PPL). (j) Same minerals association in sample 1b (XPL). (k) Hornblende-olivine association in sample 9 (XPL). (l) Hornblende-olivine-spinel association in sample 10 (XPL).

4.4 Mineral chemistry

Below, mineral chemistry data of the examined rocks is described. Representative compositions of minerals in the analyzed samples are given in Tables 4-2, 3, 4 and 5.

4.4.1 Garnet

Garnet in the migmatitic schist unit (sample 6) is dominantly almandine to pyrope with subordinate grossularite and spessartine solid-solution. Garnets in this rock show chemical zoning from core to rim with all analysis showing almandine, pyrope, grossular, spessartine

ranges of 62.0-70.6, 19.3-31.0, 3.4-4.8 and 2.3-3.5 mol.%, respectively (see Table 4-2). Element molar compositions of the core, mantle and rim shows their variations as 1.84 – 1.98 – 2.15 for Fe^{2+}, 0.07 – 0.08 – 0.15 for Mn, 0.94 – 0.77 – 0.59 for Mg and 0.34 – 0.28 – 0.21 for Ca, respectively. Fe^{2+} and Mn thus increase while Mg and Ca decrease from core to rim. Compositional profiles of garnets carried out along sections of two garnets of less inclusions, measuring 1.8 mm and 2 mm in diameter from samples 3c and 6, respectively, showed different asymmetric shapes for the different elements (see Figs. 4-4a - e). The garnet of sample 6 is rimed on the zero (0) mm end by the cordierite, biotite, quartz, sillimanite and plagioclase coronae and on the 2-mm end by contact with coarse anhedral quartz-plagioclase matrix. Fe^{2+} shows a depletion at the center of the garnet (the 1 mm point) which slightly decreased further through the mantle and ended with a sharp rise from the mantle to the rim towards the coronae. Towards the quartz-plagioclase matrix contact, however, the sharp rise of Fe^{2+} was flattened half-way (see Fig. 4-4b). Mn shows a moderate enrichment at the core followed by a steady depletion towards the outer mantle before a gentle rise towards the quartz-plagioclase contact and a sharp rise to the highest enrichment point towards the coronae (see Fig. 4-4c). Mg has an opposite trend to Fe^{2+} with high enrichment at the core which grew higher at the mantle followed by a steep decent to the rim towards the coronae, but on the other side, rose to the highest points towards the quartz-plagioclase contact (see Fig. 4-4d). Ca shows a M-shaped trend which describes an initial enrichment at the core followed by a higher enrichment at the inner mantle and a steady depletion from the outer mantle to the rim. The depletion slope however is steeper towards the quartz-plagioclase contact (see Fig. 4-4e). The garnet of sample 3c however has a featureless flat trend for all elements which seem to tie with the rim values of the sample 6 garnet. This suggests that this garnet was recrystallized at late-stage and cannot be used for *P-T* analysis.

4.4.2 Cordierite

Cordierite occurs in the metapelite (Garnet-sillimanite-biotite schist) with magnesium to iron content ratio of approximately 3:1. Hence, the X_{Mg} (= Mg/(Fe+Mg)) of cordierites also

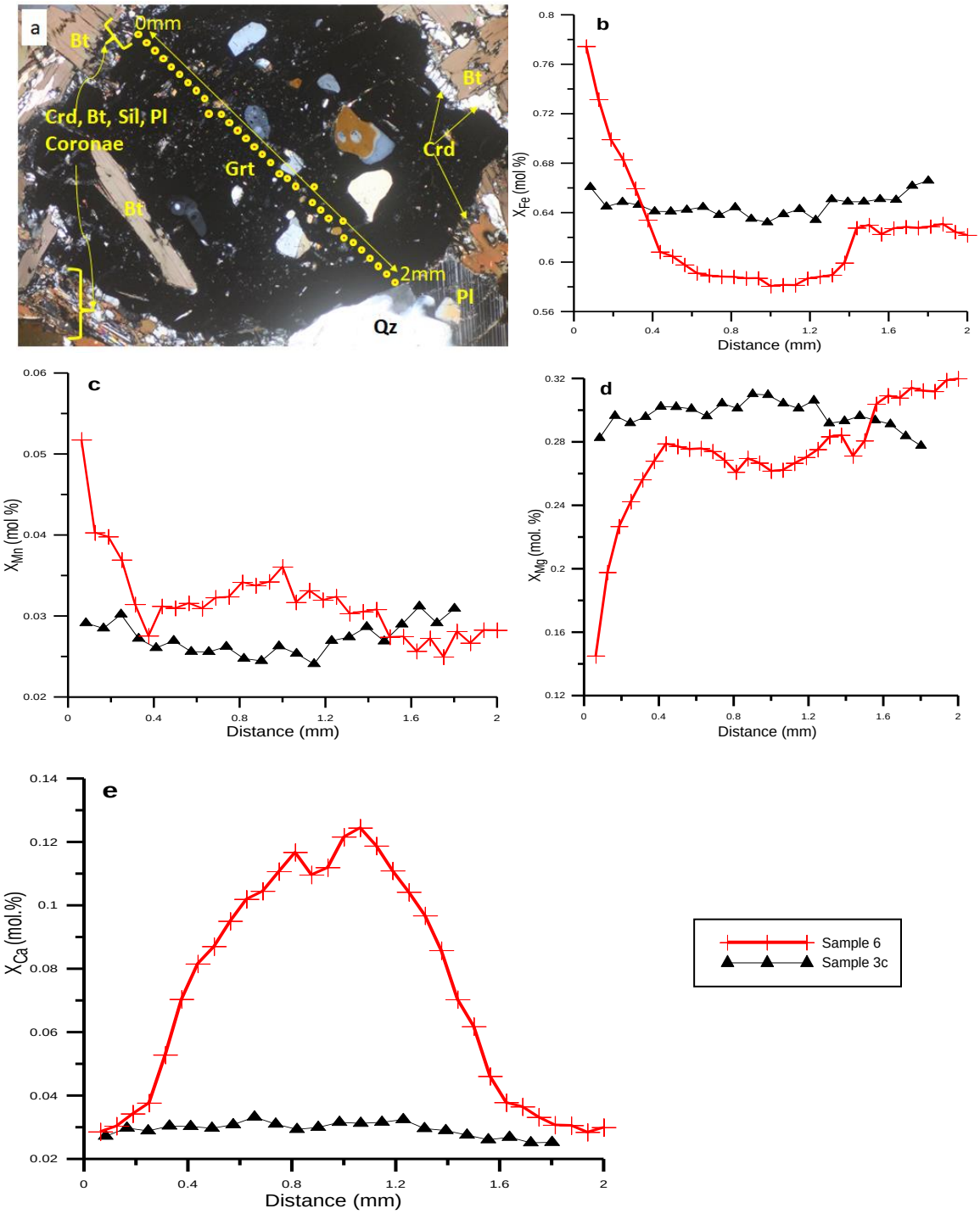

Fig. 4-4. Diagrams of garnet compositional profile analysis showing; (a) the cross-section along which analysis was done and the textural disposition of garnet and the surrounding minerals in sample 6. (b) The graph of X_{Fe} (mol. %) composition across garnet. (c) The graph of X_{Mn} (mol. %) composition across garnet. (d) The graph of X_{Mg} mol. %) composition across garnet. (e) The graph of X_{Ca} (mol. %) composition across garnet.

follow a tight range of between 0.73 and 0.74. The Mn contents of cordierites in the examined samples range between 0.008 and 0.012 pfu (see Table 4-2).

4.4.3 Biotite

Biotite occurs in all samples and has X_{Mg} which is tightly ranging between 0.54 and 0.66. In the Garnet-sillimanite-biotite schist, however, the range is even tighter between the values of 0.54 and 0.56. The titanium contents per formula unit in the biotites of the metapelitic samples range between 0.42 and 0.48 (see Table 4-2). These values of the X_{Mg} and Ti contents fall within the range of X_{Mg} = 0.28 – 1.00 and Ti = 0.04–0.17 pfu, needed for the empirical calculation of biotite geothermometry for the rocks (Henry et al. 2005).

4.4.4 Plagioclase

Plagioclase occurs in both the meta-quartz diorite (samples 1a, 1b and 11) and the metasediment (samples 3 and 6). In all samples, plagioclase is albite-rich with almost the same but wider range of values in the metasediments. In meta-quartz diorite samples, anorthite content ranges from 30.6-32.8 mol.% while in the metasediments, anorthite content ranges from 25.8-32.9 mol.% (see Table 4-3).

4.4.5 Pyroxenes

Pyroxene in the meta-quartz diorite of the study area is orthopyroxene and dominantly of hypersthene composition with calcium contents which range between 0.009 and 0.027 pfu and X_{Mg} of 0.59-0.62. Pyroxene in the meta-ultramafite (sample 9) however is of both ortho- and clinopyroxenes. The orthopyroxene has bronzite composition with X_{Mg} of 0.76 and calcium content of 0.008 pfu while the clinopyroxene is of augite composition with X_{Mg} of 0.84-0.85 and calcium content of 0.47-0.48 pfu (see Table 4-4).

4.4.6 Calcic amphibole

Amphibole occurs in samples 1a, 1b and 9. Calcium contents in the amphiboles range tightly between 1.79 and 1.82 pfu. Ti content in the amphiboles are more varied with values of 0.16-0.19, 0.17-0.18 and 0.13-0.14 pfu in samples 1a, 1b and 9, respectively. The X_{Mg} values in the amphiboles are 0.62-0.66 in sample 1, 0.61-0.62 in sample 1b and 0.78-0.79 in sample 9. Na+K contents in the amphiboles however vary between 0.46-0.63 pfu, 0.66-0.69 pfu and 0.41-0.43 pfu, respectively. A hornblende classification scheme of Locock (2014) classed all the

amphiboles as edenite, suggesting high temperature (amphibolite to granulite facies) metamorphism of the rocks (Oberti et al. 2006).

4.4.7 Other minerals

Olivine occurs in sample 9 with uniform X_{Mg} of 0.7 and lack of chromium and nickel. Spinel contains magnesium content of 0.50 pfu, iron content of 0.54-0.55 pfu, aluminum content of 1.84 pfu and 0.12-0.13 pfu values of chromium (see Table 4-4).

4.5 Metamorphic *P-T* conditions

Classical geothermobarometric analyses have been done from the chemistry of minerals in both metapelites and the metabasites of the study area (see Tables 4-2, 3 and 4) to determine the peak *P-T* conditions of metamorphism. A summary of these analyses is presented below.

4.5.1 Grt-Bt-Pl geothermobarometry

Of all the geothermometers and geobarometers, garnet-biotite-plagioclase (Grt-Bt-Pl) geothermobarometer of Ganguly et al. (1996), which could generate both the temperature and pressure values simultaneously, was applied first to determine the *P-T* conditions of migmatitic schist samples 3a and 6. These samples were chosen because they contained unique equilibrium assemblages of the desired minerals including garnet, biotite, plagioclase, cordierite and quartz. The calculated *P-T* ranges are 6.9-7.0 kbar and 698-718 ºC for sample 3a, and 5.84 kbar and 710-780 ºC for sample 6. These results were used as input for iterative calculations between the geothermometer of Kaneko and Miyano (2004) and the geobarometer of Ganguly et al. (1996).

4.5.2 Grt-Crd-Bt thermometry and Grt-Pl barometry

A combination of (1) garnet-cordierite-biotite (Grt-Crd-Bt) geothermometer of Kaneko and Miyano (2004) which is a refined garnet-biotite Fe-Mg exchange geothermometer with applications in amphibolites and granulites and (2) garnet-plagioclase (Grt-Pl) geobarometer of Ganguly et al. (1996) was employed to confirm the result obtained from the Grt-Bt-Pl geothermobarometer of Ganguly et al. (1996) above. Grt-Crd-Bt geothermometer of Kaneko and Miyano (2004) was particularly chosen because it considers the effect of Fe^{3+} and Al^{3+} contents in biotite and the software has in-built Fe^{3+} correction. Pressures of the rocks calculated from the thermobarometer above were fed into the thermometer of Kaneko and Miyano (2004) to

calculate the corresponding temperatures and the results obtained are 625-670 ºC at 7.1-7.3 kbar for sample 3 and 710-780 ºC at 5.8 kbar for sample 6. These temperature values so obtained were also used as input into the barometer of Ganguly et al. (1996) and thus, the calculations were done iteratively between this thermometer and barometer and the results approached a common point until final common values were reached at 655-665 ºC and 6 kbar for sample 3 and 710-789 ºC and 6.1-7.2 kbar for sample 6 (see Table 4-5).

4.5.3 Hbl-Pl Geothermometry

The method of the hornblende-plagioclase (Hbl-Pl) geothermometry of Holland and Blundy (1994) was used to calculate the peak temperatures of the meta-quartz diorite samples 1a and 1b which have associated hornblende and plagioclase in their equilibrium assemblages. This calculation is based on the reaction edenite + albite = richterite + anorthite – a quartz independent thermometry at 6.8 kbar. This quartz independent edenite-richterite thermometry was chosen because, according to Holland and Blundy (1994), both edenite-tremolite (quartz-dependent method) and edenite-richterite thermometers may be applied for silica-saturated rocks but in silica-undersaturated rocks or magmas, edenite-richterite thermometer alone can be applied. The value 6.8 kbar was chosen because it is the point at which the pseudosection stability field of sample 6 coincides with its garnet rim temperature (calculated). The calculated results gave the temperatures of the meta-quartz diorite as 754-766 °C (sample 1a) and 718-798 °C (sample 1b) at 6.8 kbar. A summary of the calculated temperatures and pressures are presented in Table 5 and a corresponding *P-T* graph is used to show a pictorial representation of the *P-T* distribution for the rocks of the study area.

4.5.4 Optimal thermobarometry

Optimal thermobarometry or "Average *P-T* (avPT)" calculation was also used to determine the average temperatures of formation of mineral constituents of the rocks using the method of Powell and Holland (1994). The end-members activities of the minerals generated from the EPMA raw data through the agency of AX-program (an activity-composition calculation program) of the same authors were applied to the avPT script files and run by THERMOCALC to generate the average *P-T* of the rock. THERMOCALC does this by combining the information for the several independent reactions in a least squares sense to calculate the conditions of formation. The results obtained for the representative samples are; 763 ºC at 7.1 kbar for sample 3a (not shown) and 813 ºC at 7.4 kbar for sample 6 (shown in Figs.

4-5 and 4-6 as (Av.)). A summary of the calculated temperatures and pressures are presented in Table 6, while the *P-T* diagram (Fig. 4-5) also shows the average *P-T* distribution for the rocks of the study area.

4.5.5 Mineral equilibria modeling

The equilibrium assemblage condition was constrained in pseudosection using THERMOCALC version 3.33, with the October 2009 updated version of the Holland and Powell (1998) data set (file tcds55.txt). A model system (NCKFMASHTO) was used to calculate the pseudosection (see Fig. 4-5).

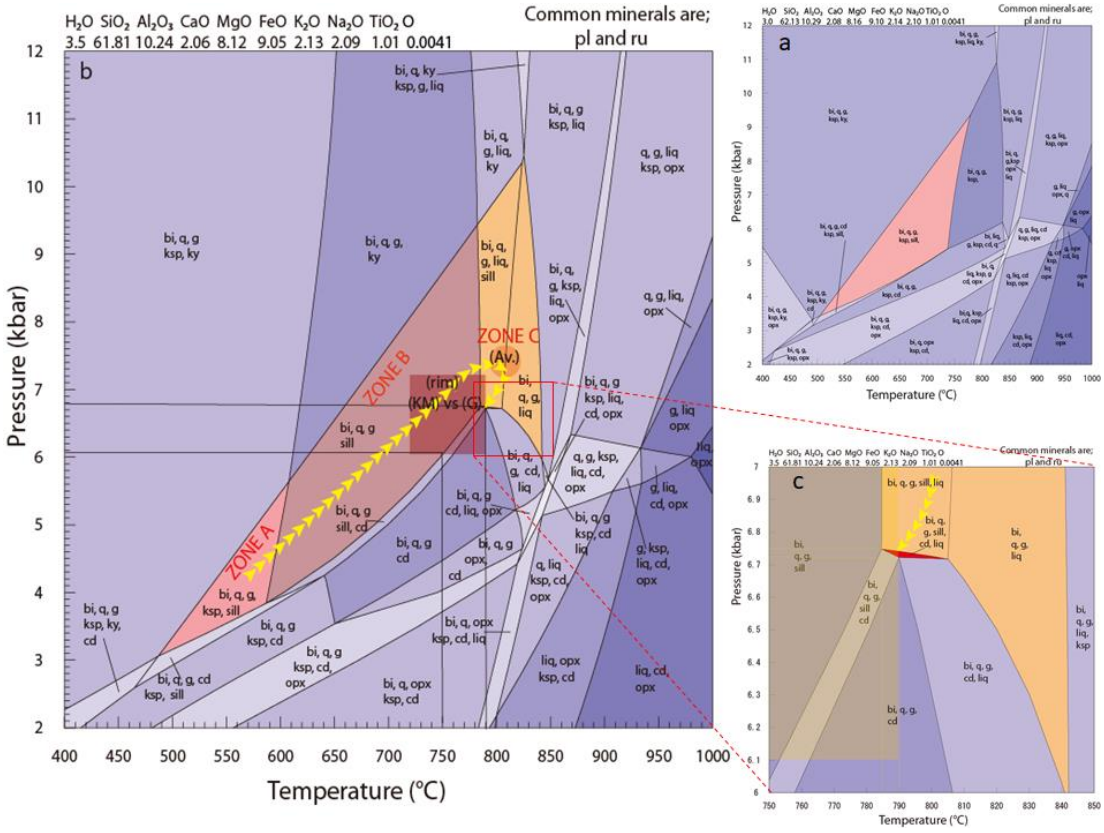

Fig. 4-5. *P–T* diagrams showing calculated pseudosections of mineral assemblages in sample 6 with the estimated *P-T* path. The bulk chemistry is in mol. % while minerals abbreviations (bi = biotite, g = garnet, q = quartz, ksp = K-feldspar, pl = plagioclase, cd = cordierite, sill = sillimanite, hb = hornblende, ru = rutile, ol = olivine, sp = spinel, ilm = ilmenite, opx = orthopyroxene, ky = kyanite, ap = apatite, liq = liquid) are after Holland and Powell (1998), (a) Pseudosection for prograde assemblage constrained with H_2O = 3.0 mol. %, (b) Pseudosection for the granulite facies assemblage constrained with H_2O = 3.5 mol. % and (c) Magnified P-T space of the equilibrium assemblage.

Fe_2O_3 constitutes less than 0.01% of the bulk chemistry of the rocks suggesting that peak metamorphism was relatively in reduced condition while MnO constitutes 0.193. Both oxides were automatically eliminated in the mole percentage calculation program. Some pelitic samples studied lacked cordierite in their assemblages or had cordierite and sillimanite in a different domain from garnet and were therefore not selected for pseudosection. Samples 3 and 6, however, possess a unique association of all essential minerals in equilibrium and were selected for conventional *P-T* calculations, while sample 6 was selected for pseudosection. For the analysis, slabs of relatively homogeneous part of the examined granulites were used for thin-section preparation, and the counterpart of the same slabs was used for chemical analysis. The equilibrium assemblage in the sample includes plagioclase + rutile + garnet + biotite + sillimanite + cordierite + quartz + liquid, while its bulk composition in molar percentages of the oxides is SiO_2 = 61.81, TiO_2 = 1.01, Al_2O_3 = 10.24, CaO = 2.06, MgO = 8.12, FeO = 9.05, K_2O = 2.13, Na_2O = 2.09, H_2O = 3.50. H_2O value of 3.5 mol.% was used because with less than this value of water, the observed equilibrium assemblage could not be constrained in the pseudosection. A water value of 3.0 is however used to constrain the *P-T* space for the prograde assemblage in another pseudosection (see Fig. 4-5a). The *P-T* space for the equilibrium assemblage (shown as red triangle in Fig. 4-5b and magnified in Fig. 4-5c) was constrained in the pseudosection between 785-805 ºC and 6.72-6.75 kbar which partly coincides with the *P-T* conditions of the garnet rims (shown as light-brown square in Figs. 4-5 and 4-6) as determined using conventional geothermometers.

4.6 Discussion

The study area is basically underlain by migmatites with felsic to mafic magma intrusions. The granitic magma seems to have been syn-tectonic as it is evidently very metamorphosed relative to the dioritic and the ultramafic magmas which seem to have been late-tectonic as evidenced by their much weaker foliations.

4.6.1 Equilibrium *P-T* condition

From petrographic studies, the mineral assemblage of the migmatitic schist sample (sample 6) showed the equilibrium mineral assemblage for the migmatites as plagioclase + rutile + garnet + biotite + sillimanite + cordierite + quartz. The equilibrium assemblage condition of the rocks as constrained in the THERMOCALC pseudosection between 785-805 ºC and 6.72-

6.75 kbar, equilibrated about the peak *P-T* but our modeling places this value on the path of early retrograde metamorphism of the rock; i.e. the rock seems to have attained a bit higher maximum *P-T* (813 ºC at 7.4 kbar) as peak *P-T* and began a retrograde progression which was probably chocked due to the absence of the already extracted melt phase and equilibrated at early retrograde point within the same granulite facies (see Figs. 4-5b, c and 4-6). This maximum *P-T* of 813 ºC at 7.4 kbar was determined using optimal thermobarometry method of Powell and Holland (1994).

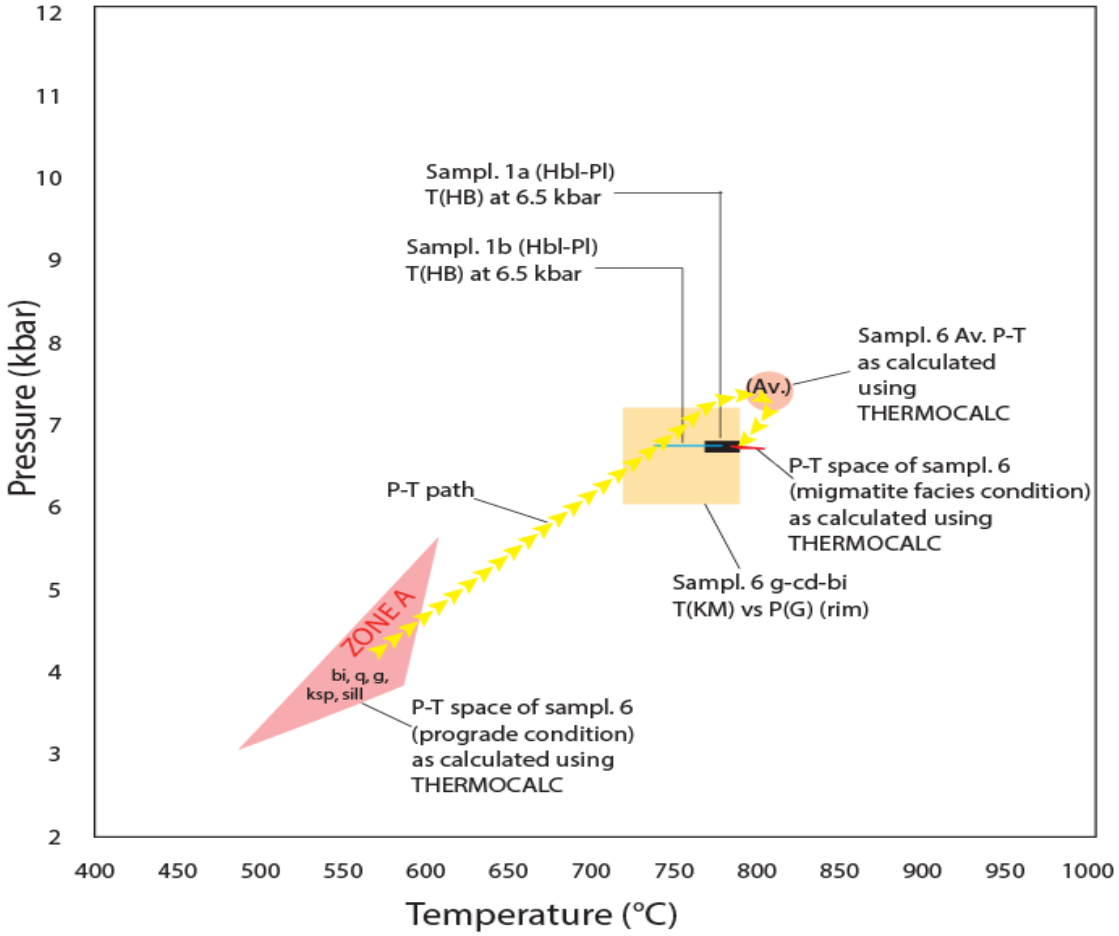

Fig. 4-6. Graphical illustration of the constrained *P-T* of representative samples using different methods. The red strip is the *P-T* equilibrium space of the mineral assemblage of sample 6 for comparison with calculated results where T(KM) is the temperature as obtained with Grt-Crd-Bt thermometer of Kaneko and Miyano (2004); P(G) is the pressure obtained with Grt-Pl barometer of Ganguly et al. (1999); T(HB) is the temperature obtained with Hbl-Pl thermometer of Holland and Blundy (1994) and AvP-T is the average pressure and temperature obtained with THERMOCALC.

A combination of conventional geothermobarometers including Grt-Bt-Pl geothermobarometer of Ganguly et al. (1996), Grt-Cd-Bt geothermometer of Kaneko and Miyano (2004) and Grt-Pl geobarometer of Ganguly et al. (1996) on the garnet-biotite cores gave the core temperature as 900-905 ºC at 11 kbar (which is abnormally high). The same analysis done for the garnet rims gave a more reasonable *P-T* range of 710-789 ºC at 6.1-7.1 kbar which coincided with the lower temperature part of the 785-805 ºC and 6.7-6.8 kbar *P-T* space of the pseudosection (low-*P* granulite facies). The result of the garnet core (900-905 ºC, 11 kbar) was rejected as the maximum *P-T* attained by the rock based on the following reasons; 1. Petrographically, the observed mineral assemblages included in garnet core could not have been stable at this temperature as proved also by the pseudosection (Fig. 4-5a). 2. At such temperature, K-feldspar would have been included as a new phase outside plagioclase in garnet or at least occurred in the matrix. Such K-feldspar would be anorthoclase or high-albite orthoclase, but this was not the case (K-feldspar in the rock occurs only as inclusions in the plagioclase cores and the chemistry does not suggest a high-albite orthoclase). 3. At granulite-facies temperatures, garnet-core versus matrix biotite thermobarometry is unreliable due to element mobility leading to core-rim homogenization (e.g. Spear and Florence 1992; Spear et al. 1990). This garnet-rim temperature (710-789 ºC, 6.1-7.1 kbar) also coincides with the temperature of the meta-quartz-diorite (753-765 °C (sample 1a) and 717-797 °C (sample 1b) at 6.5 kbar) as calculated using the Hbl-Pl thermometric methods of Holland and Blundy (1994). The equilibrium *P-T* conditions of the rock is thus regarded as the portion of the *P-T* space (785-805 ºC and 6.7-6.8 kbar) constrained in the pseudosection which coincides with the calculated garnet-rim temperatures (710-789 ºC, 6.1-7.1 kbar) and with the temperature of the meta-quartz-diorite (717-797 °C of sample 1b at 6.8 kbar). The equilibrium *P-T* condition of the study area is thus determined as 785-789 ºC and 6.7-6.8 kbar.

The equilibrium *P-T* (785-789 ºC and 6.7-6.8 kbar), corresponds to a depth of exhumation of approximately 25 km, considering the average geobaric gradient of 0.27 kbar/km for the crust. At this depth, the associated temperature (785-789 ºC) as constrained in this study is indicative of heat anomaly culminating to a heightened geothermal gradient of about 31-32 ºC/km - a common feature in granulite-facies terranes (Bohlen, 1987) (see Fig. 4-7). This depth of exhumation added to the fact that eastern Nigerian basement is topographically the highest elevated metamorphic terrane within the Nigerian Shield areas which is a proof of the rapid rate of exhumation and a characteristic of intra-continental rifting terrane.

4.6.2 P-T path analysis

A study of the minerals inclusions of the metasediments especially the garnet-sillimanite-biotite schist helps us to infer the possible *P-T* path. Conventional microscopy and EPMA backscattering images of the rocks reveal relict minerals inclusions in garnet (see Figs. 4-3a - h). These inclusions, which include quartz, biotite, K-feldspar, plagioclase, rutile and sillimanite, make up the prograde assemblage. Thus, Fig. 6a (of H_2O = 3.0 mol. %) is important to prove firstly that the assemblage above was the prograde assemblage, secondly that increase in temperature of the rock leading to migmatization and formation of the equilibrium assemblage (cordierite-sillimanite-garnet-biotite-plagioclase-rutile-quartz-liquid at H_2O = 3.5 mol. % (Fig. 4-5b)) was accompanied by higher water influx, and thirdly, that K-feldspar was removed by hydration. Fig. 6a, however, is not suitable for the description of the textural signatures of the rock samples because K-feldspars occur only as inclusions in those plagioclase fraction which themselves are inclusions in garnet (see Fig. 4-3g). The K-feldspar inclusions in plagioclase were most probably picked up at about 490-590 ºC and 3.0-5.7 kbar – a *P-T* window which may be referred to as the stability field of Bt, Grt, Qz, Kfs, Sil, Pl and Rt (zone A in Fig. 4-5b), where this prograde assemblage is stable, and K-feldspar and plagioclase grew freely. At this zone, K-feldspar grew alongside plagioclase into perfect euhedral crystals as shown in Fig. 4-3g. However, the growth of K-feldspar was suddenly stopped and overtaken by plagioclase which became the only stable feldspar phase in zone B of Fig. 6b (the stability field of Bt, Grt, Qz, Sil, Pl, Rt) (≈590-840 ºC, 3.9-10 kbar) and thus, K-feldspar relicts became inclusions in the cores of plagioclase porphyroblasts. Touret and Huizenga (2012) observed that, as one evidence of metasomatism in a cordierite-bearing granulite, K-feldspar is replaced by plagioclase and quartz under the influence of Ca and Na-bearing solutions, according to the reaction: $1.25KAlSi_3O_8 + 0.75\ Na^+ + 0.25Ca^{2+} + 2H_2O \rightarrow Na_{0.75}Ca_{0.25}Al_{1.25}Si_{2.75}O_8 + 1.25K^+ + SiO_2$……. (4-5). In the case of this study, such K^+ thus released may have been extracted in a melt phase during migmatization and any remnant may have been taken up locally in the formation of new biotites as suggested by equation (2) and observable in Figs. 4-3b and c.

Plagioclase and rutile are ubiquitous in the rock, so they are found both in the prograde and peak assemblages. Some of the early plagioclases were therefore trapped as inclusions in garnet together with their own inclusions of mainly K-feldspar and quartz. All minerals growth so far seems to have taken place within the stability field of sillimanite, which explains why sillimanite became inclusions in every growing porphyroblast including plagioclase and garnet

(see Figs. 4-3e and f), while kyanite does not appear anywhere both in the prograde or peak assemblages. Garnet porphyroblast must have started growing and gradually engulfed the prograde assemblage at middle to upper zone B. It must also have stopped growing at about the peak *P-T* in zone C (see Fig. 4-5b) as calculated using optimal *P-T* methods. The *P-T* path, however, seems to have crossed through zone C (liquid-sillimanite overlap and the sillimanite-absent, K-feldspar-absent, liquid-present fields) as constrained also by the optimal *P-T* calculation methods of Powell and Holland (1994). The path through zone C (the liquid-present phase) represents the migmatization phase of the pelite. According to the experiments of Le Breton and Thompson (1988), in sillimanite-bearing metapelites, incipient melting begins at pressure of about 6.5 kbar at 760°C following the reaction: biotite + sillimanite + plagioclase + quartz = garnet + K-feldspar + melt. The *P-T* condition of the rock returned to zone B on the path of retrograde metamorphism. The rock probably began to lose pressure quickly due to decompression or fast erosion simultaneously with temperature loss and ended up with the observed stable mineral assemblage in the cordierite-sillimanite-garnet-biotite-plagioclase-rutile-quartz-liquid stability zone (red triangle in Figs. 4-5c and 4-6) clearing a hair-pin type clockwise pattern. This decompressional retrograde path can be confirmed by the formation of the microcrystalline biotite, quartz, plagioclase, sillimanite and cordierite coronae around garnet (see Fig. 4-3d). Frijvald (1974) observed that "New biotite or quartz-biotite symplectite forms by recrystallization of biotite-rich foliae in the granulite gneisses and in part at the expense of garnet and cordierite", while Brown (1998) observed that formation of cordierite coronae around garnet takes place after the removal of the partial granitic melt and then the composition of the residue becomes appropriate for the formation of cordierite.

The study of the compositional profile of garnet shows the variations in the patterns of four major elements (Fe^{2+}, Mn, Mg and Ca). Since Fe^{2+} and Mn enrichment are inversely proportional to temperature rise, W-shaped trends of X_{Fe} and X_{Mn} with lowered central peaks for these two confirms that garnet growth began towards the peak of metamorphism and that the peak *P-T* was not so far away from garnet nucleation as the result of garnet core versus matrix biotite thermometry suggested. The nucleation of garnet was followed by further depletion of these two elements with the highest depletion recorded through the inner mantle for Fe^{2+} and outer mantle for Mn before a turn towards enrichment at the rims. Their enrichment, which signifies lowered *P-T*, peaked at the contact with cordierite corona because the replacement of garnet by cordierite corona followed a preferential absorption of magnesium into cordierite,

while Fe^{2+} and Mn were reabsorbed into the new garnet rim, and it increased their concentration. This is confirmed by the X_{Mg} value of cordierite (0.73-0.74) as against garnet rim (0.21). This means that temperature was on the rise during garnet nucleation and peaked at a higher point relative to the nucleation temperature and lowered again. Conversely, Mg and Ca enrichment, are directly proportional to temperature rise. The M-shaped trends of X_{Mg} and X_{Ca} support the result of X_{Fe} and X_{Mn} above. Towards the quartz-plagioclase contact, the shapes however differ. Mg increases beyond the core content while X_{Ca} decreases with a sharper slope than towards the coronae. This can be explained on the fact that the anhedral plagioclase is also a replacement product of the garnet rim – a possible reaction in the presence of sillimanite, according to the reaction;

Grossular + Al-silicate + Quartz => Anorthite…… (4-6) (Tuccillo et al. 1990). The removal of grossular for the formation of anorthitic plagioclase (see also equation (4-5) above) therefore concentrates the new garnet rim with residual pyrope, almandine and spessartine. These patterns thus confirm a rise from the nucleation temperature of garnet to a peak and followed by retrograde metamorphism.

This *P-T* pattern suggests that the study area underwent an initial temperature build-up and crustal thickening followed by rapid uplift and erosion, which is not consistent with frontline subduction zone nor subduction influenced magmatic-arc patterns. Such settings are normally associated with initial increase of pressure (through the kyanite field) at low temperatures followed by temperature build-up to mostly medium-range temperatures before decompression. The pattern of the *P-T* path is more reminiscent of the low ($\partial p/\partial t$) magmatic-arc setting style. It can be speculated by extrapolation of the *P-T* path to zero pressures (see Fig. 4-4) that onset of tectonism of the study area as recorded in the migmatites was dominated by initial temperature build-up due to magma under-plating and magma intrusions with the attendant crustal uplift and thinning due to convective and extensional forces. Consequent upon this is the attainment of granulite-facies grade at moderate to low pressures – a true characteristic of magmatic-arc regions. The source of the geothermal anomaly is likely due to the under-plating by the magma displaced from subduction zone and magma ascent as a result of partial melting at the upper subducting-slab surface/mantle boundaries. Currently on Earth, lower thermal gradients are associated with subduction (and early stages of collision) whereas higher thermal gradients are characteristic of magmatic-arcs and orogenic hinterlands (Brown 2006). Anomalous thermal

gradients as constrained in this study is caused by the intrusion of magmas beneath or into a given terrain rather than by increased heating as the result of increased burial (Bohlen 1987). Note that the Pan-African orogeny as a result of ocean closures had an eastward dipping subduction (Caby 2003).

Metamorphism must have been reversed at the onset of uplift. A combination of decompression forces (uplift and surface erosion) and fast cooling of the thinned crust at almost equal rates, factored the retrograde metamorphism in a manner almost equal to the rate of prograde metamorphism to trace the hair-pin style *P-T* path.

4.7 Conclusions

Compared to the *P-T* conditions recorded in other parts of the Benin-Nigerian Shield areas, the eastern Nigerian basement to the Cameroons have been reported to have higher *P-T* conditions especially with respect to the western Nigerian basement (e.g., the Zuru, Karaukarau and Wonaka Schist Belts (in northwestern Nigeria) and the Ilesha Schist Belt (in southwestern Nigeria)) which record greenschist-facies metamorphism as reported by Turner (1983) and the Cameroons where Yonta-Ngoune et al. (2010) reported a metamorphic peak of ~650 ºC at 9.5 kbar for the Boumnyebel talc-schists of Cameroon in the Pan-African Belt of Central Africa. Ferré et al. (2002), however, reported a granulite-facies metamorphism of (>800 ºC at 8 kbar) in the north-eastern Nigeria.

The equilibrium *P-T* conditions (785-789 ºC and 6.7-6.8 kbar) constrained from the pelitic unit of this research is therefore consistent with the results obtained so far in Nigerian basement, and confirms that southeastern Nigerian basement is a granulite-facies metamorphic terrane (see Fig. 8). From the result of this research also, a magmatic-arc tectonic setting is inferred for the study area as constrained also by previous researchers (e.g. Ukegbu and Beta 2009), who think that Obudu areas and southeastern Nigeria at large was formed under an arc setting.

The migmatites which form the host rocks of the study area were intruded by large volumes of syn- to late-tectonic magmas including granitic, dioritic and ultramafic compositions which show decreasing degrees of deformation in that order. The pelitic host rocks stabilized in the plagioclase + rutile + garnet + biotite + sillimanite + cordierite + quartz + liquid field constrained in the pseudosection between 785-805 ºC and 6.72-6.75 kbar, whereas the *P-T* of

stabilization as described from our controlled modeling is 785-789 ºC and 6.72-6.75 kbar. There is a marked increase therefore of metamorphic grade from the greenschist facies of the western terranes through the middle-upper amphibolite facies of the north-central terranes to the granulite facies of the eastern Nigeria – a west to east increase across the Trans-Saharan Orogenic Belt within the Nigerian Shield areas. From the result of this study, a magmatic-arc tectonic setting is inferred, although it is not confirmed for the southeastern Nigerian metamorphic basement.

Chapter 5: Tectono-Metamorphic *P-T* evolution of low-pressure granulites of Akoko areas of Ondo state, south-western Nigeria; Geothermobarometry and mineral equilibrium modelling.

5.1 Introduction

Pan-African orogeny has different structural imprints on different parts of the Trans-Saharan Orogenic Belt. By far the most dominant foliation and lineation directions recorded are the N-S to NNE-SSW directions which represent E-W to NNW-SSE compressional regimes. However, some parts of the orogenic belt are dominated by E-W trending foliation and lineation directions which unequivocally represent a different stress regime – specifically, a north-south compressional force. The Trans-Saharan Orogenic Belt was part of a large sedimentary basin which received detritus during the breakage of the Rodinia supercontinent during early Pan-African, and later became part of Gondwana hinterland after the amalgamation during late Pan-African. Many researchers agree that the sequence of the compressive/amalgamating forces which led to the closure of the sedimentary basin and subsequent formation of the Gondwana supercontinent followed an initial northward movement of the African and south American plates leading to creation of E-W trending shears, foliations and lineations encountered in all orogens affected by this tectonism. The northward movement of the plates changed direction to northeast and finally to east and southeast and consequently creating the NW-SE through N-S to NE-SW foliation, lineation and shear directions.

According to da Silva et al. (2005) in their study of the Mantiqueira Province of South America, the Pan-African orogenic stresses were absorbed into early E-W, WNW-ESE or NW-SE syn-collisional tectonics, followed by development of NE-SW or NNE-SSW transpressional (dextral) shear zones, precisely dated at ca. 790 Ma and 730–700 Ma (Brasiliano I); ca. 640–620 Ma and ca. 600 Ma (Brasiliano II), and ca. 595–560 Ma and 520–500 Ma (Brasiliano III), respectively. Caby (1998) and Egbuniwe (1982) presented a threefold subdivision for the Pan-African tectono-metamorphic events in Northern Africa: an early Pan-African tectonic-metamorphic ‘Event’ (750–700 Ma); a Main Pan-African ‘Episode’ (630–580 Ma); and a Late Pan-African ‘Episode’ (580–520 Ma). Egbuniwe (1982) suggested 3 phases of metamorphism (M1, M2 and M3) associated with 3 phases of deformation (D1, D2 and D3) within the

crystalline rocks of the basement complex in northern Nigeria. In the southwest, Boesse and Ocan (1988) recognized 3 phases of metamorphism but only 2 phases of deformation. Goodenough et al. (2014) measured the timing of magmatism within the Minna Batholith in Minna, West-Central Nigeria. The result showed that the earliest magmatism was 790–760 Ma, which was followed by 600–650 Ma, 590 Ma and 560–450 Ma episodes. All these show synchronous episodes of both magmatism and deformation across the entire Trans-Saharan Orogen. Hence, according to da Silva et al. (2005), 'the evolution of the distinct orogens is a response to continental collision processes, responsible for the development of extended deep shear systems. In most cases, the systems are the limits of distinct terranes and separate distinct records of orogenic magmatism, deformation and metamorphism'.

Black (1978) developed the concept of amalgamation of micro-continents as the final consequence of the Pan-African orogeny and Cordani et al. (2013) has suggested the trapping of several accretionary complexes and possible micro-continents within the orogenic belt during the closure of the Goiás-Pharusian Ocean. In Nigeria, the western basement province lies approximately west of Longitude 8° E, which (Grant 1978; Fitches et al. 1985; Ajibade et al. 1987) described as narrow, N-S trending and low-grade schists. These low-grade schists range from greenschist to amphibolite facies (Caby 1989; Ugwuonah and Obiora 2011) and occur in a predominantly migmatite-gneiss 'older' basement. This study area forms a part of this belt. It, however, lacks the presence of this low-grade schists but showcases large outcrops of the migmatite gneiss. Most importantly, the dominant trend of foliations and lineations is E-W to WNW-ESE and NNW-SSE. All rock units in the study area are also aligned in the E-W direction, although N-S and NE-SW foliation directions also occur.

This research was undertaking to achieve some primary objectives which in the long run must help to elucidate the Rodinea-Gondwana-recent transition story of the Trans-Saharan Orogenic Belt, using the Benin-Nigerian Shield as a laboratory. The first of these primary goals is to break into the study of the western Nigerian metamorphic basement with a view of confirming or disproving the long-held concept 'that metamorphism in the western half of Nigeria did not exceed amphibolite facies' (Rahaman 1976b; Elueze 1981; Turner 1983; Zeh and Holness 2003; Aliyu 2012). The second of the primary goals is to determine if the early to syn-tectonic metamorphic episodes (usually associated with E-W to NW-SE shear and foliation directions) produced granulite-facies terranes. Such terranes may be the lost micro-continental units in the hitherto Goiás-Pharusian Ocean, trapped within the orogenic belt during the final

ocean closures. A regional study of the minerals paragenesis and metamorphic *P-T* responses (particularly of the metasediments) to Pan-African orogeny is the way to begin to proffer solutions to these problems.

In this chapter, the petrological, mineralogical and metamorphic *P-T* study of Ikare-Erusu-Arigidi-Ogbagi areas of Ondo State, Nigeria (Lat. 07°30'N - 07°40'N and Long. 005°40'E - 005°50'E) is presented (see Fig. 5-1) and the first attempt to study the metamorphic evolution of south-western Nigerian metasediments using mineral equilibrium modeling in a complex system $Na_2O–CaO–K_2O–FeO–Fe_2O_3–MgO–Al_2O_3–SiO_2–H_2O–TiO_2$ (NCKFMASHTO) with THERMOCALC 3.33 (Powell and Holland 1988). New mineralogical and petrological data of the metamorphic suite of Ikare-Erusu-Arigidi-Ogbagi areas of Ondo State is presented in this work and discussion is argued for the evidences of granulite-facies metamorphism and *P-T* path. The result of this research will go a long way to expose the special characteristics which are peculiar to the study area and re-write the story of the western Nigerian metamorphic basement. The result will also embolden the investigation of the Rodinea-Gondwana-recent transition story and the variations in metamorphic response to orogenesis.

5.2 Field occurrence

In the study area (see Fig. 5-1), migmatites are the host rocks and they were intruded by very large volumes of granitic magma now referred to as the granite gneiss unit to the south and by an equally large charnockite pluton to the north. All rock units have been structurally aligned in the east-west direction and, although the foliation measurements are varied, they are also dominantly east-west in orientation. The granite gneiss is much more metamorphosed relative to the charnockite pluton while small bodies of the meta-basites are equally metamorphosed with the migmatite gneisses within which they occur as dykes. The east-west structural arrangement of the lithologic units in the study area is of regional significance as it is discordant to the general trend of foliations and lineations of the Trans-Saharan Orogenic Belt.

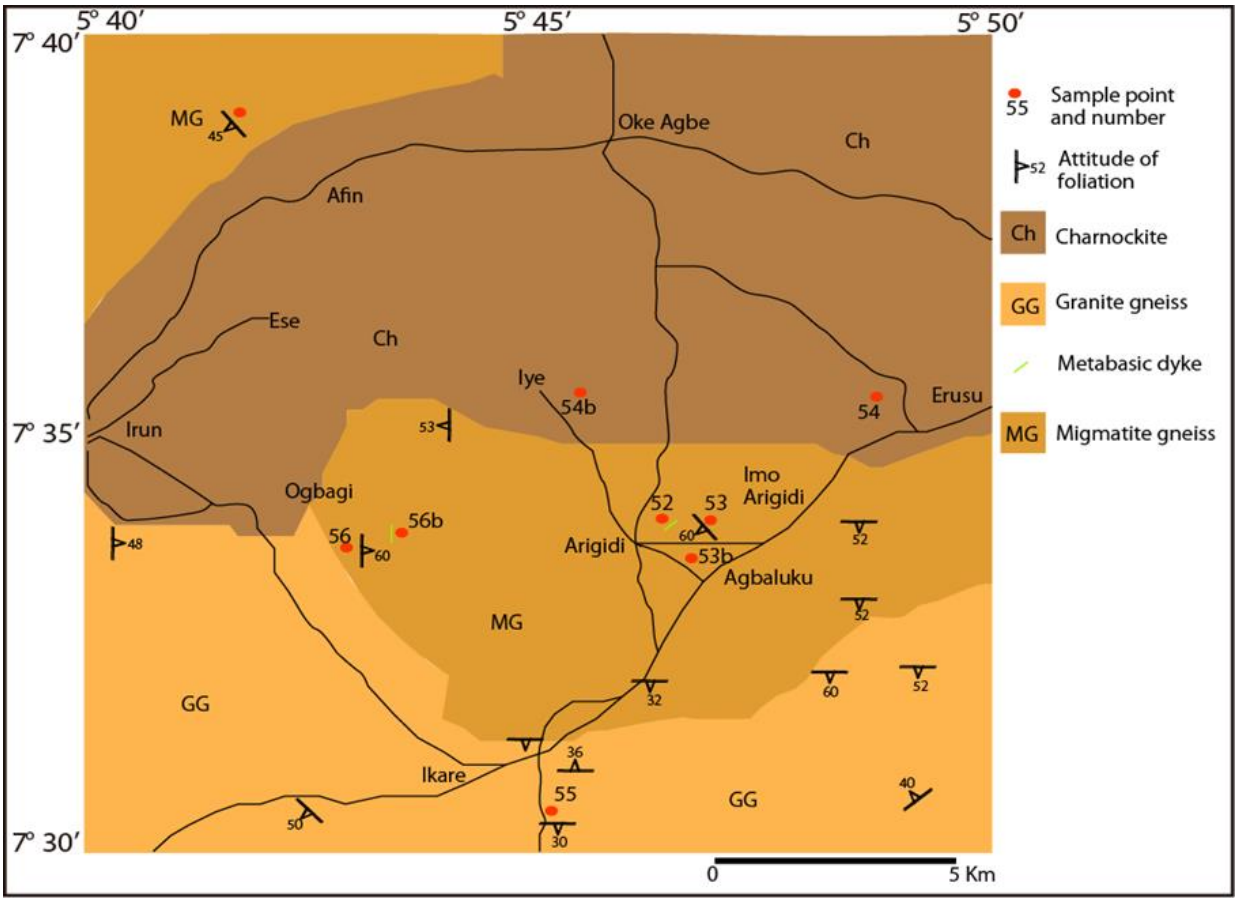

Fig. 5-1 The geological map of the study area as modified from Malomo (2004).

The study area is a very undulating terrane sculptured by the differential resistances of the different rock units to erosional processes. The two ridges of plutons bounding the study area north and south are far more resistant to erosion than the migmatite host rock. The migmatite host rock, however, has differential deformational and resistant characteristics. At locations 53 and 53b, the migmatite gneiss unit is more orderly with unidirectional (E-W) gneissose foliation (see Figs. 5-2a and b), although the unit is obviously less resistant to erosion. At location 56, however, this unit becomes plastically deformed with various degrees of drag folds, isoclinal folds, refolded folds and ptygmatic folds of quartzo-feldspathic veins (see Figs. 5-2c and d). At this point also, the unit is more indurated and attains higher elevation due to its relative resistance to erosion. The trend of foliation at this point is north-south as against the east-west orientation at locations 53 and 53B. At all exposures, the rock is mesocratic, coarse-grained with lit-per-lit injections of quartzo-feldspathic materials. The rock also reveals micro-folding of foliations and the boudinaging of quartzo-feldspathic materials. The rock is migmatitic but with a

high percentage of biotite and coarse garnet forming the dark colored bands separated by leucocratic quartzo-feldspathic layers.

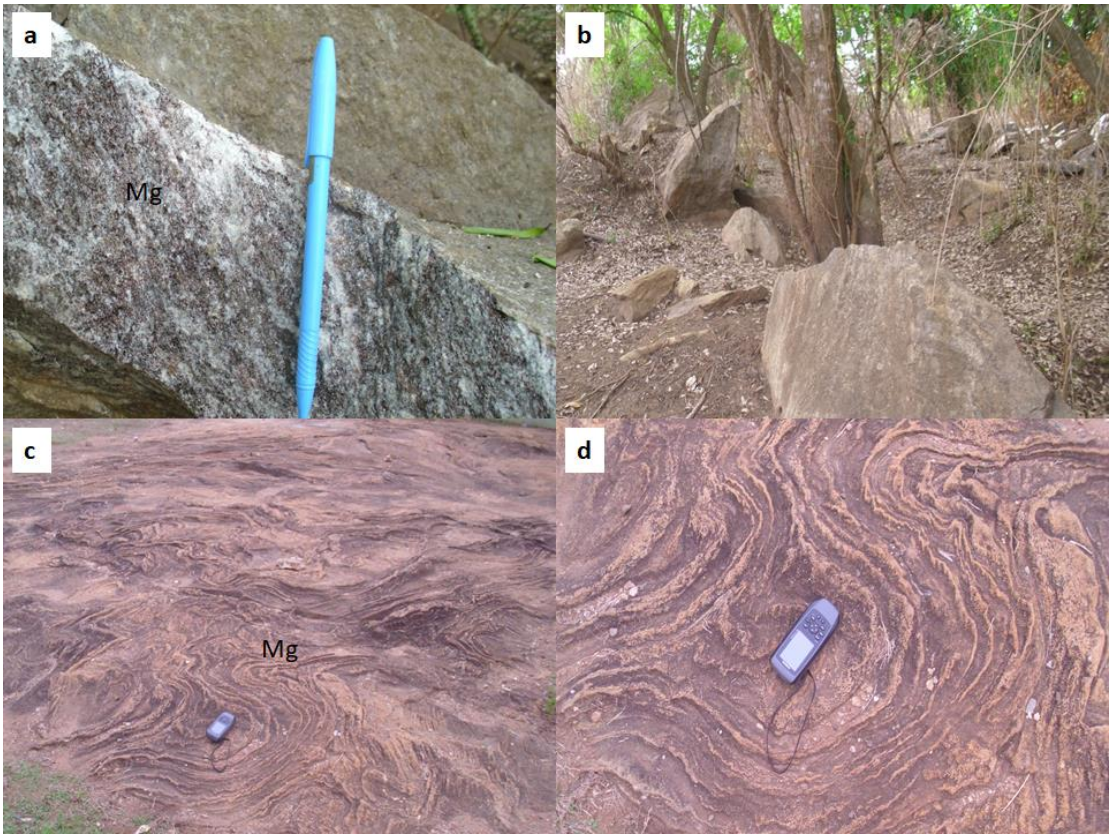

Fig. 5-2 Field photographs of representative samples discussed in this study. (a) and (b) Exposure of the migmatite gneiss unit at Imo-Arigidi (samples 53 and 53b). (c and d) The same migmatite texture at Ogbagi village (sample 56).

The metabasites are encountered at locations 52 and 56b. The rock is melanocratic and coarse grained. At location 52, the rock shows weak alignment of minerals in a preferred direction. The minerals are nematoblastic, mostly anhedral and interlocking. The largest porphyroblasts are brownish garnets which measure about 1 cm in diameter and the entire exposure is an irregular mass of mesocratic-melanocratic intrusion measuring about 30 m by 15 m in size and surrounded by the migmatite gneiss unit (host rock). At location 56b, however, the basic unit is a dyke measuring about 45 cm thick and is significantly impregnated with very coarse-grained garnets (see Figs. 5-2e and f).

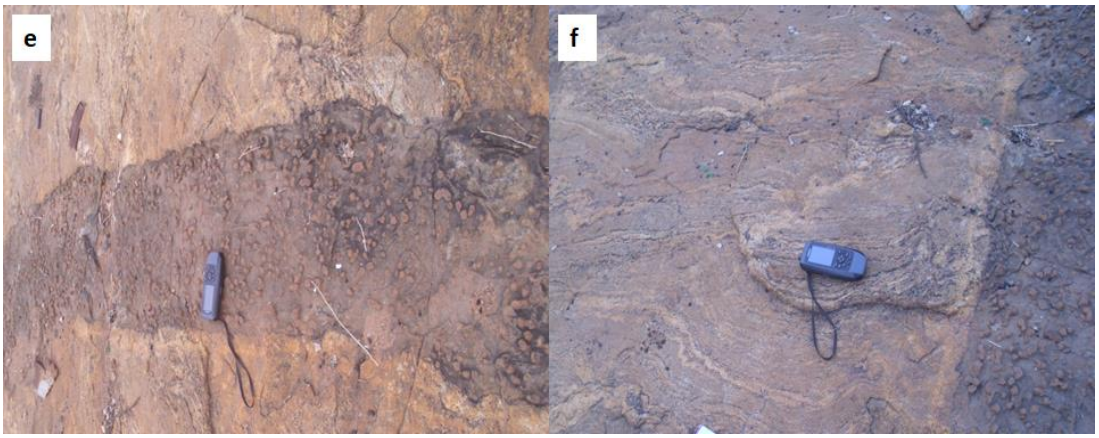

Fig. 5-2 (e) and (f) Exposure of the migmatite gneiss unit at Ogbagi village in sharp contact with the metabasite dyke (samples 56b).

Granite gneiss outcrops are hilly exposures showing massive mesocratic coarse-grained rock with alignment of minerals in a preferred direction and relicts of older materials (paleosome) and with irregular folding of foliation trends. The dominant foliation direction here is E-W. Exposures at Loc. 55 reveal a massive pluton dominated by quartzo-feldspathic mineralogy and subordinate mafic minerals. The minerals in this rock show stretched textural arrangement. The mineralogy is dominated by quartz and subordinate feldspar interlaced with tiny specks of biotite that occasionally coagulate to define the foliation. Garnet for instance mostly stretched to about 1 cm in length, while some feldspar and quartz minerals reached up to 2 cm in length in a manner synonymous with mylonitic texture (see Figs. 5-2g and h). Some hitherto stretched minerals seem to be either broken or recrystallized into smaller fragments.

Fig. 5-2 (g) and (h) Exposures of the granite gneiss unit at Ikare village (Loc. 55).

The charnockite was encountered at locations 54a and 54b. It is medium to coarse-grained and shows moderate banding of alternating medium-grained mafic and coarser-grained greenish feldspathic layers. At location 54a, it is greenish grey in color due to the mixture of some greenish mafic minerals and more dominant greyish feldspars. At location 54b, however, the rock is dark grey in color due to the dominance of mafic minerals and colorless quartz. The rock is emplaced along an E-W orientation, whereas the strike of the foliation is ENE/WSW with a dip amount of about 40º to the west.

5.3 Petrography

5.3.1 Migmatitic gneiss (host rock)

This unit is represented by samples 53b and 56. Sample 53b is coarse-grained, fairly porphyroblastic and mesocratic with alignment of minerals in a preferred direction. The mineral constituents include; garnet, biotite, quartz, plagioclase, K-feldspar, cordierite, sillimanite and spinel. Textural features such as bulbous myrmeckites and symplectites including biotite/quartz and biotite/cordierite are found in the matrix, while quartz/cordierite symplectites abound around garnets (see Figs. 5-3a, b, c and d).

The primary mineral assemblage of this rock includes; K-feldspar, plagioclase, quartz, biotite, garnet, sillimanite and spinel. Cordierite is a product of late stage reaction as it commonly surrounds garnet and sillimanite. Coarse-grained garnets are anhedral in shape and rarely contain inclusions. However, garnets are dominantly in small scattered droplets and mostly either occur near cordierite porphyroblasts or are surrounded by or in contact with cordierite/quartz symplectites (see Fig. 5-3b and d). The two noticed inclusions in garnet are quartz and magnetite. Garnet in this sample constitutes about 5-10% of the rock. Sillimanite also rarely occurs in this sample and is commonly surrounded by cordierite, biotite and plagioclase. Sillimanite make up less than 3% of the rock at this point.

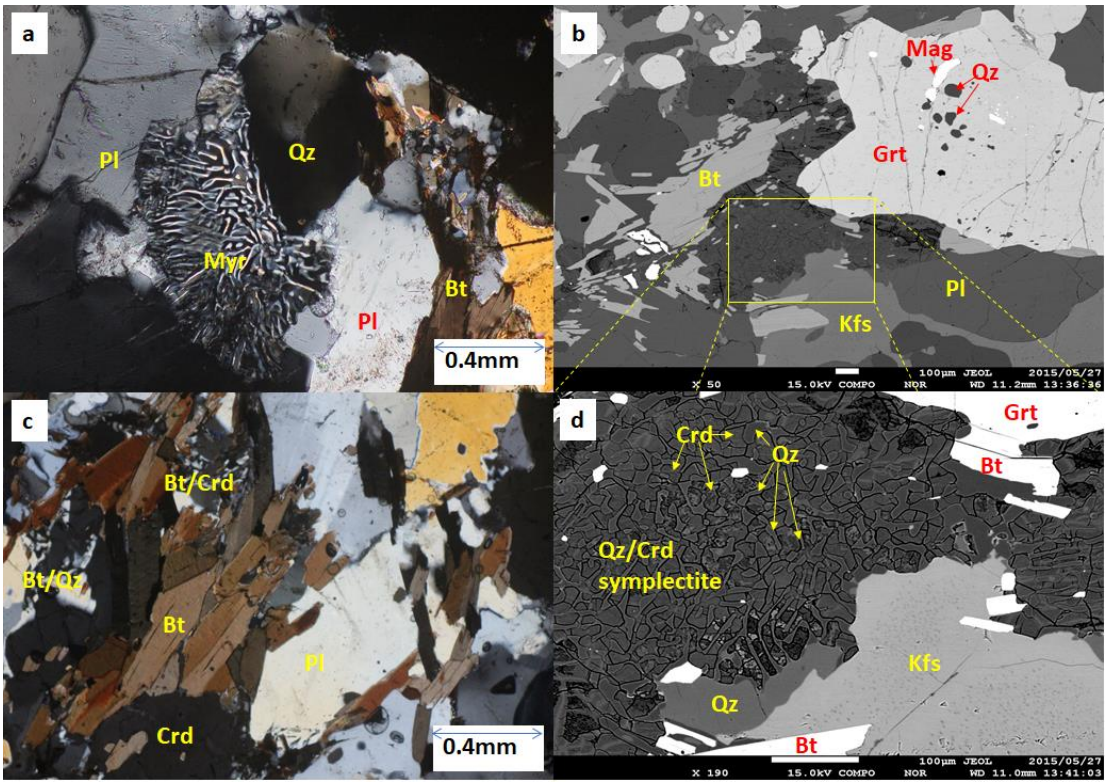

Fig. 5-3 Photomicrographs showing textures of samples discussed in this study. (a) Myrmeckitic intergrowth between quartz and plagioclase in sample 53. (b) Quartz/cordierite symplectites mantling garnet in sample 53b (BSE image). (c) Biotite/quartz and biotite/cordierite symplectites in sample 53 (XPL). (d) A magnified view of (b) (BSE image).

Biotite, which is dominantly brownish to greenish brown, is in equilibrium with cordierite, quartz, plagioclase and K-feldspar and occurs in two generations. The older and less euhedral generations form symplectites with quartz and cordierite (see Fig. 5-3c and d) and, at some points where they have contact with plagioclase, are in association with sillimanite needles. The younger generation, however, are mostly subhedral in shape with clear cleavage patterns. Their alignment defines the current foliation of the rock. They together make up about 20% of the rock.

Quartz is ubiquitous and forms the largest porphyroblasts in the rock reaching sizes of about 2.1×2.2 mm in the largest grains and about 0.15×0.1 mm in the smallest crystals. Some quartz crystals contain inclusions of sillimanite, while some quartz-plagioclase and quartz-biotite boundaries have myrmeckitic intergrowths. Quartz makes up about 35% of the rock.

Plagioclases in the rock have cloudy surfaces. The cleavage traces and twin bands are either faint or faded out at some point. The twinning style is mostly undefined-polysynthetic or

albitic, and plagioclase minerals show abundant myrmeckitic intergrowths with quartz (see Fig. 5-3a). Some plagioclase crystals show inclusions of sillimanite needles. Plagioclase together with K-feldspar constitute about 30-35% of the rock.

Sillimanite in this sample is concentrated within some irregular band with radiating and cross-cutting acicular needle sponges. It constitutes about 2% of the rock. Spinel is light greenish in plane polars. Skeletons of original spinel porphyroblast occurs in direct contact with quartz where both spinel and quartz are being altered to sillimanite, cordierite and garnet (see Fig 5-3f). It is seen to occupy the same spongy microstructure as sillimanite and is surrounded by sillimanite. The texture of spinel and quartz being altered to sillimanite, cordierite and garnet can be explained by the following reaction according to Bucher and Grapes (2011):

$$Spl + Qz = Crd + Grt + Sill \quad \text{.....(5.1)}$$

Spinel constitutes less than 1% of the rock. Ilmenite makes up about 1% of the rock.

Sample 56 is coarse-grained and mesocratic with a strong alignment of minerals in a preferred direction. The sample has grooves of intergranular diffusion channels within which lie large quantities of sillimanite needles. Mineral constituents include; quartz, biotite, cordierite, plagioclase, K-feldspar, sillimanite and garnet. Sillimanite is found in contact with many minerals including plagioclase, orthoclase, biotite and garnet - only much less with quartz (see Fig. 5-3e and f). Most sillimanite bunches are surrounded by cordierite in a replacement style. Sillimanite constitutes about 10% of the rock.

Cordierite is colorless with low relief and mostly anhedral in shape. It lacks cleavages but show partings which run orthogonal to its length. Many cordierite crystals form replacement textures around garnets, sillimanites and quartz. A single anhedral cordierite crystal measuring about 3.5 mm in length and 1.5 mm in width is observed replacing a porphyroblast of garnet and a bunch sillimanite needles. These two minerals are enveloped together and separated one from the other by cordierite in the presence of associated plagioclases, biotite and quartz (see Fig. 5-3g). Cordierite constitutes about 10% of the rock.

Plagioclase has faint traces of their twin bands. The nature of plagioclases did not allow for extinction angle measurements while plagioclase-garnet associations are among the common textural features in the rock (see Fig. 5-3h). Plagioclase constitutes about 20% of the rock.

Garnet in this sample hardly possesses inclusions though they are very robust. Garnet and sillimanite are seen being replaced by porphyroblasts of cordierite. The replacement of garnet and sillimanite by cordierite can be explained by the following reactions according to Bucher and Grapes (2011);

2Alm + 4Als + 5Qtz + nH2O = 3Crd……..……(5.2)

Quartz crystal sizes range from about 0.05×0.1 mm to as large as 1.0×3.0 mm, and it constitutes about 20% of the rock. Orthoclase makes up about 10%, biotite constitutes about 15% while garnet crystals make up about 10% of the rock. Opaque population is made up of graphite rods which constitute about 5% of the rock.

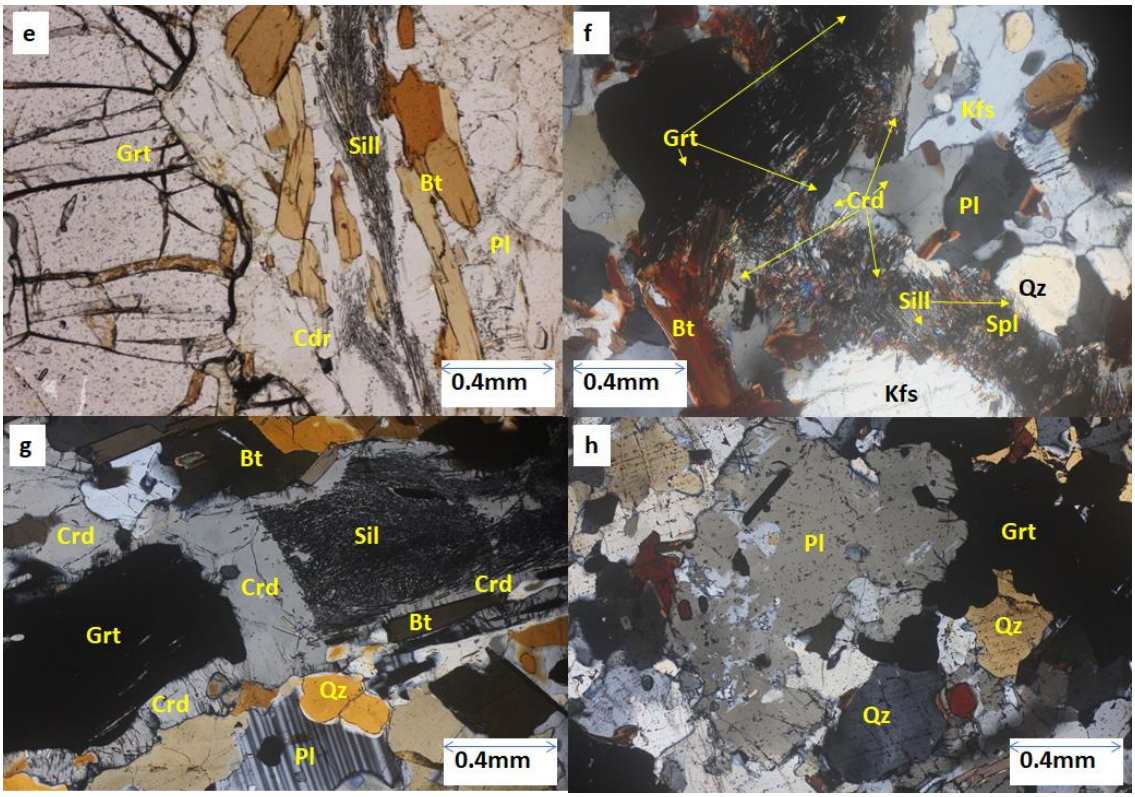

Fig. 5-3 (e) Cordierite replacing garnet and sillimanite in sample 56 (PPL). (f) Garnet-sillimanite-spinel-plagioclase-K-feldspar association in sample 53b (PPL). (g) Garnet and sillimanite and biotite being replaced by a large cordierite porphyroblast in the presence of quartz and plagioclase in sample 56 (XPL). (h) Garnet-plagioclase-quartz-biotite association in sample 56 (XPL).

5.3.2 Basic granulite (metabasites)

This unit is represented by samples 52 and 56b. Sample 52 is mesocratic and medium to coarse grained with alignment of minerals in a preferred direction. The mineral constituents include; quartz, biotite, garnet, orthopyroxene, plagioclase, apatite and zircon.

Quartz, which is colorless with low relief, is mostly anhedral in shape and many seem to be late stage as almost half of the quartz crystals in the rock tend to rap themselves around inclusions of other minerals including plagioclase, biotite, apatite, and micro-crystalline quartz. Most of the quartz crystals are irregular and elongated measuring about 0.25×1.8 mm in the largest grains and as small as 0.1×0.15 mm in the smallest grains. Quartz makes up about 20-25% of the rock.

Orthopyroxenes are restricted within some widely separated bands. They are colorless with moderate relief and show cross-cutting pyroxene cleavages. Pyroxenes are mostly coarse-grained with the smallest sizes measuring 1.0×1.6 mm, while the largest crystals measure about 1.8 mm in width and 3.0-4.0 mm in length. They are elongated along a defined direction as anhedral connected patches. In this inter-connected web-like arrangement, orthopyroxenes mantle many other crystals of mainly plagioclase and quartz (see Figs. 5-3i and j). They go into parallel extinction while others undergo slight oblique extinction. They make up 5-10% of the rock.

Garnet grows into large porphyroblast in the rock with some garnet porphyroblasts measuring approximately 2.0-2.6 mm in diameter. They are mostly anhedral to subhedral in shape. Some elongated aggregates of garnet measure about 1.2×3.5 mm. Garnet has numerous inclusions of quartz, apatite, biotite, plagioclase and opaques. Garnet makes up about 15-20% of the rock.

Plagioclase is colorless with low relief and has characteristic albite twinning. The maximum extinction angle measured is 37.5º which corresponds to labradorite composition. Average grain size of plagioclase measures about 0.5×0.5 mm. Plagioclase makes up about 25% of the rock. Biotite crystals measure between 0.05×0.1 mm in the smallest crystals to as large as 0.8×1 mm in the largest sizes. Biotite makes up about 30% of the rock. Apatite is colorless with moderate relief. It occurs both as disseminated acicular needles and as irregular patches in the

rock, occurring both in the background and as inclusions in garnet, plagioclase and quartz. It makes up less than 5% of the rock.

Sample 56b is melanocratic and porphyroblastic with medium to fine-grained groundmass and alignment of minerals in a preferred direction. The mineral constituents include; biotite, orthopyroxene, plagioclase, garnet and quartz.

Orthopyroxene in this sample occurs in skeletally growing domains and embody inclusions of apatite and microcrystalline quartz. The skeletal orthopyroxene porphyroblasts are mantling mainly plagioclase crystals (see Fig. 5-3k). It makes up about 10% of the rock.

Garnet in this sample is the main porphyroblast growing into rounded to euhedral sizes of up to 2.3 cm in diameter. Numerous inclusions of quartz, plagioclase, apatite, biotite and orthopyroxene occur in the garnet (see Fig. 5-3l). This growth of garnet and orthopyroxene can be explained by the reaction (Bowes 1989);

$$Bt = Grt + Opx + Kfs + H_2O \quad (5.3)$$

Garnet makes up about 15% of the rock.

Plagioclase also occur in lat-shaped forms, the same size as the biotites, with clear surfaces revealing unique albite twinning. Maximum extinction angle obtained is 40º which corresponds to the labradorite/bytownite composition. Plagioclase makes up about 30% of the rock. Biotite in this rock is dominantly subhedral, although euhedral biotite is also present. The mode of biotite sizes is about 0.25×0.25 mm. Biotite makes up about 25% of the rock.

Quartz population is dominated by microcrystalline sizes though one quartz grain is up to 0.25×0.25 mm in size. It makes up about 15% of the rock. Opaques (mainly ilmenite and minor magnetite) make up less than 5% of the rock. Apatite makes up less than 5% of the rock.

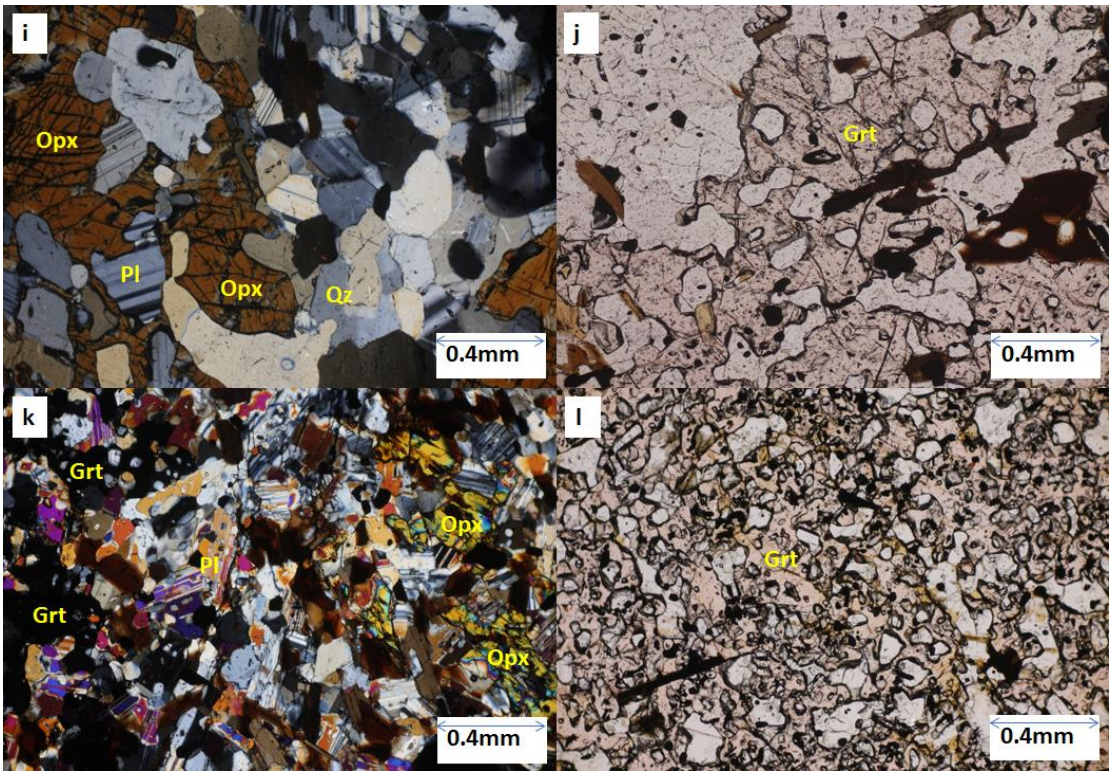

Fig. 5-3 (i) Mantling of quartz and plagioclase by a growing orthopyroxene in sample 52 (XPL). (j) Large garnet porphyroblast in sample 52 (PPL). (k) Garnet on the left and orthopyroxene on the right both growing between quartz and plagioclase crystals in sample 56b (XPL). (l) Large garnet porphyroblast with inclusions of mainly quartz and plagioclase feldspar in sample 56b (PPL).

5.3.3 Gneissic granite

This is a leucocratic coarse-grained to porphyroblastic rock with mineral alignment in a preferred direction. The mineral constituents include; quartz, microcline, plagioclase, garnet, biotite and sillimanite. This rock shows evidence that it has undergone ductile stretching in the east-west direction. Apart from the stretched features on the minerals, this rock lacks any complex textural displays.

Quartz in this rock is stretched and well fractured with most of the fracture lines being orthogonal to the direction of stretching. Quartz is anhedral and undergoes undulose extinction. It constitutes about 35% of the rock.

Garnet in this rock is rather elongated due to stretching force. It is characteristically riddled with inclusions of quartz and some small greenish biotite (see Fig. 5-3m). It measures about 0.5×1.25 mm and constitutes about 3% of the rock.

Microcline is only identifiable in the rock by faint traces of the cross-hatched twinning. All feldspars are, however, finely streaked with unusual thin lines and in the direction of stretching. Microcline makes up about 40% of the rock while plagioclase with albite twinning and thin twin bands constitute about 10% of the rock (see Fig. 5-3n).

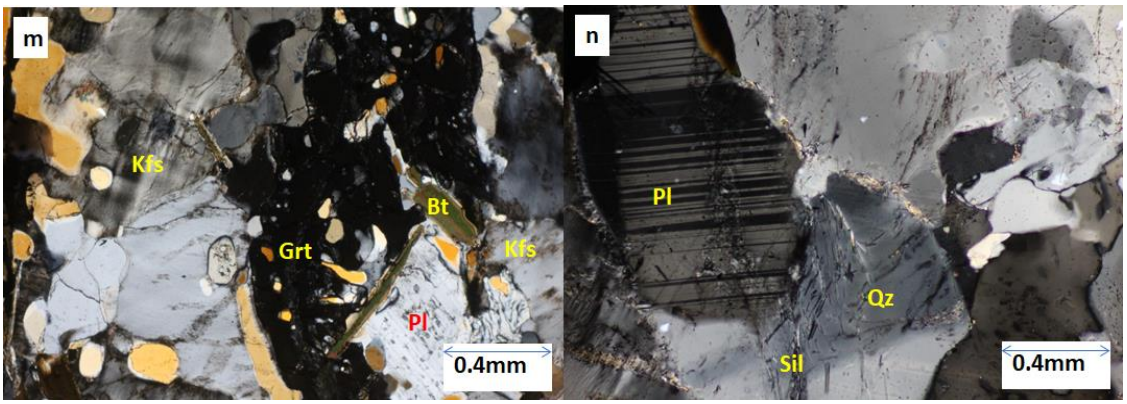

Fig. 5-3 (m) Stretched and partially crushed garnet, K-feldspar, quartz and plagioclase in sample 55 (XPL). (n) Scattered needles of sillimanite growing on plagioclase and quartz in sample 55 (XPL).

Biotite is restricted to tiny bands widely separated by larger bands of quartz and feldspar. It makes up about 10% of the rock. Sillimanite makes up less than 1% of the rock.

5.3.4 Charnockitic gneiss

This is a mesocratic rock with alignment of minerals in a preferred direction. It is medium to coarse-grained and fairly equigranular. There are numerous inclusions of microcrystalline minerals in almost all mineral phases present. These inclusions are made up dominantly of apatite, but also of quartz and zircon. Veins of quartz which measure about 0.6 mm across run through the sample creating elongated porphyroblasts of quartz in a background of equigranular mixture of quartz and other minerals. Other mineral constituents include; biotite, orthopyroxene, plagioclase and hornblende.

Quartz constitutes about 20% of the rock and biotite makes up about 5% of the rock.

Hornblende is greenish and pleochroic from light greenish brown to dark green. Skeletal patches of anhedral hornblende crystals are deep greenish and weakly pleochroic. Most hornblende crystals are light greenish brown with clear surfaces revealing the cleavages, subhedral shapes and inclusions. Their inclusions are dominated by acicular apatite and quartz. Hornblende dominates the mafic mineral population and account for about 25% of the rock.

Orthopyroxene are mainly distinguished by parallel and oblique extinctions. They together make up about 20% of the rock. Apatite constitutes about 3% of the rock while zircon is less than 1% of the rock. Ilmenite makes up about 1% of the rock.

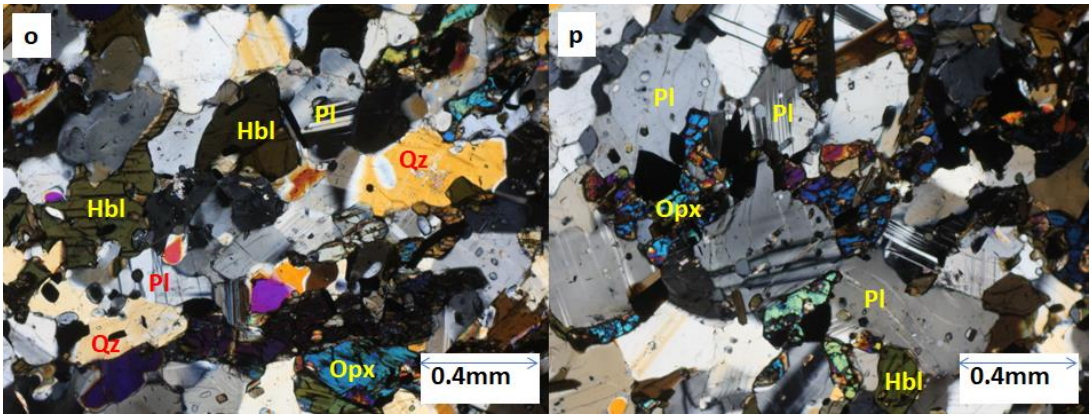

Fig. 5-3 (o) and (p) Hornblende-orthopyroxene-plagioclase-quartz association in sample 54 (XPL).

5.4 Mineral Chemistry

Below, mineral chemistry data of the examined rocks are described. Representative compositions of minerals in the analyzed samples are given in Tables 5-2, 3, 4, 5 and 6.

5.4.1 Garnet

Garnets in the study area are almandine-pyrope-grossular-sperssatine solid-solutions which are essentially homogeneous from core to rim. Differences in garnet chemistry are more pronounced from rock unit to rock unit than within a rock unit or from core to rim of a garnet. Garnets in the metabasites (samples 52 and 56B), for instance, have higher grossularite content (9.2-13.3%) than those in metagranitic and metapelitic rocks (2.2-3.4%). Spessartine contents of the garnets are also higher in the metabasites (2.1-3.7%) than in the metagranitic and metapelitic

rocks (1.0-1.2%). On the contrary, pyrope contents of the garnets are lower in the metabasites (14.7-22.0%) than in the metapelitic rocks (22.2-29.4%). Metagranitic unit, however, has the lowest pyrope content of 9.8-9.9% and highest almandine content of 85.3-85.3%. All garnets in the rocks of the study area possess high iron versus magnesium ratios with X_{Mg} ranging between 0.10 in the garnetiferous granite (sample 55) and 0.31 in the garnet-sillimanite gneiss (sample 53B). Garnet chemistry and calculated values are presented in Table 5-1.

5.4.2 Biotite

Biotites in the studied samples have varied X_{Mg} which ranged between 0.35 and 0.57. There are little or no trends attributable to rock type or unit except in the garnet sillimanite unit where X_{Mg} values are dominantly 0.52-0.59. Ti values of biotite also range between 0.44 and 0.66 pfu in all samples except in garnetiferous granite (sample 55) where the values range from 0.11-0.14 pfu. Biotite in sample 54 has Ti values of >0.6 pfu. These values are more than the ranges (Ti =0.04-0.60 apfu, X_{Mg} = 0.28 - 1.00) required according to Henry et al. (2005) for Ti-in-biotite geothermometry (see Table 5-2).

5.4.3 Orthopyroxene

Pyroxenes occur in samples 52, 54 and 56B. All pyroxenes observed in the rock units belong to the orthopyroxene series. Orthopyroxenes in the metabasites (samples 52 and 56B) have X_{Mg} values ranging between 0.40 and 0.48, while those in the charnockitic gneiss (sample 54) have X_{Mg} values which range between 0.36 and 0.37. The calcium content of all pyroxenes measured ranges between 0.01 and 0.03 pfu (see Table 5-3).

5.4.4 Calcic-amphibole

Calcic-amphibole occurs only in sample 54. All measured crystals have similar X_{Mg} values within the range of 0.37 and 0.37, with calcium content per formula unit of between 1.84 and 1.89 and Ti content of about 0.19 to 0.22 pfu. Na+K pfu content of the amphiboles ranges between 0.70 and 0.74 (see Table 5-3). Using the amphibole classification method of Leake et al. (1997), the calcic-amphibole in sample 54 plots in the field of Fe-tschermakite-hornblende (see Fig 5-4). Tschermakitic hornblende occurs in eclogites and other ultramafic rocks, amphibolites or other medium- to high-grade metamorphic rocks (Hawthorne 1983).

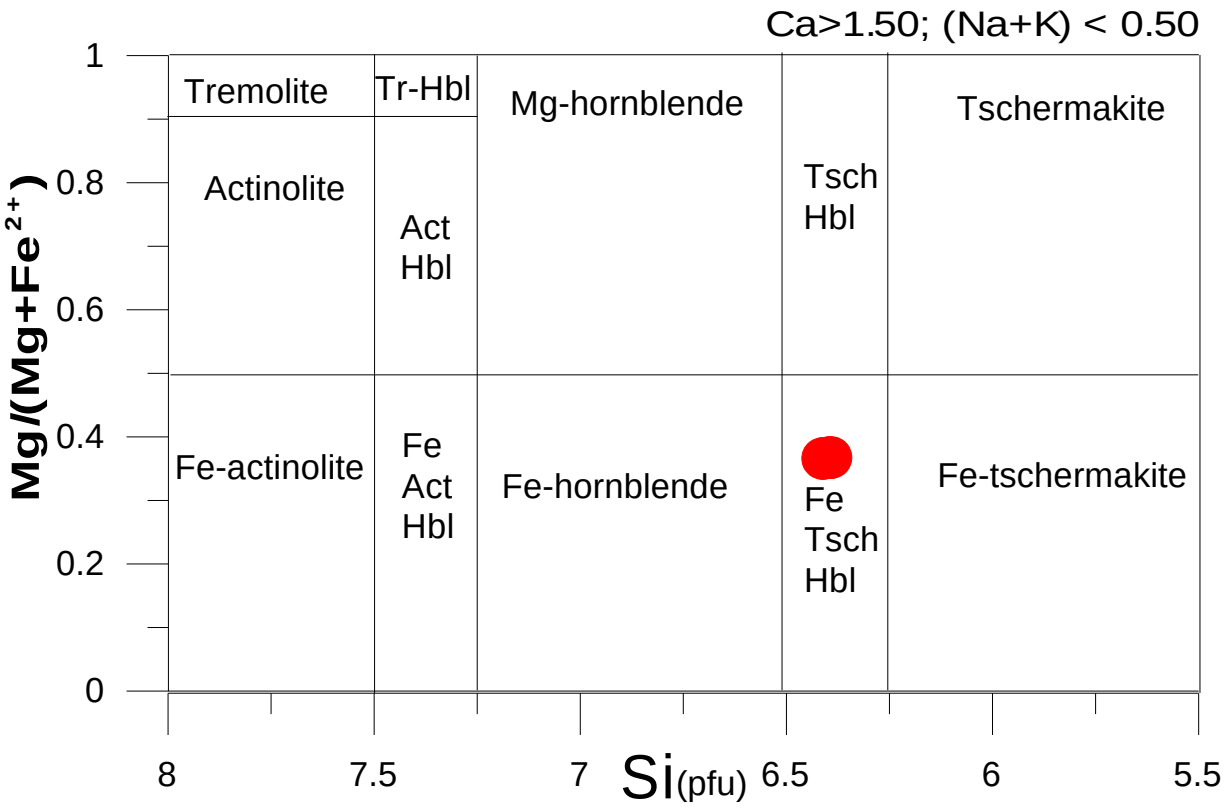

Fig. 5-4 Plot of X_{Mg} against Si^{+} for Ca-amphiboles after Leak et al. (1997).

5.4.5 Plagioclase

Plagioclase in the measured samples has varied anorthite contents with the metabasites (samples 52 and 56B) having the highest anorthite values of between $An_{67.0}$ and $An_{80.1}$. For the garnet-sillimanite gneiss (samples 53, 53B and 56), the anorthite contents of the plagioclase range between $An_{22.9}$ and $An_{33.1}$. Plagioclase in the garnetiferous granite (sample 55) has anorthite value of An_{23} while for the charnockitic gneiss (sample 54), the range is $An_{36.1}$ and $An_{39.4}$ (see Table 5-4).

5.4.6 Cordierite

Cordierite occurs in all garnet-sillimanite gneisses (the host rock) but with varied chemistry and total oxide compositions in different locations. In sample 56, the range is 97.89 to 99.09 while in sample 53, cordierite has been altered resulting in a total oxide range of 86.85 to 88.46. Cordierite in sample 56 has Na+K contents of 0.02 to 0.02 pfu, X_{Mg} range of 0.69 to 0.77,

Si range of 4.98 to 5.02 pfu and Al of 3.96 to 4.01 pfu. These suggest that cordierite in garnet-sillimanite gneisses may be of the higher-grade form $(Mg,Fe)_2Al_3(AlSi_5O_{18})$. Cordierite chemistry is presented in Table 5-5.

5.5 Metamorphic *P-T* conditions

In addition to the minerals chemistry which was used in constraining the thermo-barometric signatures of the rocks using available conventional methods, the bulk rock geochemistry of the migmatite gneiss in oxide wt.% necessary for phase equilibrium modeling was obtained. The bulk composition of sample 56 is SiO_2= 61.78, Al_2O_3 = 15.92, TiO_2 = 0.78, FeOt = 11.57, MnO = 0.1, MgO = 3.72, CaO = 1.16, Na_2O = 1.3, K_2O = 2.63, LOI = 1.17 (in wt.%). Available geothermobarometers were applied to determine peak metamorphic conditions of the pelitic schists and amphibolites. The results of *P–T* calculations are briefly summarized.

5.5.1 Garnet-biotite geothermometer

Fe–Mg exchange between garnet and biotite thermometer was used for estimating peak temperatures of metamorphism for the medium-grade pelitic metamorphic rocks. The methods of Kaneko and Miyano (2004) - a refined garnet-biotite Fe−Mg exchange geothermometer with application in amphibolites and granulites that consider the effect of Fe^{3+} and Al^{3+} contents in biotite was adopted. The result of garnet-biotite geothermometry after Kaneko and Miyano (2004) gave temperatures of 700-705 ºC for sample 52, 700 ºC for sample 53, 700 ºC for sample 53b, 590-600 ºC for sample 55, 775-780 ºC for sample 56 and 685-690 ºC for sample 56b, all at a pressure of 8 kbar.

5.5.2 Hornblende-plagioclase geothermometer

Hornblende-plagioclase geothermometer as put forward by Holland and Blundy (1994) was applied in the calculation of the peak temperatures of the metabasite (sample 54) which contained hornblende + plagioclase assemblages. This calculation is based on the reaction edenite + albite = richterite + anorthite – a quartz independent thermometry at 8 kbar. This quartz independent thermometry was chosen because it is more reliable at medium to high

temperatures and because plagioclase in the rock sample has high anorthite content ($An_{60.6-63.9}$). The calculated result gave a temperature range for the metabasite as 815-855 °C at 8 kbar.

5.5.3 Optimal thermobarometry

Optimal thermobarometry or "Average *P-T (avPT)"* calculation was carried out using the method of Powell and Holland (1994). This three-stage process begins with the raw data generated from EPMA analysis of minerals, which is fed into software called the AX-program (an activity-composition calculation program) of the same authors. The AX-program recalculates the analysis to a mineral formula and then determines the activities of mineral end-members. These end-members activities of the minerals are now applied to the *avPT* script files and run by THERMOCALC to generate the average *P-T* of the rock. THERMOCALC does this by combining the information for the several independent reactions in a least squares sense to calculate the conditions of formation. All results were obtained at greater than 95% statistical confidence level. The equations for the independent sets of reactions are presented below;

for samples 53 and 53b:

(1) gr + q + 2sill = 3an

(2) 2py + 5q + 4sill = 3crd

(3) 2alm + 5q + 4sill = 3fcrd

(4) east + py + 3q = phl + crd

(5) 10phl + 21sill = san + 9east + 6crd + H_2O

(6) 5ann + 6fcrd = 5san + 9alm + 5H_2O + 3sill,

for sample 56:

(1) gr + q + 2sill = 3an

(2) 2py + 5q + 4sill = 3crd

(3) 2alm + 5q + 4sill = 3fcrd

(4) 2phl + 9q + 6sill = 3crd + 2san + 2H_2O

(5) 3fcrd + 4ann + 3q = 6alm + 4san + $4H_2O$.

Their corresponding calculations and average *P-T* results are presented in Table 5-6. Optimal *P-T* result as calculated for the migmatite gneiss samples gave conditions of 7.4 ± 1.8 kbar and 893 ± 118°C for sample 53, 8.0 ± 1.6 kbar and 921 ± 110 °C for sample 53B, 7.7 ± 1.8 kbar and 971 ± 138 °C for sample 56, giving an average of 7.7 ± 1.7 kbar and 910 ± 122 °C for the migmatite rock unit. This result is shown pictorially in Fig. 5-5 below.

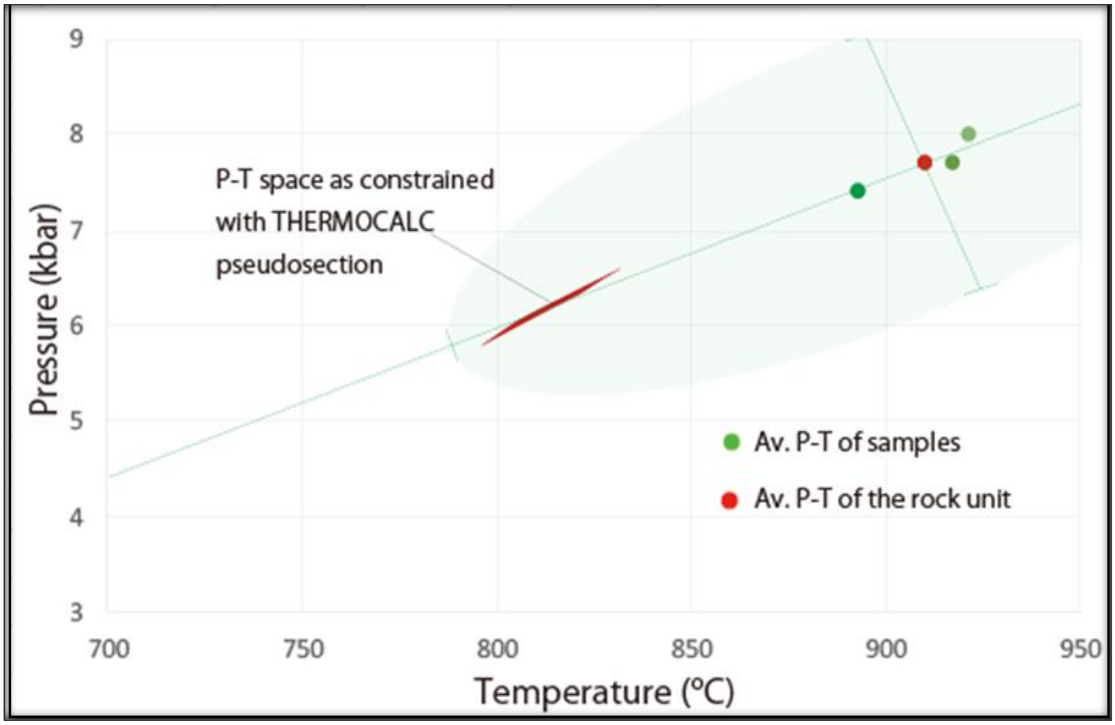

Fig. 5-5 A graphical plot of the optimal thermobarometry analysis in comparison with the P-T space constrained with THERMOCALC pseudosection.

5.5.4 Mineral equilibria modeling

The equilibrium assemblage condition was constrained in pseudosection using THERMOCALC version 3.33, with the October 2009 updated version of the Holland and Powell (1998) data set (file tcds55.txt). A model system (NCKFMASHTO) was used to calculate the pseudosection (see Fig. 5-6). Fe_2O_3 constitutes 0.78% of the bulk chemistry of the rocks suggesting that peak metamorphism was relatively in reduced condition while MnO constitutes 0.1%. Manganese was automatically eliminated in the mole percentage calculation program. All pelitic samples studied contain similar mineralogy though the minerals occur at different

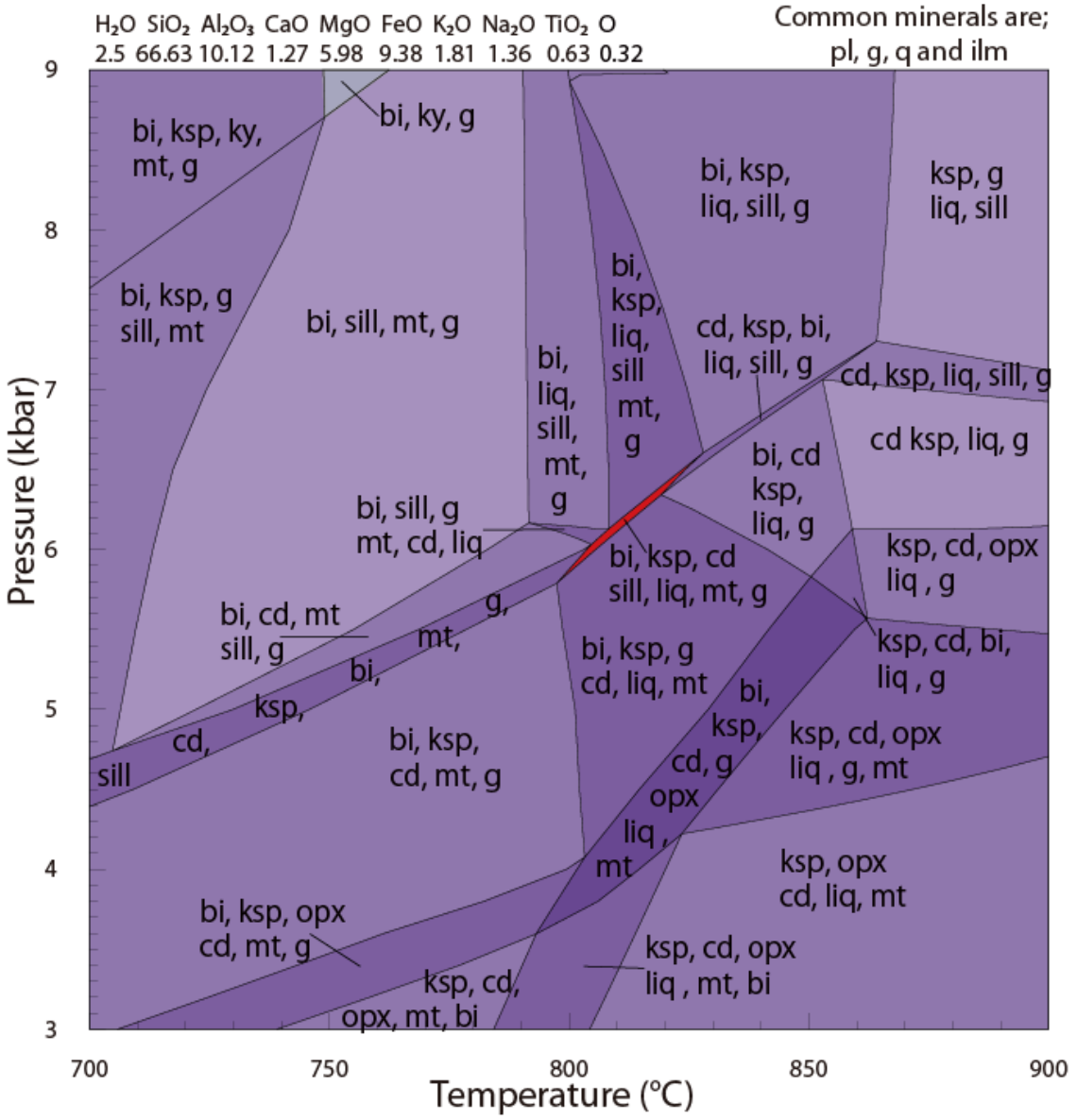

Fig. 5-6 *P–T* diagram showing calculated pseudosections of mineral assemblages in sample 56. The bulk chemistry is in mol. % while minerals abbreviations (bi = biotite, g = garnet, q = quartz, ksp = K-feldspar, pl = plagioclase, cd = cordierite, sill = sillimanite, hb = hornblende, ru = rutile, ol = olivine, sp = spinel, ilm = ilmenite, opx = orthopyroxene, ky = kyanite, ap = apatite, liq = liquid) are after Holland and Powell (1998)

quantities. Samples 53 and 53b were, however, found to have alterations and were not considered fit for pseudosection. Sample 56 was therefore selected for pseudosection calculation. For the analysis, a slab of relatively homogeneous part of the examined granulite was used for thin-section preparation, and the counterpart of the same slab was used for chemical analysis. Bulk rock composition for the rock was determined by X-ray fluorescence spectroscopy at

Activation Laboratories, Canada. The equilibrium peak assemblage in the sample includes: plagioclase + K-feldspar + garnet + biotite + sillimanite + cordierite + quartz + liquid + magnetite + ilmenite while the bulk composition in molar percentages of the oxides in the sample is SiO_2 = 66.63, TiO_2 = 0.63, Al_2O_3 = 10.12, CaO = 1.27, MgO = 5.98, FeO = 9.38, K_2O = 1.81, Na_2O = 1.36, O = 0.32, H_2O = 2.5. H_2O values of 2.5 mol.% for the sample was used because with less than this value of water, the observed equilibrium assemblage could not be constrained in the pseudosections.

The *P-T* spaces for the equilibrium assemblage (shown in red in Fig. 5-6) was constrained in the pseudosection between 790-830 ºC and 5.8-6.6 kbar for sample 56.

5.6 Discussion

The study area is basically underlain by migmatites with felsic to mafic magma intrusions. The east-west alignment of all rock units seems to suggest a greater influence of the early Pan-African episodes (Egbuniwe 1982; Boesse and Ocan 1988; Caby 1998; da Silva et al. 2005; Goodenough et al. 2014) on this part of the Nigerian basement. This fact is also supported by the dominance of the E-W foliations and very importantly the linear stretching of the minerals of the granite gneiss in that E-W direction. The granitic magma was emplaced earlier than the charnockitization of the northern pluton. This is indicated by the higher degree of metamorphism of the granite gneiss relative to the charnockite pluton and the fact that the granite gneiss bears the earlier (E-W) foliation direction while the charnockite has much weaker and dominantly N-S to NNE-SSW aligned foliations. The migmatite, however, showcases all available foliation directions beginning with the dominant E-W through NW-SE to N-S and NE-SW directions (see Fig. 5-1).

5.6.1 Equilibrium *P-T* condition

From petrographic studies, the mineral assemblage of the migmatitic gneiss showed the equilibrium mineral assemblage for the migmatites as garnet + biotite + quartz + plagioclase + K-feldspar + cordierite + sillimanite + spinel for samples 53 and 53b and garnet + biotite + quartz + plagioclase + K-feldspar + cordierite + sillimanite for sample 56. The equilibrium assemblage condition of the rock is constrained using THERMOCALC pseudosection between 790-830 ºC and 5.6-6.6 kbar (see Figs. 5-5 and 5-6).

The granite gneiss has the mineral composition of quartz + microcline + plagioclase + garnet + biotite + sillimanite. This garnet-biotite-sillimanite association in the presence of K-feldspar is index for the high-pressure, upper-amphibolite facies metamorphic grade of the KFASH (Mg-deficient) system (Bucher and Grapes 2011). In the metabasite units, however, the assemblage is quartz + biotite + garnet + orthopyroxene + plagioclase. This orthopyroxene-garnet association in metabasites on the other hand is an indication of the granulite-facies metamorphic grade. In the charnockite, the assemblage is biotite + orthopyroxene + plagioclase + hornblende. This is also a typical granulite facies assemblage.

A combination of conventional geothermobarometers including Grt-Bt-Pl geothermobarometer of Ganguly et al. (1996), Grt-Cd-Bt geothermometer of Kaneko and Miyano (2004) and Grt-Pl geobarometer of Ganguly et al. (1996) on the garnet-biotite pairs of the migmatite gneiss samples gave the core and rim temperatures as 700 ºC and 660 ºC for sample 53, 710-720 ºC and 673 ºC for sample 53b, and 775-780 ºC and 750-755 ºC for sample 56, respectively, at 6 kbar. These temperature values are indicative of upper-amphibolite facies (for samples 53 and 53b) to granulite facies (for sample 56). The values may, however, be indicative of retrograde metamorphism in all the migmatite gneiss samples when compared to the results of the THERMOCALC pseudosection. More importantly, this record shows indications of polymetamorphism of the rocks as recorded in one rock unit. For the granite gneiss, however, this same analysis gave much lower core values as 585-590 ºC. Due to the stretching of the garnet crystals, the analyzed samples were very elongate and thin. There is thus no real difference between the cores and rims. More so, ideal garnet-biotite pairs for analysis was difficult making temperature calculations unattainable.

Optimal *P-T* analysis of the rocks gave an average of 7.7 ± 1.74 kbar and 910 ± 122 °C for the migmatite gneiss rock unit. The optimal *P-T* calculation is rooted in linear programming and determines the lines of the equations of minerals formation and averages the different lines in a least-square sense for the rock. Three samples of the migmatite gneiss unit gave close results whose average is as above. This strongly suggests that the equilibrium *P-T* of the rock will most probably lie within the vicinity of this average. The variances of the pressure and temperature (± 1.7 kbar and ± 122 °C) are determined from the standard deviations by (v = s.d. × 2) and within it lies the *P-T* space of equilibration as constrained using THERMOCALC pseudosection (see Fig. 5-5). A regression line for the three samples passing through the average point also passes

through the *P-T* space of the pseudosection. According to Baldwin (2016), average *P-T* can certainly give thermobarometric information on low variance mineral assemblages, but pseudosections are likely to provide the most powerful tools for thermobarometry.

The equilibrium *P-T* conditions of the rock is thus regarded as the *P-T* space (790-830 ºC and 5.6-6.6 kbar) constrained in the pseudosection. This *P-T* corresponds to a depth of exhumation of approximately 22 km, considering the average geobaric gradient of 0.27 kbar/km for the crust. At this depth, the associated temperature (790-830 ºC) as constrained in this study is indicative of heat anomaly culminating to a heightened geothermal gradient of about 36-38 ºC/km - a common feature in granulite-facies terranes (Bohlen 1987). This depth of exhumation is a proof of the rapid rate of exhumation.

5.6.2 *P-T* path analysis

The *P-T* path of the study area is difficult to fully constrain within the scope of this work. To start with, most mineral porphyroblasts including garnet lack inclusions of prograde assemblage minerals. Some garnet porphyroblasts, however, contain inclusions of quartz and magnetite only (see Fig. 5-3b) while some others contain sillimanite only. Samples 53 and 53b contain cordierite-quartz symplectites growing between garnet and K-feldspar (see Figs. 5-3b and d). The formation of cordierite-quartz symplectites from garnet, biotite and sillimanite is a sign of decompression which could be a consequence of rapid rate of exhumation. From the western end of the migmatite gneiss unit, sample 56 showcases similar textures including replacement of garnet and sillimanite by cordierite porphyroblast (see Fig. 5-3e and g). These textures observed unequivocally signifies a decompressive regime. However, the occurrence of another texture where sillimanite and garnet have replaced spinel-quartz association leaving behind skeletons of spinel in an envelope of sillimanite needles (see Fig 5-3f) may be indicative of near isobaric cooling from a higher temperature granulite facies according to the reaction: Spl + Qz = Grt + Sill + Crd. According to Bucher and Frey (1994), a study of the equilibria between Grt-Crd-Sill-Qz reveals that at approximately 800°C under varied pressure conditions, different forward reactions are favored depending on X_{FeO} of the rock. The reaction Grt + Sill + Crd = Spl + Qz occurs at $X_{FeO} = 0.65 > x \geq 0$, the reaction Crd = Spl + Qz occurs at $0.85 > x > 0.65$, while the reaction Grt + Sill = Spl + Qz occurs at $0.9 > x > 0.85$. The X_{FeO} of the rocks of this study is constrained as 0.649, which favors the first reaction and confirms that a decompressive reaction

of the study sample will follow the part of Spl + Qz = Grt + Sill + Crd. Bucher and Grapes (2011), in an isobaric T–XFe section at 6 kbar showing the distribution of stable assemblages in metapelites in the FMASH system with Qtz-saturation, however, showed that the assemblage Grt + Crd + Sill + Spl is stable at 800-950°C and X_{Fe} of 0.55-0.8. The association of Spl + Qz represents a temperature range of >950 °C (Bucher and Grapes 2011). It follows that the *P-T* path of the study area may have followed cooling of the rock from such high temperature conditions. On the contrary, however, chemistry of spinel in the study samples show appreciable ZnO content (15.15-15.55 wt%). Structural formula determination reveals that the spinel in the samples of this study is hercynite-gahnite-spinel solution with formula: $(Fe_{0.49}Zn_{0.33}Mg_{0.25})Al_2O_4$. Such spinels also have been reported from parageneses including (l:) pelitic metasedimentary rocks which have undergone high-grade regional metamorphism (Gable and Sirns 1969; Frost 1973; Wagner and Crawford 1975) or contact metamorphism (Loomis 1972; Atkra 1978); and (2) mafic metavolcanic or metasedimentary rocks rich in cordierite and gedrite (Robinson and Jaffe 1969; Gable and Sims 1969; James et al.1978). Stoddard (1979), studied these two parageneses and showed that such ternary, zincian spinels resulted from the dehydration of Zn-enriched staurolites but he was quick to add that the spinels of his study were not in contact with quartz even though the rocks of the two parageneses commonly contained quartz. The situation of spinel in this study, however, is that the spinels contain appreciable ZnO w% and at the same time are in direct contact with quartz (see Fig 5-3f). The prograde path therefore is simply indeterminate at this level.

The granite gneiss (granitic pluton) and the metabasites (basic dykes) evidently intruded the migmatite (sediment) during the early phase of the initial (north-south) tectonic episode. They were also metamorphosed in the duration of the same (north-south) tectonic episode, perhaps at the late-stage of the compressional regime. This compressional regime created the E-W orientation of foliations and lineations preserved in both the granite gneiss and the migmatite gneiss. In Bauchi area of north eastern Nigeria, the emplacement of the fayalite-bearing monzonite is constrained by Dada and Respaut (1989) to a U–Pb age at 638±3 Ma which, considering the syn-tectonic character of the intrusion, is interpreted as the age of granulite-facies metamorphism.

The charnockitization of the northern pluton of the study area indicates low water activity – a condition which could be attained at later stage in metamorphism when water must have been extracted from the rock through partial melting or fluid infiltration. This condition probably

occurs at deep crustal levels, where the rock is associated with moderate to high pressures and CO_2 activity dominates (Frost et al. 2000). Condie and Allen (1984) constrained a pressure range of 5-6 kbar and 7.5-8 kbar for the charnockites of southern India, while Frost et al. (2000) constrained a pressure of 5-6 kbar and 775-800 °C for the charnockites formed at deeper levels of the Louis Lake batholith, a calc-alkalic pluton exposed in Wind River Range of western Wyoming. Exhumation of the charnockites of the study area may have come with sudden uplift. Such exhumation from deeper levels to the surface could have been rapid leading to rapid decompression and cooling to establish the low-pressure granulite facies constrained in samples 53 and 53b.

5.7 Conclusions

The migmatites which form the host rocks of the study area were intruded by large volumes of syn- to late-tectonic magmas including granitic and mafic compositions. The pelitic host rocks stabilized in the plagioclase + K-feldspar + garnet + biotite + sillimanite + cordierite + quartz + liquid field constrained in the pseudosection between 790-830 ºC and 5.6-6.6 kbar. The study area has signatures of early to late tectono-metamorphic episodes of the Pan-African orogeny. From the analysis of the mineralogy of the rocks, the *P-T* path cannot be easily and correctly constrained due to the occurrence in the rock of garnets and feldspar porphyroblasts with little to no inclusions making it almost impossible to constrain the prograde assemblage. The charnockite pluton in the study area may represent the deeper crustal level relative to the granite gneiss which may have intruded the migmatite gneiss at shallower crustal levels. This study envisages two stages of retrograde metamorphism including an initial near-isobaric cooling followed by a rapid decompression. The rapid exposure of deeper crustal facies is possibly due to differential uplift and erosion.

Chapter 6: Discussion and conclusions

This study has so far taken us through three case-study areas including Keffi (north-central Nigeria), Obudu (south-east Nigeria) and Akoko Ondo (south-west Nigeria) within the Nigerian Shield of Trans-Saharan Orogenic Belt. Based on the detailed studies of these localities, discussions and conclusions are drawn as presented in this chapter.

6.1 Metamorphism

In Keffi area, the metamorphic grade of the Schist Belt is upper-amphibolite. Many other basement areas of Nigeria also registered greenschist-amphibolite-facies grade. The Zuru, Karaukarau and Wonaka Schist Belts (in northwestern Nigeria) and the Ilesha Schist Belt (in southwestern Nigeria) were reported to have attained the greenschist-facies metamorphism (Turner 1983). Zeh and Holness (2003) constrained the *P*–*T* conditions of 590±20°C at 5±0.5 kbar for the Ilesha Schist Belt. Ige et al. (1998) constrained a temperature range of 570-625°C from Mokuro and llesha Schist Belt. Aliyu (2012) constrained epidote-amphibolite facies for Maru Schist Belt in northwestern Nigeria. Elueze (1981) constrained amphibolite-facies for Zungeru-Birnin-Gwari Schist Belt in northwestern Nigeria. In Iseyin-Oyan River Schist Belt in the southwestern Nigeria, Rahaman (1976b) also constrained amphibolite-facies grade. The granulite-facies terrane of Akoko area of this study retains the E-W foliation directions described as belonging to the earlier episodes of Pan-African orogeny indicating that granulite-facies metamorphism of the Pan-African orogeny most probably occurred during the earlier phases of the orogeny. This supposition is consistent with the U–Pb age reported in Dada and Respaut (1989) (638±3 Ma) which is interpreted as the age of granulite-facies metamorphism. It also suggests that the granulite-facies metamorphism of Obudu area may have occurred during the earlier phases of the orogeny and the N-S to NNE-SSW foliation directions of Obudu area may be a later invent. On the other hand, the granulite-facies metamorphism recorded in the migmatites of Akoko and Obudu areas can be tied to the proximity of these migmatites to heat sources. These migmatite terranes are intruded by large plutons. In Obudu area, it is a combination of granitic, dioritic and ultramafic intrusions while in Akoko area, the migmatite was intruded by a large granitic pluton signifying also that the age of granulite-facies metamorphism is also the age of intense magmatic activity.

Keffi area of north-central Nigeria shows the characteristics of magmatic arc setting of subduction-influenced metamorphism with higher dP/dT, while the Obudu area of eastern

Nigeria shows the characteristics of magmatic arc setting of low dP/dT type. The Akoko area of western Nigeria also shows characteristics synonymous with intra-continental rifting terrane with low dP/dT. These characteristics are shown below (Fig. 6-1a) on a diagram of metamorphic patterns by belts in relation to apparent thermal gradients and pictorially and graphically in Fig. 6-1b.

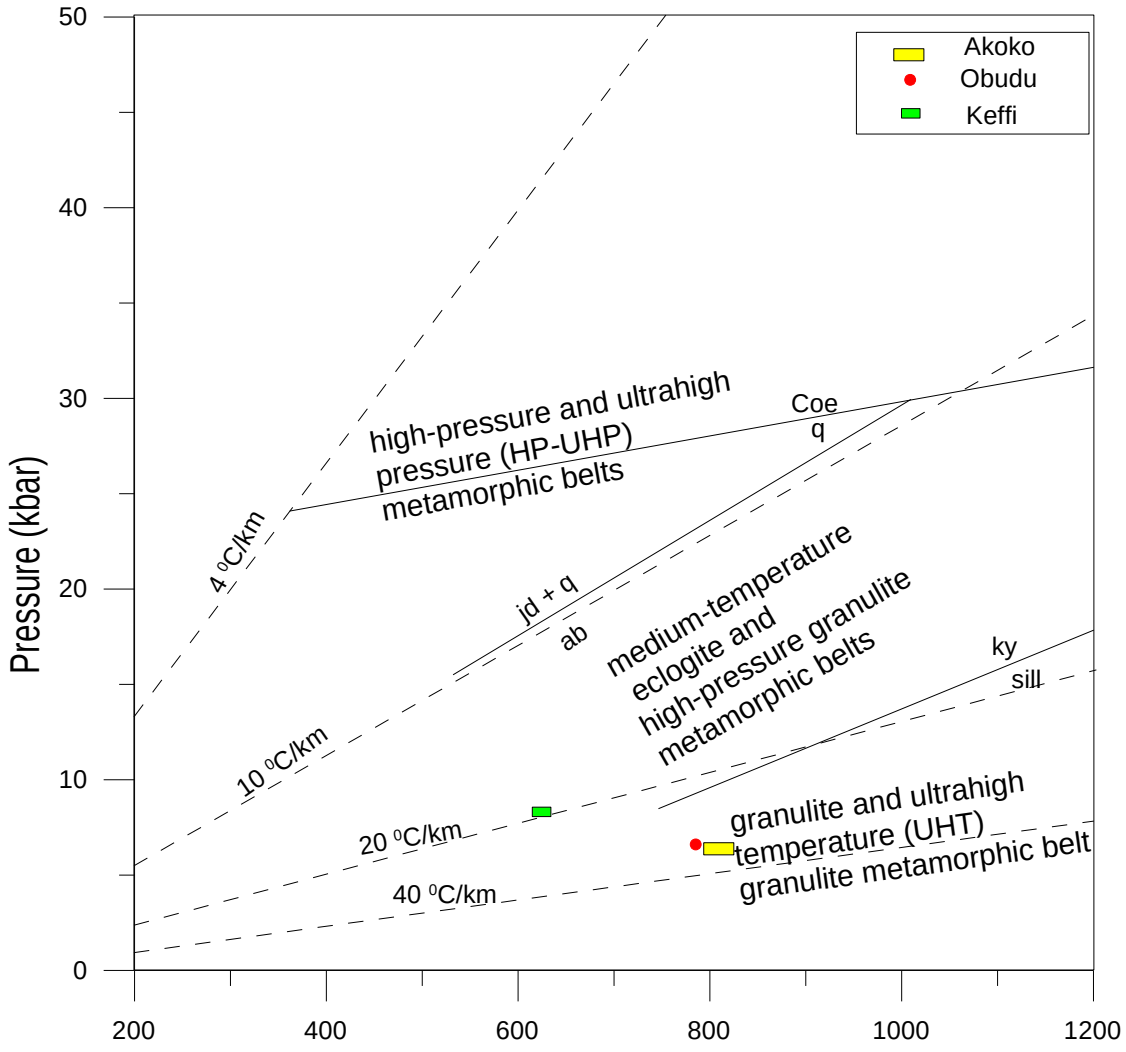

Fig. 6-1a Metamorphic patterns by belts in relation to apparent thermal gradients showing the position of *P-T* spaces for the study areas in the granulite-facies region. Modified from Brown (2006). Where Coe = coesite, Qtz = quartz, Jd = jadeite, Ab = albite, Ky = kyanite, Sill = sillimanite.

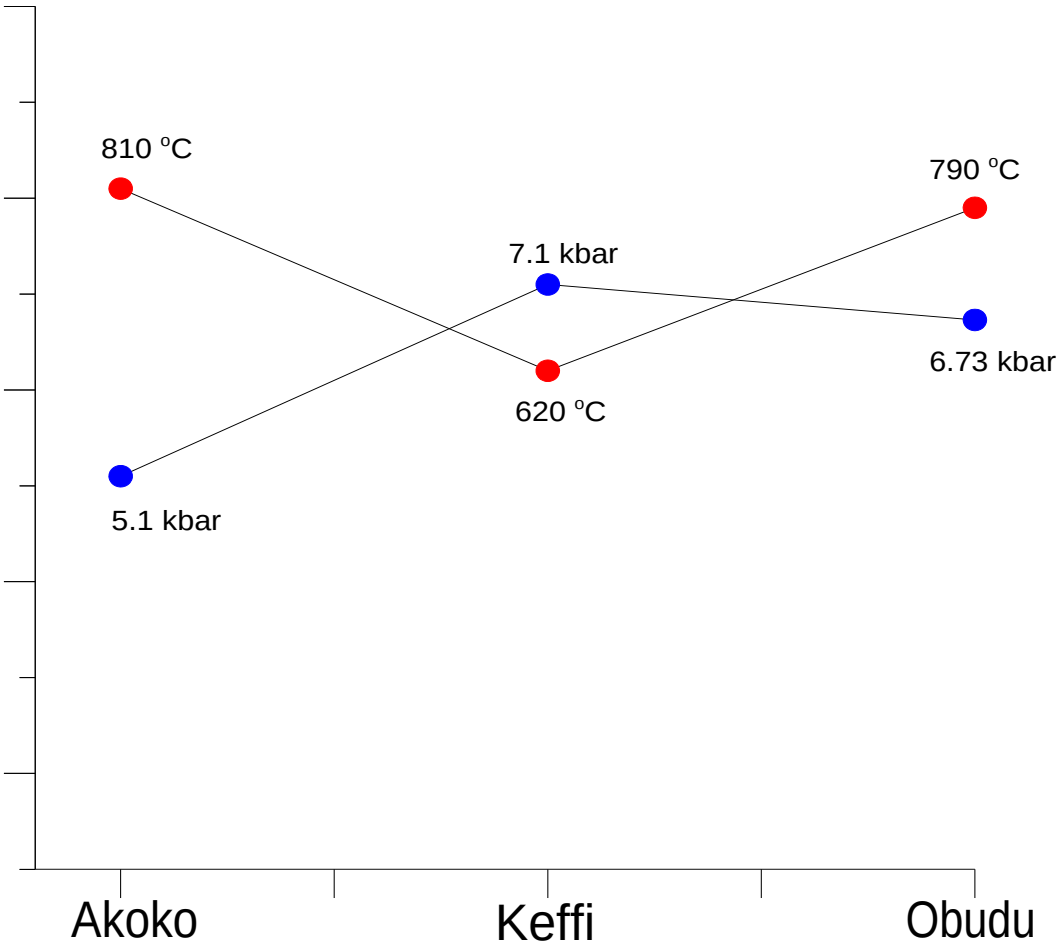

Fig. 6-1b Graphical representation of the distribution of pressure-temperature values at the three case study areas of the Nigerian basement complex

6.2 Tectonism

The metasediments including gneisses and schists absorbed and preserved the sketch of tectonic events, recording both the direction of the compressive forces and the degree of metamorphism. The late Pan-African events obliterated the original impressions of the earlier episodes of Pan-African tectonism in most parts of the basement as observed in Keffi and Obudu areas where almost all foliation and lineation directions are N-S to NNE-SSW. In Keffi area, many anticlines and synclines are observed with their axes aligned in N-S to NNE-SSW directions (see Fig. 3-2). Many researchers have dated the episodes of Pan-African tectonism and noted that the E-W foliation directions are the earliest while the N-S to NNE-SSW directions are the latest. In Akoko area, however, E-W foliation and lineation directions dominate.

Analyses of the metabasic samples from the three locations studied show inconsistent plots of same samples within arc-related fields on different diagrams. Since the Trans-Saharan Orogenic Belt is a suture zone, ordinarily, one would expect metabasaltic intrusives to plot in the calc-alkali basalt fields in variation diagrams. In the TiO_2 – (MnO×10) – (P_2O_5×10) diagram, however, sample 13 of Keffi plots in the IAT field while sample 68 of Obudu plots in the Bon region of CAB. Samples 52 and 56b of Akoko plot in the IAT/OIA boundary leaving only sample 12 of Keffi in the CAB field. In the Ti/100 – Zr – Y×3 diagram, sample 13 of Keffi plots in the within-plate basalt field while sample 68 of Obudu plots in the MORB field (see Fig. 6-2a). These trends may suggest that, in the suturing of the Orogenic Belt, many different tectonic settings including extensional settings, which reigned during ocean expansion, collisional settings initiated during ocean closure and associated calc-alkaline intrusive activities as a result of subducting slabs of oceanic micro-plates, may have left their imprints on the final products of the orogeny – in this case, the Trans-Saharan Belt.

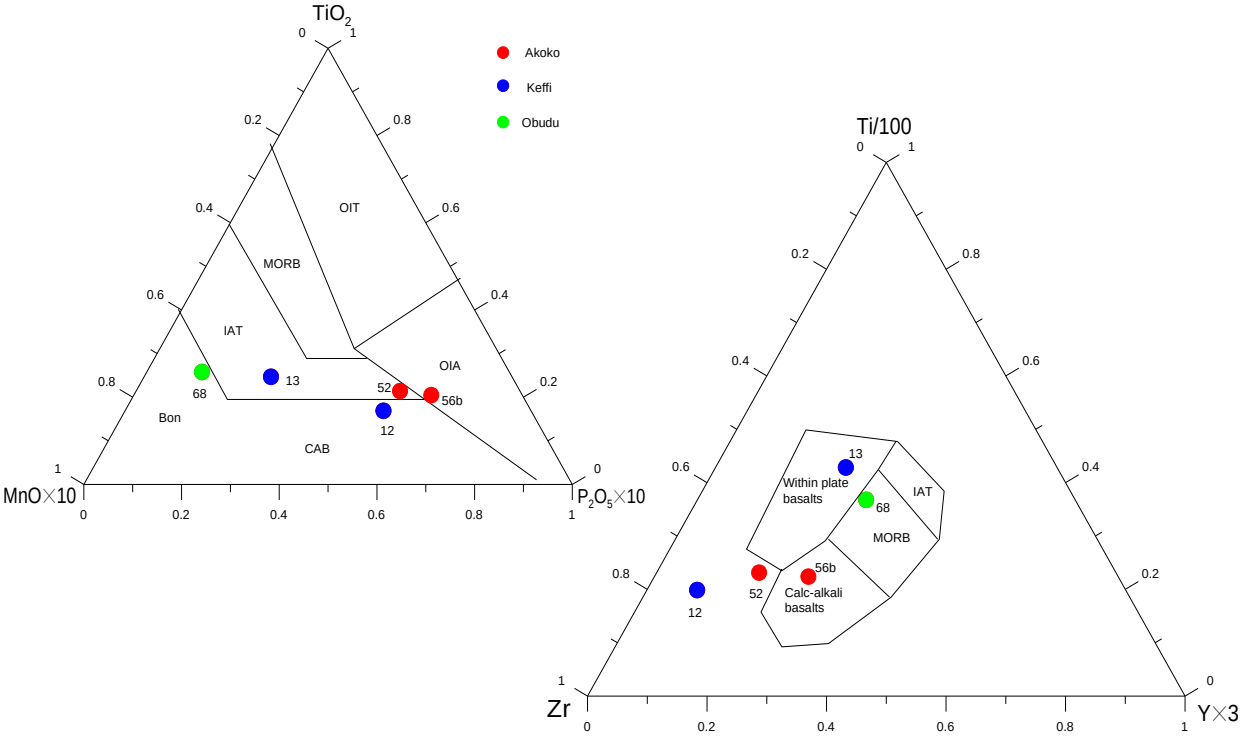

Fig. 6-2a Elemental discrimination diagrams of the metabasites of the study areas.

The results of THERMOCALC pseudo-sections of the three case-study areas show that no iron oxide phase is stable in the eastern Nigeria basement, ilmenite is stable in the central Nigerian basement while ilmenite and magnetite are stable in the western Nigerian basement.

This observation shows increase in oxygen activity in the rocks during metamorphism from east to west. The western Nigeria metasediment signature of high oxidation state, indicated by high $Fe^{3+}/(\Sigma Fe)$ = 0.06 as against 0.001 value for eastern Nigeria metasediment, may suggest that western Nigeria migmatite gneisses are metamorphosed ocean floor sediments which may have come in contact with highly oxidizing fluids that could be generated during serpentinite breakdown in subduction zones (Debret and Sverjensky 2017).

Furthermore, the occurrence of granulite-facies terranes of low dP/dT magmatic arc settings at both the eastern and western flanks of the Nigerian shield and a higher dP/dT setting at the center may strongly suggest the existence of two opposing subductions at the eastern and western margins of the belt occasioned by the opposing movements of the Congo and West-African Cratons, respectively. This phenomenon accidentally corresponds with the observations of Caby et al. (2003) on the Central-Western Hoggar area of the same Trans-Saharan Orogen (e.g. see Fig. 62b).

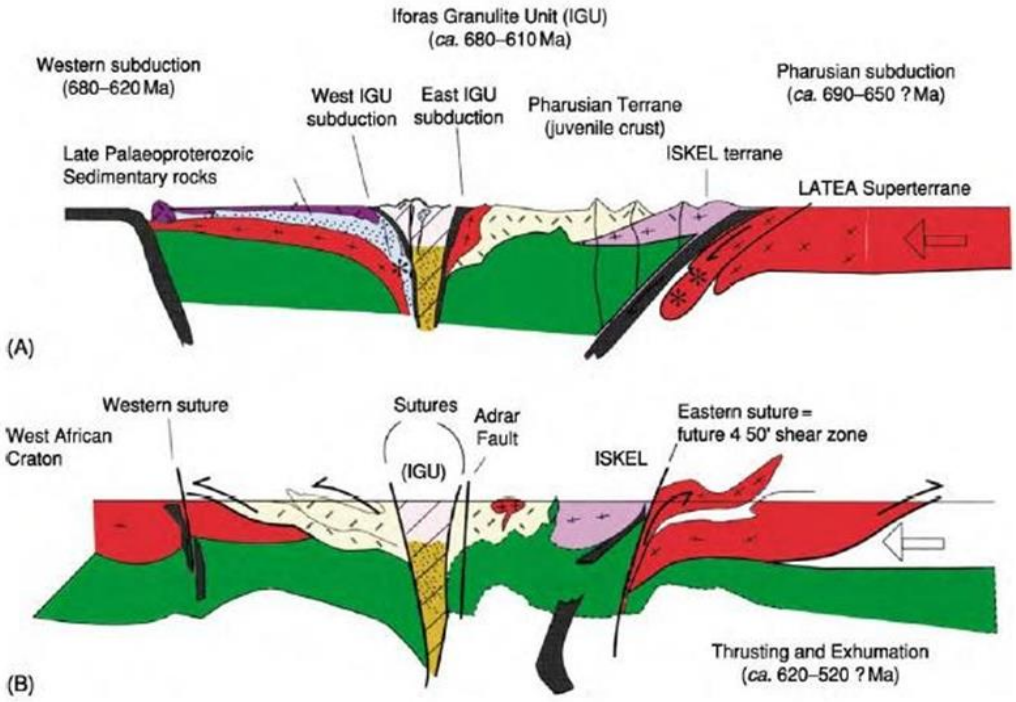

Fig 6-2b Diagrams showing the geodynamic evolution of western central Hoggar (Trans-Saharan Belt) between ~ 900 and ~ 520 Ma. Stars denote high pressure rocks now exposed. (Reproduced with permission from Caby R (2003) Terrane assembly and geodynamic evolution of central western Hoggar: a synthesis)

This study therefore adopts a modified model of Caby et al. (2003) (see Fig. 6-2c) as an effective model for the regional metamorphism/tectonism of the Trans-Saharan Orogenic Belt within the Benin-Nigerian Shield.

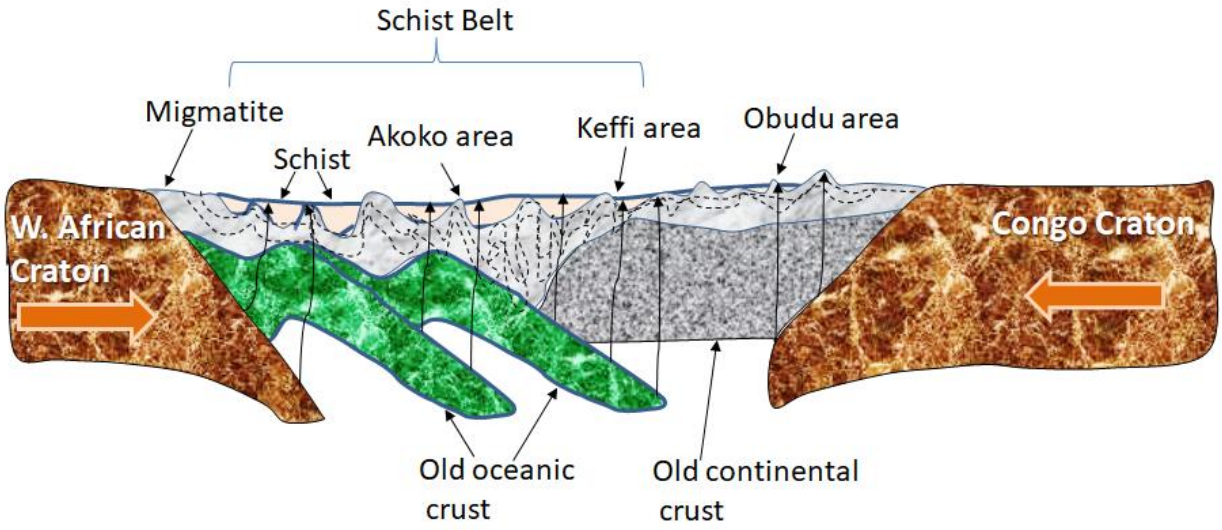

Fig. 6-2c Diagram showing the geodynamic evolution of the Benin-Nigerian shield (Trans-Saharan Orogenic Belt)

6.3 Conclusions

This study made the first detailed map of Keffi Schist Belt and observed that all pelitic samples contain Grt + Bt + Pl + Qz + Chl + Ilm, but the staurolite-bearing assemblage contains staurolites and subordinate retrograde chlorites in addition. *P–T* equilibration is within the range of 6.4-7.7 kbar and 610-630°C which is the highest *P-T* value recorded in literature for Nigerian Schist Belt (basement cover) with a clockwise *P-T* path.

In Obudu area, migmatite gneiss stabilized in granulite-facies grade at equilibrium *P-T* condition of 785-805 ºC and 6.72-6.75 kbar. The stable mineral assemblage of the rocks includes Grt + Bt + Sill + Crd + Pl + Rt + Qz + Liq. The prograde, peak and retrograde conditions of the migmatites define a clockwise *P-T* path and a magmatic-arc setting.

The metamorphic signatures including mineral assemblages and *P-T* paths constrained on the different case study areas reveal very significant variations in metamorphic response to orogenesis of a single orogenic belt.

Akoko area in southwestern Nigeria has been characterized as a granulite-facies terrane with a dominant (early Pan-African) E-W foliation and lineation directions and stable mineral assemblage of Grt + Bt + Sill + Crd + Pl + Kfs + Qz + Ilm + Mt + Liq. A *P-T* condition of 790-830 ºC, 5.6-6.6 kbar is constrained for this area.

The results of this study have proved that below the greenschist-facies basement cover exists granulite-facies terranes in parts of Western Nigeria Basement of even higher grade relative to the east. Hence, regional metamorphism of Pan-African orogeny in Nigerian shield areas as it affects the younger metasediments can be said not to have exceeded the amphibolite-facies grade, while most granulite-facies terranes are associated with intrusive activities of granitoid magmas into the migmatites.

The occurrence of low-pressure granulite terranes in both the eastern and western Nigeria and higher-pressure and medium-temperature magmatic arc setting within Nigerian centre (Keffi) show that it is likely that Nigeria is built out of two or more different opposing tectonic domains as observed also by Caby (2003) for Central-Western Hoggar.

It is based on the observation from this study that every part of this Orogenic Belt was equally affected by granulite-facies metamorphism during the early Pan-African (north-south) orogenic phases as recorded in the migmatite gneisses of this study. The late Pan-African (east-west) orogenic phases impacted maximum of amphibolite-facies metamorphism on the Orogenic Belt as recorded in the younger metasediments of Keffi Schist Belt.

Comparative analysis of pseudosections across the Nigerian Shield reveals a rapid increase in iron oxide contents of the metasediments from east to west which may signify that the migmatites in the eastern Nigerian basement were deposited on continental areas whereas the migmatites of the western terrane were deposited in a more pelagic environment.

Acknowledgements

I am very grateful first and foremost to God almighty by whose providence, I happen to be here for this research. This research work is partly sponsored by the Tertiary Education Trust Fund of Nigeria which provided the initial funds for my studies in University of Tsukuba, Japan. I am specially indebted to my supervisor Prof. T. Tsunogae for his patience, gentle guidance and invaluable academic impacts with which he ensured the success of this study. I am also grateful

to Prof. Y. Arakawa, Prof. K. Hayashi and Dr. M. Kurosawa for their invaluable academic impacts and supervisory roles.

I am very grateful to my family members (Ikechukwu, Ngozi, Chukwuma,Chukwudi, Osondu, Nkechi, Chinedu, Chika, Kelechi and Chidiebere).

I also acknowledge the assistance of the 2015/2016/2017 Ph.D. and M.Sc. students of petrology (Koizumi, Endo, Saito, Takamura, Kuribara, Takahashi, Minako, Minami, Airi, Massi, Li Tang, Pang Meng, Hikari, Eri) of the Graduate School of Life and Environmental Sciences, University of Tsukuba, Ibaraki, Japan, for their good academic interactions and assistance in carrying out the EPMA analysis.

This work was also partly sponsored by a Grant-in-Aid for Scientific Research (B) to Tsunogae from the Japanese Society for the Promotion of Science (JSPS) (No. 26302009).

And to all people of Japan, may you continue to lead the world in peace and harmony, in science and research. And may God continue to protect you and bless you all.

References;

Affaton P, Rahaman MA, Trompetre R, Sougy J., 1991. The Dahomeyide orogen: tectonothermal evolution and relationships with the Volta Basin, in: Dallmeyer RD, Lec'orc'he JP. (eds.), The West-African Orogens and Circum-Atlantic Correlatives. IGCP, Special Publications. Springer Verlag, Berlin, pp. 107-122.

Ajibade AC, Woakes M, Rahaman MA., 1987. Proterozoic crustal development in the Pan-African regime of Nigeria, in: Kroner A. (ed.), Proterozoic Lithospheric Evolution, Geophysical Union Geodynamics Series 17, 259-271.

Ajibade AC, Wright JB., 1989. The Togo Benin Nigeria Shield: evidence of crustal aggregation in the Pan-African Belt. Tectonophysics 65, 125-129.

Aliyu AI., 2012. Formation of Atoll Garnets in the banded iron formation of Maru Schist Belt. American International Journal of Contemporary Research 2, 210-221.

Ananaba SE, Ajakaye DE., 1987. Evidence of tectonic control of mineralization in Nigeria from lineament density analysis. A Landsat study. International Journal of Remote Sensing 8, 1445-1452.

Atkin BP., 1978. Hercynite as a breakdown product of staurolite from within the aureole of the Ardara Pluton. Mineralogical Magazine, 42, 237 -239.

Baldwin J., 2016. THERMOCALC Average PT Calculations. University of Montana. https://serc.carleton.edu/ research_education/equilibria/avpt.html

Bendaoud A, Ouzegane K, Godard G, Liégeois JP, Kienast JR, Bruguier O, Drareni A., 2008. Geochronology and metamorphic *P-T-X* evolution of the Eburnean granulite-facies metapelites of Tidjenouine (Central Hoggar, Algeria): witness of the LATEA metacratonic evolution. Geological Society, London, Special Publications 297, 111-146.

Berman RG., 1990. Mixing properties of Ca-Mg-Fe-Mn garnets. American Mineralogist 75, 328-344.

Black R, Caby A, Moussine-Pouchkirn E, Bayer JM, Bertranda MF, Abre J, Lesquera A., 1979. Evidence for late Precambrian plate tectonics in W. Africa. Nature 278, 223-226.

Black R, Latouche L, Liégeois JP, Caby R, Bertrand JM., 1994. Pan-African displaced terranes in the Tuareg shield (central Sahara). Geology 22, 641–644.

Boesse TN, Ocan OO., 1988. Geology and evolution of the Ife-Ilesha Schist belt southwestern Nigeria. Symposium on Benin-Nigeria geo-traverse of Proterozoic geology and tectonics of high grade terranes 87-107.

Bohlen SR., 1987. Pressure-temperature-time paths and a tectonic model for the evolution of granulites. Journal of Geology 95, 617-632.

Boullier AM., 1991. The Pan-African belt in the Hoggar shield (Algeria, Mali and Nigeria): a review, in: Dalmeyer RD, Lécorché JP. (eds.), The West African Orogen and Circum-Atlantic Correlatives. Springer Verlag, Berlin, pp. 85-105.

Bowes DR., 1989. The Encyclopedia of Igneous and Metamorphic Petrology; Van Nostrand Reinhold.

Brown M., 1998. Unpairing metamorphic belts: P–T paths and a tectonic model for the Ryoke Belt, southwest Japan. Journal of Metamorphic Geology 16, 3-22.

Brown M., 2006. A duality of thermal regimes is the distinctive characteristic of plate tectonics since the Neoarchean. Geology 34, 961-964.

Bruguier O, Dada S, Lancelot JR., 1994. Early Archean component (>3.5 Ga) within a 3.05 Ga orthogneiss from northern Nigeria: U–Pb zircon evidence. Earth and Planetary Science Letters 125, 89-103.

Bucher K, Frey M., 1994. Petrogenesis of Metamorphic Rocks. Springer-Verlag Berlin Heidelberg 319p.

Bucher K, Grapes R., 2011. Petrogenesis of Metamorphic Rocks. Springer-Verlag Berlin Heidelberg 419p.

Burke K, Dewey JF., 1972. Orogeny in Africa, *in* Dessauvagie TFW, Whiteman AJ, (eds.), Proceedings of the Ibadan Conference on African Geology, Ibadan, Nigeria. pp. 583-608.

Caby R., 1989. Precambrian terranes of Benin, Nigeria and Northeast Brazil and the late Proterozoic South Atlantic fit. Geological Society of America Special Paper 230, 145-158.

Caby R., 2003. Terrane assembly and geodynamic evolution of Central-Western Hoggar: a synthesis. Journal of African Earth Sciences 37, 133-159.

Caby R, Bertrand JML, Black R., 1981. Pan-African Ocean closure and continental collision in the Hoggar-Iforas segment, central Sahara, in: Kroner A. (ed.), Precambrian Plate Tectonics. Elsevier, Amsterdam, pp. 407-434.

Cahen L, Snelling NJ, Delhal J, Vail JR., 1984. The Geochronology and Evolution of Africa. Clarendon Press, Oxford. pp. 455-496.

Castaing C, Triboulet C, Feybesse JL, Chevremont P., 1993. Tectonometamorphic evolution of Ghana, Togo and Benin in the light of the Pan-African/Brasiliano orogeny. Tectonophysics 218, 323-342.

Cawood PA, Kröner AW, Collins J, Timothy M, Kusky AW, Mooney D, Windley BF., 2009. Accretionary orogens through Earth history; Geological Society, London, Special Publications 318, 1-36.

Cordani UG, Pimentel MM, Ganade de Araújo CE, Basei MAS, Fuck RA, Girardi VAV., 2013. Was there an ediacaran clymene ocean in central South America? American Journal of Science 313, 517-539.

da Silva LC, McNaughton NJ, Armstrong R, Hartmann LA, Fletcher IR., 2005. The neoproterozoic Mantiqueira Province and its African connections: a zircon-based U–Pb geochronologic subdivision for the Brasiliano/Pan-African systems of orogens. Precambrian Research 136, 203–240.

Dada SS., 1998. Crust-forming ages and Proterozoic crustal evolution in Nigeria: a reappraisal of current interpretations. Precambrian Research 87, 65-74.

Dada SS., 2006. Proterozoic Evolution of Nigeria, in: Oshin, O. (ed.), The Basement Complex of Nigeria and its Mineral Resources. Petrochemical Services Ltd. Ibadan, Nigeria, pp. 29-45.

Dada SS., 2008. Proterzoic evolution of the Nigeria-Boborema province, Geological Society London Special publication 294, 121-136.

Dada SS, Respaut JP., 1989. La monzonite a fayalite de Bauchi (bauchite): Nouveau emoin d'ún magmatisme syntectonique pan-africain au nord du Nigeria. Compte Rendus Academie des Sciences de Paris 309, 887-892.

Dasgupta S, Sengupta P, Fukuoka M, Bhattacharya PK., 1991. Mineral chemistry and reaction textures in metabasites from the Eastern Ghats belt, India and their implications. Journal of Geology 99, 124-133.

Debret B, Sverjensky D A., 2017. Highly oxidising fluids generated during serpentinite breakdown in subduction zones. Science reports 7, 10351.

Deer WA, Howie RA, Zussman J., 1966. An introduction to the rock-forming minerals. Addison Wesley Longman Limited. Edinburgh Gate, England. 687p.

Egbuniwe IG., 1982. Geotectonic evolution of Maru Belt, northwestern Nigeria, unpublished Ph.D thesis of the University of Wales, U.K.

Ekwueme BN., 1991. Geology of the area around Obudu Cattle Ranch, southeastern Nigeria. Journal of Mining and Geology 27, 129-134.

Ekwueme BN., 2003. The Precambrian Geology and Evolution of the Southeastern Nigerian Basement Complex. University of Calabar Press, Calabar.

Ekwueme BN, Kroner A., 1998. Single zircon evaporation ages from the Oban Massif, southeastern Nigeria. Journal of African Earth Sciences 26, 195-205.

Elueze AA., 1981. Geochemistry and petro-tectonic setting of metasedimentary rocks of the schist belt of Ilesha area, SW Nigeria. Journal of Mining Geology 19, 194-197.

Ephraim BE., 2005. Petrology and geochemistry of basement rocks in northeast Obudu area, Bamenda Massif, southeastern Nigeria. Unpublished PhD thesis, University of Calabar.

Ephraim BE, Ekwueme BN, Moazzen M, Modjarrad M., 2008. P-T conditions of Pan-African orogeny in southeastern Nigeria. Central European Geology 51, 359-378.

Ferré EC, Caby R., 2006. Granulite facies metamorphism and charnockite plutonism: examples from the Neoproterozoic Belt of northern Nigeria. Proceedings of the Geologists' Association 118, 47-54.

Ferré E, Déléris J, Bouchez JL, Lar AU, Peucat JJ., 1996. The Pan-African reactivation of contrasted Eburnean and Archaean provinces in Nigeria: structural and isotopic data. Journal of the Geological Society, London 153, 719-728.

Ferré EC, Gleizes G, Caby R., 2002. Obliquely convergent tectonics and granite emplacement in the Trans-Saharan belt of Eastern Nigeria: a synthesis. Precambrian Research 114, 199-219.

Fitches WR, Ajibade AC, Egbuniwe IG, Holt RW, Wright JB., 1985. Late Proterozoic schist belts and plutonism in NW Nigeria. Journal of Geological Society, London 142, 319-337.

Frijvald M., 1974. Low-pressure re-metamorphism of granulite and orthogneiss complexes in the Křišťanov and Prachatice Massifs (Southern Bohemia). Mineralogical Magazine 39, 612-613.

Fritz H, Abdelsalam M., Ali KA, Bingen B, Collins AS, Fowler AR, Ghebreab W, Hauzenberger CA, Johnson PR, Kusky TM Macey P Muhongo S Stern RJ, Viola G, 2013. Orogen styles in the East African Orogen: A review of the Neoproterozoic to Cambrian tectonic evolution. Journal of African Earth Sciences 86, 65-106.

Frost BR, Frost CD, Hulsebosch TP, Swapp SM., 2000. Origin of the Charnockites of the Louis Lake Batholith, Wind River Range, Wyoming. Journal of Petrology 41, 1759–1776.

Condie KC, Allen P., 1984 Origin of Archaean Charnockites from Southern India. In: Kröner A, Hanson GN, Goodwin AM. (eds) Archaean Geochemistry. Springer, Berlin, Heidelberg, pp 182-203.

Gable DJ, Sims PK., 1969. Geology and regional metamorphism of some high-grade cordierite gneisses. Front Range, Colorado. Geological Society of America Special Paper 128p.

Ganguly J, Cheng W, Tirone M., 1996. Thermodynamics of aluminosilicate garnet solid solution: new experimental data, an optimized model, and thermometric applications. Contribution to Mineralogy and Petrology 126, 137-151.

Goodenough KM, Lusty PAJ, Roberts NMW, Key RM, Garba A., 2014. Post-collisional Pan-African granitoids and rare metal pegmatites in western Nigeria: Age, petrogenesis, and the 'pegmatite conundrum' Lithos 200, 22-34.

Goscombe B, Gray D, Hand M., 2003. Variation in metamorphic style along the northern margin of the Damara Orogen, Namibia. Journal of Petrology 45, 1261-1295.

Grant NK., 1978. Structural distinction between a metasedimentary cover and a underlying basement in the 600 m.y. old Pan-African domain of northwestern Nigeria, West Africa. Geological Society of America Bulletin 89, 50-58.

Hawthorne FC., 1983. The crystal chemistry of the amphiboles. Canadian mineralogist 21, 368-386.

Henry DJ, Guidotti CV, Thomson JA., 2005. The Ti-saturation surface for low-medium pressure metapelitic biotites: implications for geothermometry and Ti substitution mechanisms. American Mineralogist 90, 316-328.

Holland T, Blundy J., 1994. Non-ideal interactions in calcic amphiboles and their bearing on amphibole-plagioclase thermometry. Contributions to Mineralogy and Petrology 116, 433-447.

Holland TJB, Powell R., 1998. An internally-consistent thermodynamic dataset for phases of petrological interest. Journal of Metamorphic Geology 16, 309-344.

Holt RW., 1982. The geotectonic evolution of the Anka belt in the Precambrian Basement Complex of N.W. Nigeria. Unpublished PhD thesis, Open Univ., Milton Keynes.

Ige OA, Okrusch M, Schussler U, Schmadicke E, Cook NJ., 1998. The metamorphosed mafic-ultramafic complex of Mokuro, llesha Schist Belt, southwestern Nigeria. Journal of African Earth Sciences 26, 593-616.

Joy BR, Evans BW., 2014. Clinoferrogedrite in the contact-metamorphosed Biwabik Iron Formation, Northeastern Minnesota. Canadian Mineralogist 52**,** 533-554.

James RS, Grieve RAF, Pauk L., 1978. The petrology of cordierite-anthophyllite gneisses and associated mafic and pelitic gneisses at Manitouwadge, Ontario. American Journal of Science 2, 4l-63.

Loomis IP., 1972. Contact metamorphism of pelitic rocks by the Ronda ultramafic intrusion, southern Spain. Geological Society of America 83, 2449-2473.

Kaneko Y, Miyano T., 2004. Recalibration of mutually consistent garnet-biotite and garnet cordierite geothermometers. Lithos 73, 255-269.

Kawakami T, Motoyoshi Y., 2004. Timing of attainment of spinel + quartz coexistence in the garnet-sillimanite leucogneiss from Skallevikshalsen, Lützow-Holm Complex, East Antarctica. Journal of Mineralogical and Petrological Sciences 99, 311-319.

Kennedy WQ., 1964. The structural differentiation of Africa in the Pan-African (±500 my) tectonic episode. Leeds University Annual Reports of the Institute of African Geology 8. 48-49.

Kerr PF., 1977. Optical Mineralogy. McGraw-Hill Inc. New York. 390p.

Kleemann U, Reinhardt J., 1994. Garnet-biotite thermometry revisited: The effect of Alvi and Ti in biotite. European Journal of Mineralogy 6, 925-941.

Kogbe CA., (Ed.), 1989. Geology of Nigeria. Rock View Publishing Company Jos, Nigeria, pp. 325-34.

Korikovsky SP, Larikova TL, Gerasimov VY., 2009. Retrograde Andalusite and Staurolite Coronas around Spinel in Garnet–Cordierite–Sillimanite–Biotite Gneisses of the Dzirula Massif (Georgia). Doklady Earth Sciences 425, 283-286.

Kretz R., 1983. Symbols for rock-forming minerals. American Mineralogist 68, 277-279.

Kröner A, Stern RJ., 2004. Pan-African Orogeny - North African Phanerozoic Rift Valley; Encyclopedia of Geology, Elsevier, Amsterdam 1, 1-12.

Kursky TM, Abdesalam M, Stern RJ, Turker RD, 2003. Evolution of the East African and related orogens, and the assembly of Gondwana. Precambrian Research 123, 81-85.

Le Breton N, Thompson AB., 1988. Fluid absent (dehydration) melting of biotite in metapelites in the early stages of crustal anatexis. Contributions to Mineralogy and Petrology 99, 226-237.

Leake BE., 1968. A catalog of analyzed calciferous and sub-calciferous amphiboles together with their nomenclature and associated minerals. Geological Society of America, Special Paper 98, 1-44.

Leake BE, Woolley AR, Arps CES, Birch WD, Gilbert MC, Grice JD, Hawthorne FC, Kato A, Kisch HJ, Krivovichev VG, Linthout K, Laird J, Mandarino JA, Maresch WV, Nickel EH, Rock NMS, Schumacher JC, Smith DC, Stephenson NCN, Ungaretti L, Whittaker EJW, Youzhi G., 1997. Nomenclature of amphiboles: Report of the Subcommittee on Amphiboles of the International Mineralogical Association, Commission on New Minerals and Mineral Names. American Mineralogist 82, 1019-1037.

Li SH, Unsworth MJ, Booker JR, Wei WB, Tan HD, Jones AG., 2003. Partial melt or aqueous fluid in the mid-crust of Southern Tibet? Constraints from INDEPTH magnetotelluric data. Geophysical Journal International 153, 289-304.

Li ZX, Bogdanova SV, Collins AS, Davidson A, De Waele B, Ernst RE, Fitzsimons ICW, Fuck RA, Gladkochub DP, Jacobs J, Karlstrom KE, Lu S, Natapov LM, Pease V, Pisarevsky SA, Thrane K, Vernikovsky V., 2008. Assembly, configuration, and break-up history of Rodinia: a synthesis. Precambrian Research 67, 179-210.

Liégeois JP, Black R, Navez J, Latouche L., 1994. Early and late Pan-African orogenies in the Aïr assembly of terranes (Tuareg shield, Niger). Precambrian Research 67, 59-88.

Locock AJ., 2014. An Excel spreadsheet to classify chemical analyses of amphiboles following the IMA 2012 recommendations. Computers & Geosciences 62, 1-11.

Malomo S., 2008. Geological Map Obudu area. Geological Survey of Nigeria, Abuja. Scale 1:100 000, 291 sheet.

McCurry P., 1976. The Geology of northern Nigeria – A review, in: Kogbe, C. (ed.), Geology of Nigeria, Lagos, Nigeria, Elizerbethan Publishers, pp. 15-39.

Morimoto N, Fabries J, Ferguson AK, Ginzburg IV, Ross M, Seifert FA, Zussman J, Aoki K, Gottardi G., 1988. Nomenclature of pyroxenes. Mineralogical Magazine 52, 535-550.

Morimoto T, Santosh M, Tsunogae T, Yoshimura Y., 2004. Spinel + Quartz association from the Kerala khondalites, southern India: evidence for ultrahigh-temperature metamorphism. Journal of Mineralogical and Petrological Sciences 99, 257-278.

Mvondo H, den Brok SWJ, Mvondo Ondoa J., 2003. Evidence of symmetric extension and exhumation of the Yaounde´ nappe (Pan-African fold belt, Cameroon). Journal of African Earth Sciences 36, 215-231.

Oberti R, Cámara F, Della Ventura G, Iezzi G, Benimoff AI., 2006. "Parvo-mangano-edenite, parvo-manganotremolite, and the solid solution between Ca and Mn^{2+} at the M4 site in amphiboles". American Mineralogist 91, 526-532.

Obiora SC., 2005. Field Descriptions of Hard Rocks with examples from the Nigerian Basement Complex, 1st ed. Snap Press Nigeria limited. Enugu.

Okezie CN., 1974. Geological Map of Nigeria, Scale 1:2,000,000. Geological Survey of Nigeria, Abuja.

Onyeagocha AC, Ekwueme BN., 1990. Temperature-pressure distribution patterns in metamorphosed rocks of the Nigerian Basement Complex - a preliminary analysis. Journal of African Earth Sciences 11, 83-93.

Oyinloye AO., 2011. Geology and Geotectonic Setting of the Basement Complex Rocks of south Western Nigeria; Implications on Provenance and Evolution. In: Dar IA (ed.), Earth and Environmental Intech Publishers Croatia, 98-118.

Pereira MD, Bea F., 1994. Cordierite-producing reactions in the PEÑA NEGRA Complex, Avila Batholith, Central Spain: The key role of cordierite in low-pressure anatexis. The Canadian Mineralogist 32, 763-780.

Pidgeon RT, Van Breemen O, Oyawoye MO., 1976. Pan-African and earlier events in the basement complex of Nigeria. 25th IGC, Sydney., Abstracts 3, 667.

Powell R, Holland TJB., 1988. An internally consistent dataset with uncertainties and correlations; 3. Applications to geobarometry, worked examples and a computer program. Journal of Metamorphic Geology 6, 173-204.

Powell R, Holland TJB., 1994. Optimal geothermometry and geobarometry. American Mineralogist 79, 120-133.

Rahaman MA., 1976a. Review of the basement geology of south-western Nigeria, in; Kogbe CA. (ed.), Geology of Nigeria, Elizabethan Publishers, Lagos, pp. 41-58.

Rahaman MA., 1976b. Progressive polyphase metamorphism in pelitic schists around Aiyetoro, Oyo State, Nigeria. Journal of Minning and Geology 13, 33-44.

Rahaman MA., 1988. Recent advances in the study of the basement complex of Nigeria, in: Precambrian Geology of Nigeria. Geological Survey of Nigeria, pp. 11-43.

Robinson P, Jaffe HW., 1969. Aluminous enclaves in gedrite-cordierite gneiss from southwestern New Hampshire. American Journal of Science 267, 389-421.

Santosh M., 1987. Cordierite gneisses of south Kerala, India; Petrology, fluid inclusions and implications for crustal uplift history. Contributions to Mineralogy and Petrology 96, 343-356.

Spear FS, Florence FP., 1992. Thermobarometry in granulites: Pitfalls and new approaches. Journal of Precambrian Research 55, 209-241.

Spear FS, Kohn MJ, Florence F, Menard T., 1990. A model for garnet and plagioclase growth in pelitic schists: Implications for thermobarometry and P-T path determinations: Journal of Metamorphic Geology 8, 683-696.

Stoddard EF., 1979. Zinc-rich hercynite in high-grade metamorphic rocks: a product of the dehydration of staurolite. American Mineralogist 64, 736-741.

Touret JLR, Huizenga JM., 2012. Fluid-assisted granulite metamorphism: A continental journey. Gondwana Research 21, 224–235.

Tuccillo ME, Essene EJ, Van der Pluijm BA., 1990, Growth and retrograde zoning in garnets from high-grade metapelites; Implications for pressure-temperature paths. Geology 18, 839-842.

Turner DE., 1983, Upper proterozoic schists belts in the Nigerian sector of the Pan-African province of West Africa. Precambrian Research 21, 55-79.

Ugwuonah EN., Obiora SC., 2011. Geothermometric and Geobarometric signatures of metamorphism in the Precambrian Basement Complex rocks around Keffi, North-central Nigeria. Ghana Journal of Science 51, 73-87.

Ukaegbu VU, Beka FT., 2009, Rare-earth and trace element imprints on the origin and tectonic setting of gabbro-diorite complex in the Pan-African belt of Southeast Obudu Plateau, Nigeria. Chinese Journal of Geochemistry 28, 239-247.

Umberto GC, Marcio MP, Carlos EG, Reinhardt AF., 2013. The significance of the Transbrasiliano-Kandi tectonic corridor for the amalgamation of West Gondwana. Brazillian Journal of Geology, São Paulo 43, 583-597.

Umeji AC, Caen-Vachette M., 1991. Geochronology of a rhyolite dyke from Nassarawa-Egon in Central Nigeria. Geologische Rundschau 80, 171-177.

Wagner ME, Crawford ML., 1975. Polymetamorphism of the Precambrian Baltimore Gneiss in southeastern Pennsylvania. American Journal of Science 275, 653-682.

Westerhof AB, Härmä P, Isabirye E, Katto E, Koistinen T, Kuosmanen E, Lehto T, Lehtonen M I, Mäkitie H, Manninen T, Mänttäri I, Pekkala Y, Pokki J, Saalmann K, Virransalo P, 2014. Geology and Geodynamic Development of Uganda with Explanation of the 1:1,000,000 - Scale Geological Map. Geological Survey of Finland 55, 387 p.

Whitney DL, Evans BW., 2010. Abbreviations for names of rock-forming minerals. American Mineralogist 95, 185-187.

Woakes M, Rahaman MA, Ajibade AC., 1987. Some metallogenic features of the Nigerian basement. Journal of African Earth Sciences 6, 655-664.

Wright EP., 1971. Basement Complex. Geological Survey of Nigeria Bulletin, 32, 12-47.

Wu CM., 2015. Revised empirical garnet–biotite–muscovite–plagioclase geobarometer in metapelites. Journal of Metamorphic Geology 33, 167-176.

Yonta-Ngoune C, Nkoumbou C, Barbey P, Le Breton N, Montel J, Villieras F., 2010. Geological context of the Boumnyebel talcschists (Cameroon): inferences on the Pan-African belt of central Africa. Geoscience, 1-8.

Zeh A, Holness MB., 2003. The effect of reaction overstep on garnet microtextures in metapelitic rocks of the Ilesha Schist Belt, SW Nigeria. Journal of Petrology 44, 967-994.

Appendix I: Methodology

I.1 Field investigation

The field work of this research is the basis upon which the entire study rests and by which the study is relevant. So, from the onset, a detailed and painstaking approach was giving to the field work. It began with intensive table study of the Nigerian basement geology to isolate areas with the best representative characteristics. These characteristics includes for instance; areas that have received little to no attention in previous literatures, areas with special structural outcrops and areas that may possibly expose outcrops of all lithostratigraphic units of the basement geology. This exercise was followed by investigative field works. The first of these which began on 2nd October 2014, lasted for ten days and took me through the southeastern Nigerian basement covering Netim and Obudu in northern Cross-River state through Ushongo and Wukari to Takum and from Sabongida stalin village to Jalingo in Benue state, through Gombe state and Bauchi in the Northeast Basement to Jos and Kigimi-Katabu vilages in Kaduna state and lastly to Abuja in central Nigeria. The second phase of the investigative field work was from 19th March 2015 till 26th March 2015. This field work which covered some southwestern areas started in Abeokuta-Ibadan areas, took me to Ilorin villages in Kwara state and from Minna to Kaduna areas and through Abuja to Keffi-Akwanga areas to Toto and Laminga villages and to Imo-Arigidi, Ikare and Ogbagi areas in Akoko, Ondo state and lastly to Igarra villages in Edo state.

After a comprehensive table study of the work so far, in combination with the detailed field work, I carried out in Keffi areas during my Second-Degree project, four case study areas were isolated for this study which includes Keffi (North-central Nigeria), Obudu (Southeastern Nigeria), Akoko (Southwestern Nigeria) and Igarra (Southwestern Nigeria). The first three areas were fully studied and reported in this work while the knowledge gathered in the field work and preliminary laboratory studies of the fourth area are all part of the knowledge we now showcase.

Detailed field work on Obudu areas took place between 30th March 2015 and 8th April 2015 while that of Igarra and Akoko areas were mapped on 17th December 2015 to 24th December 2015 and 19th January 2016 to 25th January 2016 respectively. These detailed field works precipitated the information used to redraw the geologic maps of the two areas, remove

the schistose unit which appears in the geologic map of Akoko area of (Malomo, 2006) and identify two tectono-metamorphic signatures on the same migmatite gneiss unit of Akoko area.

I.2 Petrology and EMPA

Electron microprobe analysis (EMPA) for mineral chemistry was carried out using an electron microprobe analyzer (JEOL JXA8530F) at the Chemical Analysis Division of the Research Facility Center for Science and Technology, University of Tsukuba, Japan. The analyses were performed under conditions of 15 kV accelerating voltage and 10 nA sample current, and the data were regressed using an oxide-ZAF correction program supplied by JEOL.

I.3 Whole rock geochemistry

For the analysis, the counterpart slabs of relatively homogeneous part of the examined granulites used for thin-section preparation, was used for chemical analysis. Bulk rock compositions for the rocks were determined by X-ray fluorescence spectroscopy at Activation Laboratories, Canada.

Appendix II: Analytical data

Table 3-1. Modal analysis of the rocks discussed in this study.

	Metasediments (schist)					Metabasites	
Sample No.	K1	K10a	K10b	K17	K26	K12	K16
Quartz	55-60	30-35	25-30	55-60	50-55	5-10	15-20
Plagioclase	3-5	10-15	10-15	2-5	2-5	15-20	15-20
K-feldspar/ Microcline	<3			<2			
Biotite	30-35	30-35	30-35	35-40	25-30	20-25	
Muscovite	2-5	15-20	15-20	<5			
Staurolite		2-5					
Garnet	5-10	2-5	2-5	<2	<3		
Clinopyroxene						30-35	
Hornblende						18-23	60-70
Chlorite		<2	5-10		15-20		
Zircon	<1	<2		<1			
Apatite	<1	2-5	1-2				
Titanite						1-2	2-5
Ilmenite		<5	<10	<3	2-5	1-2	2-5
Graphite				<2			

Table 3-2. Chemistry of garnet (O=12) from staurolite-garnet-biotite schist (sample K10a) and garnet-biotite schist (samples K1, K26 and K17).

Sample No.	K10a			K1		K26		K17	
Remarks	Core	Mantle	Rim	Core	Rim	Core	Rim	Core	Rim
SiO_2	37.60	37.45	37.60	37.34	37.08	36.95	37.04	37.02	37.25
Al_2O_3	21.08	21.10	21.26	20.43	20.42	20.54	20.72	20.98	20.70
TiO_2	0.00	0.04	0.00	0.00	0.03	0.00	0.01	0.00	0.00
Cr_2O_3	0.00	0.00	0.02	0.03	0.02	0.04	0.00	0.04	0.00
FeO*	33.10	32.83	32.37	29.74	29.86	32.11	31.60	27.36	26.23
MnO	5.87	5.83	6.26	8.76	8.39	7.27	7.37	12.51	13.05
MgO	2.84	2.75	2.41	2.50	2.62	2.29	2.21	1.65	1.32
CaO	1.10	1.35	1.69	2.05	1.97	1.40	1.11	1.63	2.39
Na_2O	0.00	0.01	0.01	0.07	0.06	0.01	0.00	0.03	0.06
K_2O	0.00	0.00	0.01	0.00	0.00	0.00	0.00	0.00	0.00
Total	101.62	101.40	101.67	100.93	100.47	100.61	100.06	101.22	101.00
Si	2.997	2.992	2.996	3.070	3.068	3.003	3.042	3.050	3.022
Al	1.980	1.986	1.996	1.932	1.930	1.975	1.951	1.944	1.963
Ti	0.000	0.002	0.000	0.001	0.001	0.001	0.001	0.001	0.001
Cr	0.000	0.000	0.001	0.001	0.001	0.001	0.001	0.001	0.001
Fe^{2+}	2.206	2.192	2.156	2.116	2.131	2.177	2.143	2.137	2.160
Mn	0.396	0.394	0.422	0.411	0.407	0.414	0.412	0.411	0.413
Mg	0.337	0.328	0.287	0.293	0.307	0.314	0.302	0.303	0.308
Ca	0.094	0.116	0.144	0.134	0.117	0.119	0.127	0.125	0.123
Na	0.000	0.002	0.002	0.001	0.001	0.001	0.001	0.001	0.001
K	0.000	0.000	0.001	0.000	0.000	0.000	0.000	0.000	0.000
Total	8.013	8.014	8.007	7.963	7.966	8.008	7.982	7.977	7.995
Mg/(Fe+Mg)	0.133	0.130	0.117	0.122	0.126	0.126	0.123	0.124	0.125
Alm %	72.7	72.4	71.6	71.6	72.0	72.0	71.8	71.8	71.9
Sps %	13.1	13.0	14.0	13.9	13.7	13.7	13.8	13.8	13.8
Prp %	11.1	10.8	9.5	9.9	10.4	10.4	10.1	10.2	10.2
Grs %	3.1	3.8	4.8	4.5	3.9	3.9	4.2	4.2	4.1

FeO* as total Fe

Table 3-3. Chemistry of muscovite (O=22) and plagioclase (O=8) in staurolite-garnet-biotite schist (sample K10a), garnet-biotite schist (samples K1 and K17), metabasic schist (sample K12) and amphibolite (sample K16).

	K10a			K1		K17		K12		K16	
Mineral name	Ms		Pl	Ms	Pl	Ms	Pl	Pl	Pl	Pl	Pl
Remarks	Core	Core	Core	Matrix	Core	Matrix	Core	Core	Rim	Core	Rim
SiO_2	46.20	46.88	65.32	46.15	64.30	44.88	61.55	59.16	59.40	58.60	59.23
Al_2O_3	35.18	36.51	22.79	35.33	22.72	34.52	24.77	25.65	26.08	26.09	26.47
TiO_2	0.39	0.39	0.01	0.37	0.00	0.65	0.00	0.03	0.01	0.00	0.00
Cr_2O_3	0.00	0.05	0.00	0.02	0.00	0.00	0.01	0.05	0.01	0.00	0.00
FeO*	1.34	1.11	0.09	0.87	0.04	1.15	0.20	0.04	0.19	0.03	0.05
MnO	0.03	0.01	0.05	0.00	0.00	0.01	0.08	0.01	0.03	0.00	0.04
MgO	0.56	0.33	0.00	0.52	0.00	0.70	0.00	0.00	0.03	0.00	0.00
CaO	0.05	0.01	3.55	0.01	3.77	0.00	5.92	7.60	7.56	7.78	7.94
Na_2O	1.53	1.72	10.08	1.37	9.96	0.81	8.37	7.43	7.41	7.37	7.39
K_2O	8.88	8.89	0.06	8.98	0.08	10.22	0.06	0.09	0.16	0.15	0.10
Total	94.18	95.89	102.03	93.61	100.86	92.94	100.94	100.06	100.88	100.01	101.20
Si	6.184	6.150	2.829	6.196	2.818	6.130	2.711	2.641	2.632	2.620	2.617
Al	5.549	5.643	1.163	5.588	1.173	5.556	1.286	1.349	1.362	1.375	1.378
Ti	0.040	0.038	0.000	0.037	0.000	0.067	0.000	0.001	0.000	0.000	0.000
Cr	0.000	0.005	0.000	0.002	0.000	0.000	0.000	0.002	0.000	0.000	0.000
Fe^{2+}	0.150	0.121	0.003	0.097	0.001	0.131	0.007	0.001	0.007	0.001	0.002
Mn	0.003	0.001	0.002	0.000	0.000	0.002	0.003	0.000	0.001	0.000	0.002
Mg	0.112	0.064	0.000	0.104	0.000	0.143	0.000	0.000	0.002	0.000	0.000
Ca	0.007	0.002	0.165	0.001	0.177	0.000	0.279	0.363	0.359	0.372	0.376
Na	0.398	0.437	0.846	0.357	0.846	0.214	0.714	0.643	0.636	0.639	0.632
K	1.516	1.488	0.003	1.537	0.004	1.779	0.003	0.005	0.009	0.009	0.006
Total	13.959	13.950	5.014	13.919	5.020	14.022	5.004	5.006	5.009	5.016	5.012
An %			16.3		17.3		28.1	36.1	36.1	36.8	37.3

FeO* as total Fe

Table 3-4. Chemistry of staurolite (O=48), chlorite (O=28), biotite (O=22), clinopyroxene (O=6), magnesio-hornblende (O=23) and actinolite (O=23) in staurolite-garnet schist (sample K10a), metabasites (samples K12 and K16) and garnet-biotite schists (samples K1, K17, and K26).

Sample No.	K10a				K12					K16			K1	K17	K26
Mineral name	St		Chl	Bt	Cpx		Bt	Mg-Hbl		Act	Mg-Hbl		Bt	Bt	Bt
Remarks	Matrix	Rim	Core	Matrix	Core	Rim	Matrix	Core	Rim	Core	Core	Rim	Matrix	Matrix	Matrix
SiO_2	27.49	27.27	24.80	36.45	53.91	53.99	37.80	49.78	48.30	53.32	45.65	46.14	35.72	35.38	35.32
Al_2O_3	53.70	54.14	23.51	19.34	1.04	0.79	14.72	7.05	7.86	3.30	9.52	9.53	19.54	19.24	19.88
TiO_2	0.52	0.52	0.08	1.55	0.00	0.06	2.34	0.58	0.93	0.09	1.09	0.97	1.53	2.05	1.79
Cr_2O_3	0.03	0.00	0.00	0.03	0.04	0.00	0.12	0.12	0.13	0.02	0.00	0.00	0.05	0.01	0.14
FeO*	13.75	13.80	23.51	18.88	7.40	8.12	15.07	12.23	12.93	13.41	16.44	16.76	18.83	19.13	17.96
MnO	0.34	0.33	0.21	0.09	0.39	0.51	0.23	0.36	0.42	0.34	0.34	0.35	0.10	0.29	0.19
MgO	1.75	1.73	15.38	10.57	13.66	13.46	14.60	14.31	13.57	14.96	10.83	10.73	10.32	9.27	9.62
CaO	0.00	0.01	0.01	0.00	23.86	23.97	0.00	12.42	12.33	12.51	12.39	12.27	0.01	0.00	0.00
Na_2O	0.07	0.07	0.01	0.40	0.39	0.30	0.11	0.79	0.87	0.42	0.98	0.91	0.33	0.16	0.46
K_2O	0.00	0.00	0.02	8.83	0.02	0.01	9.63	0.56	0.70	0.19	0.95	0.88	8.79	9.08	8.78
ZnO	0.90	1.08								0.00					
Total	98.55	99.0	87.65	96.26	100.70	101.20	94.61	98.21	98.04	98.55	98.19	98.55	95.21	94.60	94.13
Si	7.957	7.872	5.178	5.449	1.990	1.991	5.694	7.187	7.035	7.649	6.785	6.826	5.403	5.411	5.390
Al	18.314	18.415	5.782	3.407	0.045	0.034	2.612	1.200	1.348	0.558	1.667	1.661	3.482	3.468	3.574
Ti	0.112	0.112	0.012	0.174	0.000	0.002	0.264	0.063	0.102	0.010	0.122	0.108	0.174	0.235	0.205
Cr	0.008	0.000	0.000	0.003	0.001	0.000	0.014	0.014	0.015	0.003	0.000	0.000	0.006	0.001	0.016
Fe^{2+}	3.326	3.330	4.103	2.360	0.228	0.250	1.898	1.476	1.575	1.608	2.042	2.073	2.381	2.446	2.291
Mn	0.084	0.080	0.037	0.012	0.012	0.016	0.029	0.044	0.051	0.041	0.043	0.044	0.013	0.038	0.024
Mg	0.753	0.745	4.782	2.354	0.751	0.739	3.276	3.078	2.944	3.197	2.398	2.364	2.325	2.111	2.187
Ca	0.001	0.003	0.002	0.000	0.943	0.947	0.000	1.921	1.923	1.921	1.972	1.945	0.001	0.000	0.000
Na	0.039	0.038	0.002	0.114	0.028	0.022	0.032	0.221	0.246	0.116	0.283	0.261	0.096	0.049	0.137
K	0.001	0.001	0.005	1.684	0.001	0.000	1.850	0.104	0.130	0.034	0.179	0.166	1.695	1.771	1.708
Zn	0.192	0.231													
Total	30.790	30.827	19.923	15.572	4.001	4.001	15.670	15.306	15.369	15.136	15.491	15.449	15.575	15.530	15.532
Mg/(Fe+Mg)	0.185	0.18	0.54	0.4993	0.75	0.77	0.63	0.68	0.65	0.67	0.54	0.53	0.49	0.46	0.49

FeO* as total Fe

Table 3-5. Summary of calculated temperatures (°C) and pressures (kbar) of the schist samples

Sample No.	P (W)	T (KM)	T (HB)
K10	5.3	610-615	
K1	6.4	620-630	
K17	3.2	590-600	
K26		590-595	
K12			665-690
K16			650-700

P(W): Garnet-biotite-muscovite-plagioclase barometry after Wu (2015), T (KM): Garnet-biotite thermometry with Fe3+ correction after Kaneko and Miyano (2004), T (HB): Hornblende-plagioclase thermometry after Holland and Blundy (1994). P at 600oC and T at 7 kbar.

Table 3-6. Independent sets of reactions and their corresponding calculations (for x(H_2O) = 1.0)

Independent sets of reactions :	**P (at 597ºC)**	**sd(P)**	**a**	**sd(a)**	**b**	**c**	**ln K**	**sd(ln K)**
1. 12ames + 5alm + 9q = 8clin + 3daph + 2mst	2.0	10.98	17.16	9.27	0.05576	-4.004	-8.027	6.095
2. 36ames + 55alm + 27q = 33daph + 40py + 6mst	7.6	19.75	1810.83	70.20	-0.01070	-13.258	-241.320	35.788
3. mu + 2phl + 6q = 3cel + py	9.3	2.92	81.84	1.28	0.04805	-4.398	-11.608	1.815
4. 2east + 6q = mu + cel + py	7.1	2.11	36.60	1.25	0.02416	-3.798	-4.266	1.122
5. 6mu + 10east + ames + 39q = 16cel + 2mst	9.7	2.17	191.41	9.50	0.44531	-29.942	-39.662	9.105
6. 8ann + 2fst + 15q = 8mu + daph + 9alm	7.6	2.83	47.08	9.14	-0.05762	-9.111	10.039	3.415
7. 31cel + 6phl + 4fst = 21mu + 16fcel + 2clin + 13py	9.1	14.72	634.09	12.26	-0.76744	9.348	-9.640	19.432
8. mu + 3fcel + 2phl + 6q = 6cel + alm	7.2	5.23	10.73	2.22	0.08689	-4.559	-7.341	3.366
9. 39cel + 2fst = 18mu + 8fcel + 13phl + 46q + 4H_2O	9.2	3.73	-78.12	13.92	-1.00228	39.403	80.678	20.742

	avP	**sd**	**avT**	**sd**	**cor**	**fit**
lsq	9.3	2.0	597	18	-0.064	1.39

Where sd= standard deviation, P = pressure, T = temperature, a = activities, b and c = equilibrium parameters, K = slope of reaction curves, av = average, cor = correlation coefficient, fit = goodness of fit, lsq = least-square values.

End-members and abbreviations are those used in THERMOCALC of Powell and Holland (1988).

Table 4-1. Modal analysis of the rocks discussed in this study.

Sample no.	Rock type[a]	Qz	Ksp	Pl	Bt	Grt	Sil	Crd	Hbl	Opx	Cpx	Ol	Spl	Mag	Ilm	Ti	Ap	Ru	Zr
1a	3	**		****	*+				.	*+				.	.	.			.
1b	3	**		****	*+				.	*+				.	.	.			.
2	1	****	**	**	*												.		.
3a	2	**		**	***	*+	*	*+					.		.	.	.	.	.
3b	2	**		**	***	*+	*	*+					.		.	.	.	.	.
3c	2	**		**	***	*+	*	*+					.		.	.	.	.	.
3d	2	**		**	***	*+	*	*+					.		.	.	.	.	.
4	2	**		**	***	*+	*	*+					.		.	.	.	.	.
5	2	**		**	***	*+	*	*+					.		.	.	.	.	.
6	2	**		**	***	*+	*	*+							.	.	.	.	.
7a	2	**		**	***	*+	*	*+							.	.	.	.	.
7b	2	**		**	***	*+	*	*+							.	.	.	.	.
8	1	****	**	**	*												.		.
9	4								****		*	**	*	*	.				
10	4								****		*	**	*	*	.				
11	3	**		****	*+				.	*+				.	.	.			.
13	1	****	**	**	*												.		.
14	1	****	**	**	*												.		.
15	1	****	**	**	*												.		.
16	1	****	**	**	*												.		.

****+ =(>59), **** = (50-59), ***+ = (40-49), *** = (30-39), **+ = (20-29), ** = (15-19), *+ = (10-14), * = (5-9), . = (<5);

[a]1: Granite gneiss, 2: Garnet-sillimanite-biotite schist, 3: Meta-quartz-diorite, 4: Meta-ultramafite

Table 4-2. Chemistry of biotite, garnet and cordierite from the Meta-quartz diorite (Older granite suite) and migmatitic schist (Younger metasediment suite)

	Meta-Quartz Diorite			Migmatitic schist											
	Sample 1			Sample 3				Sample 6							
Mineral name	Bt			Grt core	Grt rim	Bt		Grt core	Grt mantle	Grt rim	Bt		Crd	
No. of O	22	22	22	12	12	22	22	12	12	12	22	22	18	18
SiO_2	36.95	36.96	37.77	37.62	37.79	36.22	36.25	38.65	38.67	37.28	35.61	35.66	48.80	48.52
Al_2O_3	14.31	14.38	14.29	21.18	21.37	18.17	17.83	21.59	21.69	21.25	17.11	17.57	32.90	33.33
TiO_2	5.39	5.02	4.64	0.02	0.06	3.90	3.73	0.01	0.00	0.00	3.89	4.19	0.00	0.00
Cr_2O_3	0.07	0.03	0.01	0.01	0.00	0.10	0.07	0.02	0.01	0.00	0.14	0.13	0.00	0.00
FeO*	14.56	13.68	14.20	32.00	31.70	16.91	16.65	28.24	30.20	31.95	16.61	16.46	5.93	6.10
MnO	0.01	0.07	0.10	1.58	1.80	0.11	0.09	1.12	1.21	2.26	0.05	0.08	0.09	0.10
MgO	14.11	15.21	14.98	5.70	6.44	11.22	11.39	8.09	6.49	4.79	11.04	10.87	9.45	9.36
CaO	0.00	0.08	0.00	1.21	1.07	0.00	0.00	1.75	1.26	1.08	0.01	0.02	0.00	0.01
Na_2O	0.00	0.01	0.02	0.00	0.07	0.14	0.12	0.02	0.00	0.00	0.10	0.11	0.06	0.07
K_2O	9.72	9.25	9.71	0.01	0.00	9.33	9.26	0.02	0.04	0.00	9.04	9.17	0.01	0.00
Total	95.16	94.77	95.95	99.38	100.29	96.10	95.40	99.49	99.55	98.61	93.64	94.37	97.24	97.50
Si	5.538	5.519	5.598	2.997	2.978	5.400	5.437	3.012	3.033	3.002	5.451	5.417	5.021	4.986
Al	2.526	2.528	2.495	1.988	1.984	3.192	3.151	1.982	2.004	2.016	3.086	3.145	3.989	4.036
Ti	0.607	0.618	0.517	0.001	0.003	0.436	0.421	0.000	0.000	0.000	0.448	0.478	0.000	0.000
Cr	0.009	0.004	0.001	0.001	0.000	0.012	0.008	0.001	0.000	0.000	0.017	0.016	0.000	0.000
Fe^{2+}	1.824	1.825	1.759	2.132	2.089	2.108	2.087	1.839	1.980	2.151	2.125	2.091	0.510	0.524
Mn	0.001	0.006	0.012	0.107	0.120	0.014	0.011	0.074	0.080	0.154	0.006	0.010	0.008	0.008
Ni	0.000	0.000	0.000	0.000	0.000	0.000	0.000	0.000	0.000	0.000	0.000	0.000	0.000	0.000
Mg	3.150	3.136	3.307	0.676	0.756	2.492	2.544	0.938	0.758	0.575	2.517	2.460	1.449	1.433
Ca	0.000	0.000	0.000	0.104	0.090	0.000	0.000	0.146	0.106	0.093	0.002	0.003	0.000	0.001
Na	0.000	0.022	0.006	0.000	0.011	0.040	0.035	0.003	0.000	0.000	0.030	0.032	0.012	0.014
K	1.858	1.866	1.835	0.001	0.000	1.774	1.771	0.002	0.004	0.000	1.764	1.776	0.002	0.001
Total	**15.517**	**15.541**	**15.558**	**8.008**	**8.032**	**15.468**	**15.465**	**7.998**	**7.966**	**7.990**	**15.446**	**15.428**	**10.991**	**11.003**
Mg/(Fe+Mg)	0.633	0.632	0.653	0.241	0.266	0.542	0.549	0.34	0.28	0.21	0.54	0.54	0.74	0.73
Fe/(Fe+Mg)	0.367	0.368	0.347	0.759	0.734	0.458	0.451	0.66	0.72	0.79	0.46	0.46	0.26	0.27
Alm %				70.63	68.4			61.4	67.71	72.36				
Sps %				3.5	3.9			2.5	2.7	5.2				
Prp %				22.4	24.7			31.3	25.93	19.34				
Grs %				3.4	3.0			4.9	3.6	3.1				

FeO* as total Fe

Table 4-3. Chemistry of plagioclases from the meta-quartz diorite unit (samples 1a and 11) and the migmatite unit (samples 3a and 6)

	Sample 1a			Sample 11		Sample 3a	Sample 6		
Comment	Pl core	Pl core	Pl rim	Pl core	Pl rim	Pl	Pl core	Pl core	Pl rim
SiO_2	59.22	60.60	59.88	60.50	61.09	61.83	60.36	60.81	60.78
Al_2O_3	24.57	25.41	25.81	24.02	24.56	24.93	24.12	24.03	23.96
TiO_2	0.01	0.00	0.07	0.01	0.03	0.00	0.00	0.00	0.01
Cr_2O_3	0.00	0.00	0.05	0.00	0.00	0.02	0.00	0.00	0.00
FeO*	1.01	0.13	0.26	0.12	0.31	0.03	0.04	0.06	0.13
MnO	0.02	0.00	0.04	0.00	0.03	0.00	0.02	0.01	0.00
MgO	0.55	0.00	0.02	0.00	0.02	0.00	0.00	0.00	0.00
CaO	6.81	6.97	7.01	6.32	6.48	6.07	5.92	6.01	5.97
Na_2O	7.65	8.72	8.30	7.15	7.34	9.63	7.89	7.87	7.96
K_2O	0.44	0.48	0.49	1.15	0.62	0.24	0.18	0.18	0.13
Total	100.28	102.37	101.93	99.31	100.48	102.74	98.54	99.01	98.99
Si	2.653	2.657	2.636	2.719	2.709	2.692	2.720	2.728	2.728
Al	1.297	1.313	1.339	1.272	1.283	1.279	1.281	1.270	1.267
Ti	0.000	0.000	0.002	0.000	0.001	0.000	0.000	0.000	0.000
Cr	0.000	0.000	0.002	0.000	0.000	0.001	0.000	0.000	0.000
Fe^{2+}	0.038	0.005	0.010	0.004	0.011	0.001	0.002	0.002	0.005
Mn	0.001	0.000	0.002	0.000	0.001	0.000	0.001	0.000	0.000
Mg	0.037	0.000	0.002	0.000	0.002	0.000	0.000	0.000	0.000
Ca	0.327	0.327	0.331	0.304	0.308	0.283	0.286	0.289	0.287
Na	0.664	0.741	0.708	0.622	0.630	0.812	0.689	0.684	0.693
K	0.025	0.027	0.027	0.066	0.035	0.013	0.011	0.010	0.008
Total	5.042	5.071	5.058	4.988	4.981	5.081	4.989	4.984	4.988
An%	32.1	29.9	31.0	30.6	31.6	25.5	29.0	29.4	29.1
Ab%	65.4	67.7	66.4	62.7	64.8	73.3	69.9	69.6	70.2
Or%	2.5	2.5	2.6	6.6	3.6	1.2	1.1	1.0	0.8

FeO* as total Fe

Table 4-4. Chemistry of hornblende, orthopyroxene, clinopyroxene, spinel and olivine in the rocks of the study area.

	Meta-quartz diorite						Meta-ultramafite							
	Sample 1a		Sample 1b		Sample 11		Sample 10							
Mineral name	Hbl	Opx	Hbl	Opx	Opx		Hbl	Edenite	Spinel		Olivine		Opx	
No. of O	23	6	23	6	6	6	23	23	4	4	4	4	6	6
SiO_2	44.92	52.96	44.58	52.28	52.50	52.58	45.47	52.89	0.05	0.04	38.28	38.45	54.78	54.79
Al_2O_3	9.45	0.99	10.15	1.01	0.84	0.71	12.52	6.61	56.98	56.52	0.01	0.02	2.68	2.63
TiO_2	1.68	0.05	1.52	0.01	0.05	0.10	1.17	0.40	0.00	0.01	0.00	0.02	0.10	0.15
Cr_2O_3	0.05	0.00	0.04	0.00	0.03	0.00	0.40	0.13	5.96	6.02	0.00	0.01	0.11	0.16
FeO*	13.83	24.49	14.12	23.80	24.76	24.64	7.70	6.25	23.60	23.81	26.24	26.55	15.24	15.25
MnO	0.23	0.67	0.19	0.62	0.62	0.69	0.16	0.11	0.19	0.18	0.35	0.37	0.33	0.30
MgO	12.92	20.87	12.79	21.48	20.46	20.02	16.26	19.17	12.18	12.04	35.80	35.99	27.47	27.15
CaO	11.48	0.49	11.40	0.49	0.66	0.63	11.63	12.32	0.04	0.01	0.00	0.00	0.24	0.25
Na_2O	1.59	0.00	1.67	0.02	0.00	0.00	1.43	0.61	0.03	0.02	0.00	0.01	0.03	0.00
K_2O	0.92	0.01	0.95	0.00	0.00	0.00	0.09	0.04	0.00	0.00	0.01	0.01	0.00	0.01
ZnO	0.10	0.10	0.00	0.16	0.00	0.00	0.00	0.00	0.00	0.00	0.00	0.00	0.00	0.00
Total	97.18	100.61	97.40	99.87	99.92	99.39	96.85	98.61	99.44	99.11	101.00	101.77	100.97	100.74
Si	6.681	1.980	6.621	1.967	1.981	1.994	6.536	7.332	0.001	0.001	1.006	1.005	1.947	1.953
Al	1.656	0.043	1.775	0.045	0.037	0.032	2.121	1.079	1.840	1.835	0.000	0.001	0.112	0.110
Ti	0.188	0.001	0.170	0.000	0.001	0.003	0.126	0.041	0.000	0.000	0.000	0.000	0.003	0.004
Cr	0.006	0.000	0.004	0.000	0.001	0.000	0.046	0.015	0.109	0.111	0.000	0.000	0.003	0.004
Fe^{3+}									0.000	0.000				
Fe^{2+}	1.720	0.766	1.753	0.749	0.781	0.781	0.925	0.725	0.541	0.548	0.577	0.580	0.453	0.454
Mn	0.029	0.021	0.024	0.020	0.020	0.022	0.020	0.000	0.004	0.004	0.008	0.008	0.010	0.009
Mg	2.863	1.162	2.828	1.204	1.150	1.131	3.483	3.959	0.497	0.494	1.402	1.401	1.455	1.441
Ca	1.828	0.020	1.813	0.020	0.027	0.026	1.790	1.830	0.001	0.000	0.000	0.000	0.009	0.009
Na	0.459	0.000	0.480	0.001	0.000	0.000	0.397	0.164	0.001	0.001	0.000	0.000	0.002	0.000
K	0.175	0.000	0.180	0.000	0.000	0.000	0.016	0.006	0.000	0.000	0.000	0.000	0.000	0.000
Zn	0.011	0.003	0.000	0.004	0.000	0.000	0.000	0.000	0.000	0.000	0.000	0.000	0.000	0.000
Total	15.617	3.997	15.649	4.011	3.998	3.988	15.461	15.164	2.995	2.996	2.994	2.995	3.994	3.986
Xmg	0.62	0.60	0.62	0.62	0.60	0.59	0.79	0.85	0.48	0.47	0.71	0.71	0.76	0.76

FeO* as total Fe

Table 4-5. Summary of calculated temperatures (°C) and pressures (kbar) of the representative rock samples.

Geothermobarometer	Sample	Comment	Temperature(°C)	Pressure(kbar)
The results of iterative calculation between Grt-Pl geobarometer of Ganguly et al. (1996) and Grt-Bt-Crd thermometer of Kaneko and Miyano (2004);	6	Grt core	900-905	11
		Grt rim	710-789	6.1-7.1
	3a	Grt core	702-716	7.1-7.3
		Grt rim	655-665	6
The results of optimal thermobarometry after Powell and Holland (1994).	6		813	7.4
	3a		763	7.1
Hbl-Pl thermometer after Holland and Blundy (1994).	1a	Hbl./ Pl cores	753-765	6.5
	1b	Hbl./ Pl cores	771-797	6.5
The results of THERMOCALC pseudosection after Holland and Powell (1998)	6		785-805	6.72-6.75

Table 5-1. Chemistry of garnets from garnet-sillimanite gneiss (samples 53, 53B and 56), meta-basite (samples 52 aand 56B) and garnet-biotite granite (sample 55)

Sample No.	Sample 52			Sample 53			Sample 53B				Sample 55		Sample 56				Sample 56B		
No. oxygen	12	12	12	12	12	12	12	12	12	12	12	12	12	12	12	12	12	12	12
Remarks	core 1	mantle 1	rim 1	core	core	rim	rim	rim	core	core			rim	rim	core	core	core	rim	rim
SiO_2	37.42	37.44	37.33	38.47	38.22	38.86	38.62	38.44	38.88	38.72	36.34	36.42	38.62	38.57	38.17	38.65	37.58	38.10	39.05
Al_2O_3	21.09	21.24	21.38	21.67	21.72	22.26	21.89	21.68	21.99	21.63	20.50	20.76	21.99	21.88	21.90	21.73	20.98	21.57	21.09
TiO_2	0.01	0.00	0.00	0.00	0.04	0.00	0.03	0.00	0.00	0.01	0.00	0.00	0.00	0.03	0.00	0.00	0.01	0.07	0.06
Cr_2O_3	0.05	0.05	0.00	0.03	0.06	0.07	0.05	0.08	0.06	0.04	0.01	0.00	0.04	0.09	0.04	0.05	0.01	0.01	0.00
FeO*	33.05	32.09	32.90	33.09	33.07	34.14	32.59	32.61	31.42	31.19	37.63	37.28	31.98	31.82	31.32	30.59	30.63	30.93	30.31
MnO	1.10	1.02	1.10	0.56	0.56	0.52	0.56	0.54	0.50	0.55	0.75	0.75	0.47	0.51	0.45	0.47	1.03	1.12	1.66
MgO	3.77	3.83	3.79	6.85	6.77	5.75	6.70	6.64	7.53	7.70	2.44	2.40	6.94	6.84	7.38	7.32	5.57	5.73	4.48
CaO	3.72	4.06	3.77	0.82	0.81	0.92	0.79	0.80	1.00	0.99	1.06	1.09	1.10	1.02	1.25	1.22	3.25	3.33	4.79
Na_2O	0.01	0.04	0.01	0.03	0.00	0.04	0.00	0.02	0.03	0.00	0.04	0.03	0.02	0.00	0.01	0.00	0.04	0.00	0.00
K_2O	0.00	0.00	0.01	0.00	0.00	0.00	0.00	0.00	0.00	0.00	0.01	0.00	0.00	0.01	0.00	0.00	0.01	0.01	0.00
Total	100.22	99.82	100.30	101.63	101.35	102.57	101.26	100.86	101.41	100.93	98.78	98.72	101.24	100.80	100.60	100.03	99.12	100.86	101.43
Si	2.986	2.989	2.975	2.986	2.976	2.995	2.997	2.999	2.997	3.000	2.990	2.991	2.992	2.999	2.973	3.013	2.995	2.981	3.043
Al	1.984	1.999	2.007	1.982	1.993	2.021	2.002	1.993	1.997	1.975	1.988	2.009	2.008	2.005	2.010	1.996	1.970	1.989	1.936
Ti	0.001	0.000	0.000	0.000	0.002	0.000	0.002	0.000	0.000	0.001	0.000	0.000	0.000	0.002	0.000	0.000	0.000	0.004	0.004
Cr	0.003	0.003	0.000	0.002	0.003	0.004	0.003	0.005	0.004	0.003	0.001	0.000	0.003	0.005	0.002	0.003	0.000	0.001	0.000
Fe^{2+}	2.205	2.142	2.192	2.147	2.153	2.199	2.115	2.127	2.025	2.020	2.588	2.560	2.071	2.069	2.039	1.994	2.041	2.024	1.974
Mn	0.074	0.069	0.074	0.037	0.037	0.034	0.037	0.036	0.033	0.036	0.052	0.052	0.031	0.034	0.030	0.031	0.070	0.074	0.110
Mg	0.449	0.455	0.450	0.792	0.785	0.659	0.774	0.772	0.864	0.889	0.300	0.294	0.801	0.792	0.856	0.850	0.661	0.668	0.520
Ca	0.318	0.347	0.322	0.068	0.068	0.076	0.065	0.066	0.082	0.082	0.094	0.096	0.091	0.085	0.104	0.102	0.278	0.279	0.399
Na	0.001	0.006	0.001	0.004	0.000	0.006	0.000	0.003	0.005	0.000	0.006	0.005	0.002	0.000	0.001	0.000	0.005	0.000	0.000
K	0.000	0.000	0.001	0.000	0.000	0.000	0.000	0.000	0.000	0.000	0.001	0.000	0.000	0.001	0.000	0.000	0.001	0.001	0.000
Total	8.020	8.013	8.022	8.024	8.024	7.995	7.998	8.004	8.005	8.011	8.019	8.007	8.004	7.994	8.021	7.988	8.023	8.020	7.986
Mg/(Fe+M	0.169	0.175	0.17	0.269	0.267	0.231	0.268	0.266	0.299	0.306	0.104	0.103	0.279	0.277	0.296	0.299	0.245	0.248	0.209
Alm %	72.4	71.1	72.1	70.5	70.8	74.1	70.7	70.9	67.4	66.7	85.3	85.3	69.2	69.4	67.3	67.0	66.9	66.5	65.7
Sps %	2.4	2.3	2.4	1.2	1.2	1.1	1.2	1.2	1.1	1.2	1.7	1.7	1.0	1.1	1.0	1.0	2.3	2.4	3.6
Prp %	14.7	15.1	14.8	26.0	25.8	22.2	25.9	25.7	28.8	29.4	9.9	9.8	26.8	26.6	28.3	28.5	21.7	22.0	17.3
Grs %	10.4	11.5	10.6	2.2	2.2	2.6	2.2	2.2	2.7	2.7	3.1	3.2	3.0	2.9	3.4	3.4	9.1	9.2	13.3

FeO* as total Fe

Table 5-2. Chemistry of biotites from garnet-sillimanite gneiss (samples 53, 53B and 56), meta-basite (samples 52 aand 56B) and garnet-biotite granite (sample 55)

Sample no.	52			53		53B		54		55		56	56B		
No. of oxygen	22	22	22	22	22	22	22	22	22	22	22	22	22	22	22
SiO_2	35.66	35.32	35.39	36.30	36.31	36.38	36.25	35.44	32.58	35.69	35.08	35.75	35.78	35.60	36.82
Al_2O_3	14.62	15.72	15.35	17.28	17.12	17.68	17.52	13.55	12.69	18.21	18.13	17.31	15.86	15.82	14.79
TiO_2	5.29	4.54	4.58	4.67	5.28	4.25	4.25	5.23	5.30	0.94	1.21	5.07	5.23	4.92	3.85
Cr_2O_3	0.11	0.00	0.00	0.19	0.23	0.16	0.14	0.03	0.04	0.00	0.02	0.16	0.03	0.03	0.00
FeO*	22.53	20.34	19.76	15.56	15.88	15.22	15.24	23.72	23.57	20.00	20.15	16.78	18.65	18.26	17.49
MnO	0.06	0.05	0.04	0.00	0.02	0.04	0.04	0.11	0.05	0.01	0.00	0.01	0.01	0.01	0.09
MgO	8.61	10.28	10.71	11.68	11.30	12.54	12.41	8.36	7.21	8.86	8.54	10.30	10.61	10.66	13.03
CaO	0.02	0.00	0.00	0.00	0.00	0.00	0.00	0.00	0.12	0.00	0.00	0.00	0.02	0.00	0.40
Na_2O	0.13	0.12	0.10	0.05	0.04	0.05	0.09	0.02	0.09	0.04	0.05	0.07	0.09	0.12	0.11
K_2O	9.17	8.82	9.18	9.85	9.88	9.74	9.83	9.49	8.80	9.51	9.53	9.61	9.13	9.09	8.62
ZnO	0.17	0.18	0.00	0.04	0.08	0.14	0.05		0.05			0.08	0.13	0.00	
Total	96.38	95.37	95.11	95.63	96.16	96.22	95.89	95.93	90.49	93.26	92.70	95.15	95.52	94.51	95.20
Si	5.483	5.416	5.435	5.427	5.410	5.392	5.398	5.524	5.432	5.569	5.523	5.404	5.432	5.451	5.560
Al	2.649	2.840	2.778	3.044	3.007	3.089	3.074	2.488	2.493	3.348	3.363	3.083	2.838	2.855	2.631
Ti	0.612	0.523	0.529	0.525	0.592	0.474	0.475	0.613	0.664	0.110	0.143	0.576	0.597	0.567	0.437
Cr	0.013	0.000	0.000	0.023	0.027	0.019	0.017	0.004	0.005	0.000	0.002	0.019	0.003	0.004	0.000
Fe^{2+}	2.896	2.608	2.537	1.945	1.978	1.886	1.897	3.090	3.286	2.609	2.653	2.120	2.367	2.338	2.208
Mn	0.008	0.007	0.005	0.000	0.003	0.005	0.005	0.014	0.007	0.001	0.000	0.001	0.001	0.002	0.011
Mg	1.972	2.347	2.449	2.600	2.508	2.770	2.753	1.941	1.791	2.059	2.004	2.319	2.399	2.432	2.931
Ca	0.003	0.000	0.000	0.000	0.000	0.000	0.000	0.000	0.021	0.000	0.000	0.001	0.003	0.000	0.065
Na	0.039	0.035	0.029	0.015	0.012	0.013	0.027	0.005	0.027	0.011	0.014	0.021	0.025	0.036	0.031
K	1.797	1.725	1.798	1.878	1.877	1.841	1.867	1.885	1.870	1.892	1.913	1.851	1.767	1.775	1.660
Zn	0.020	0.021	0.000	0.005	0.009	0.015	0.006	0.000	0.006	0.000	0.000	0.008	0.015	0.000	0.000
Total	15.492	15.521	15.560	15.462	15.426	15.507	15.528	15.563	15.604	15.599	15.614	15.406	15.446	15.458	15.533
Mg/(Fe+Mg)	0.41	0.47	0.49	0.57	0.56	0.59	0.59	0.39	0.35	0.44	0.43	0.52	0.5	0.51	0.57
Na+K	1.84	1.76	1.83	1.89	1.89	1.85	1.89	1.89	1.9	1.9	1.93	1.87	1.79	1.81	1.69

FeO* as total Fe

Table 5-3. Chemistry of orthopyroxenes from meta-basites (samples 52 and 56B) and charnockitic gneiss (sample 54), and hornblende from the charnockitic gneiss (sample 54)

Sample No.	Sample 52				Sample 54						Sample 56B			
Mineral Name	Opx				Opx			Hbl			Opx			
No. oxygen	6	6	6	6	6	6	6	23	23	23	6	6	6	6
Remarks														
SiO_2	49.43	49.81	49.73	49.76	49.28	49.48	49.10	40.98	40.82	41.37	50.42	50.54	50.56	50.60
Al_2O_3	1.16	1.40	1.38	1.29	0.59	0.53	0.56	11.23	10.70	10.92	1.76	1.79	1.77	1.73
TiO_2	0.10	0.05	0.13	0.09	0.07	0.09	0.09	1.60	1.86	1.67	0.07	0.11	0.10	0.09
Cr_2O_3	0.00	0.03	0.04	0.03	0.01	0.04	0.00	0.03	0.00	0.05	0.00	0.00	0.02	0.02
FeO*	34.76	34.95	34.65	34.12	36.41	36.04	36.18	21.51	21.84	22.31	31.21	31.39	31.04	31.36
MnO	0.45	0.37	0.41	0.41	1.11	1.15	1.23	0.21	0.35	0.26	0.35	0.33	0.28	0.27
MgO	13.28	13.11	13.12	13.65	11.82	11.98	11.79	7.01	7.12	7.23	15.80	16.12	15.83	16.02
CaO	0.50	0.50	0.50	0.37	0.77	0.58	0.52	11.33	11.22	11.11	0.28	0.28	0.26	0.23
Na_2O	0.03	0.06	0.02	0.07	0.03	0.00	0.01	1.34	1.41	1.31	0.02	0.00	0.00	0.01
K_2O	0.00	0.02	0.01	0.00	0.00	0.00	0.01	1.70	1.55	1.56	0.00	0.01	0.01	0.00
Total	99.71	100.31	100.05	99.97	100.08	99.89	99.48	96.92	96.87	97.77	100.00	100.80	99.87	100.46
Si	1.966	1.968	1.968	1.967	1.977	1.984	1.981	6.396	6.392	6.412	1.960	1.951	1.964	1.958
Al	0.054	0.065	0.064	0.060	0.028	0.025	0.027	2.065	1.974	1.993	0.081	0.081	0.081	0.079
Ti	0.003	0.002	0.004	0.003	0.002	0.003	0.003	0.188	0.218	0.194	0.002	0.003	0.003	0.003
Cr	0.000	0.001	0.001	0.001	0.000	0.001	0.000	0.003	0.000	0.006	0.000	0.000	0.001	0.001
Fe^{2+}	1.156	1.154	1.146	1.128	1.221	1.208	1.220	2.808	2.859	2.890	1.014	1.013	1.008	1.014
Mn	0.015	0.013	0.014	0.014	0.038	0.039	0.042	0.028	0.046	0.034	0.011	0.011	0.009	0.009
Mg	0.787	0.771	0.773	0.804	0.706	0.716	0.708	1.630	1.660	1.668	0.914	0.927	0.916	0.923
Ca	0.021	0.021	0.021	0.015	0.033	0.025	0.023	1.893	1.882	1.844	0.012	0.012	0.011	0.009
Na	0.002	0.005	0.002	0.005	0.003	0.000	0.001	0.405	0.428	0.393	0.002	0.000	0.000	0.001
K	0.000	0.001	0.000	0.000	0.000	0.000	0.000	0.337	0.310	0.308	0.000	0.000	0.000	0.000
Total	4.005	4.000	3.996	4.002	4.008	4.000	4.004	15.753	15.771	15.744	3.999	4.005	3.993	4.000
Mg/(Mg+Fe)	0.41	0.40	0.40	0.42	0.37	0.37	0.37	0.37	0.37	0.37	0.47	0.48	0.48	0.48

FeO* as total Fe

Table 5-4. Chemistry of plagioclase from the garnet-sillimanite gneiss (samples 53, 53B and 56), meta-basite (samples 52 and 56B) and garnet-biotite granite (sample 55)

Sample No.	Sample 52			Sample 53		Sample 53B			Sample 54			Sample 55			Sample 56		Sample 56B		
No. oxygen	8	8	8	8	8	8	8	8	8	8	8	8	8	8	8	8	8	8	8
SiO_2	50.55	50.51	48.76	63.62	63.47	63.01	61.92	61.97	58.27	59.00	59.43	61.85	61.48	61.44	60.24	59.98	48.68	48.94	48.60
Al_2O_3	32.46	32.02	32.33	24.04	23.50	24.12	24.61	24.03	26.00	26.07	25.80	23.28	23.06	23.07	25.04	25.62	33.61	33.52	33.79
TiO_2	0.05	0.00	0.00	0.00	0.00	0.03	0.00	0.00	0.00	0.00	0.00	0.00	0.01	0.01	0.02	0.01	0.01	0.01	0.00
Cr_2O_3	0.00	0.00	0.00	0.00	0.00	0.00	0.00	0.00	0.01	0.00	0.00	0.06	0.00	0.01	0.00	0.03	0.03	0.00	0.00
FeO*	0.15	0.02	1.04	0.08	0.00	0.20	0.09	0.00	0.15	0.06	0.05	0.01	0.03	0.00	0.00	0.22	0.06	0.05	0.08
MnO	0.00	0.04	0.05	0.01	0.02	0.03	0.02	0.00	0.00	0.00	0.02	0.01	0.03	0.04	0.04	0.00	0.00	0.01	0.00
MgO	0.00	0.00	0.42	0.01	0.00	0.00	0.01	0.00	0.01	0.00	0.00	0.00	0.00	0.00	0.00	0.01	0.00	0.00	0.02
CaO	14.76	14.28	15.30	4.98	4.79	5.25	5.87	5.48	8.33	7.93	7.53	4.80	4.83	4.74	6.62	6.98	16.02	15.85	15.93
Na_2O	3.83	3.89	3.02	8.91	8.91	8.84	8.51	8.54	7.08	7.19	7.36	8.89	8.94	8.94	7.92	7.78	2.88	2.88	2.78
K_2O	0.08	0.09	0.06	0.21	0.42	0.28	0.26	0.34	0.30	0.32	0.36	0.29	0.28	0.21	0.23	0.18	0.05	0.05	0.06
Total	101.91	100.91	101.04	101.90	101.10	102.05	101.44	100.44	100.16	100.58	100.55	99.19	98.66	98.46	100.13	100.80	101.33	101.32	101.24
Si	2.269	2.285	2.221	2.767	2.782	2.747	2.718	2.741	2.610	2.625	2.642	2.766	2.766	2.768	2.681	2.657	2.202	2.212	2.199
Al	1.716	1.707	1.736	1.232	1.214	1.239	1.273	1.253	1.372	1.367	1.352	1.227	1.222	1.224	1.313	1.337	1.792	1.785	1.802
Ti	0.002	0.000	0.000	0.000	0.000	0.001	0.000	0.000	0.000	0.000	0.000	0.000	0.000	0.000	0.001	0.000	0.000	0.000	0.000
Cr	0.000	0.000	0.000	0.000	0.000	0.000	0.000	0.000	0.000	0.000	0.000	0.002	0.000	0.000	0.000	0.001	0.001	0.000	0.000
Fe^{2+}	0.005	0.001	0.040	0.003	0.000	0.007	0.003	0.000	0.006	0.002	0.002	0.000	0.001	0.000	0.000	0.008	0.002	0.002	0.003
Mn	0.000	0.001	0.002	0.000	0.001	0.001	0.001	0.000	0.000	0.000	0.001	0.000	0.001	0.002	0.002	0.000	0.000	0.000	0.000
Mg	0.000	0.000	0.028	0.001	0.000	0.000	0.001	0.000	0.001	0.000	0.000	0.000	0.000	0.000	0.000	0.001	0.000	0.000	0.001
Ca	0.709	0.692	0.747	0.232	0.225	0.245	0.276	0.260	0.400	0.378	0.359	0.230	0.233	0.229	0.316	0.331	0.776	0.767	0.772
Na	0.333	0.341	0.266	0.751	0.757	0.747	0.724	0.732	0.615	0.620	0.634	0.771	0.779	0.780	0.683	0.668	0.253	0.252	0.244
K	0.004	0.005	0.003	0.012	0.023	0.015	0.014	0.019	0.017	0.018	0.020	0.016	0.016	0.012	0.013	0.010	0.003	0.003	0.003
Total	5.040	5.034	5.045	4.998	5.001	5.013	5.015	5.008	5.020	5.011	5.009	5.013	5.019	5.016	5.009	5.013	5.029	5.023	5.024
An	68.05	67.00	73.72	23.61	22.91	24.70	27.62	26.20	39.41	37.85	36.11	22.96	23.01	22.66	31.60	33.13	75.43	75.25	76.00
Ab	31.95	33.00	26.28	76.39	77.09	75.30	72.38	73.80	60.59	62.15	63.89	77.04	76.99	77.34	68.40	66.87	24.57	24.75	24.00
Na+K	0.34	0.35	0.27	0.76	0.78	0.76	0.74	0.75	0.63	0.64	0.65	0.79	0.80	0.79	0.70	0.68	0.26	0.26	0.25
K/Na+k	0.01	0.01	0.01	0.02	0.03	0.02	0.02	0.03	0.03	0.03	0.03	0.02	0.02	0.02	0.02	0.01	0.01	0.01	0.01
Xab	0.68	0.67	0.74	0.24	0.23	0.25	0.28	0.26	0.39	0.38	0.36	0.23	0.23	0.23	0.32	0.33	0.75	0.75	0.76
Xan	0.32	0.33	0.26	0.76	0.77	0.75	0.72	0.74	0.61	0.62	0.64	0.77	0.77	0.77	0.68	0.67	0.25	0.25	0.24

FeO* as total Fe

Table 5-5. Chemistry of other minerals from garnet-sillimanite gneiss (samples 53, 53B and 56), meta-basite (samples 52 aand 56B) and charnockitic gneiss (sample 54)

Sample No.	Sample 52		Sample 53				Sample 53B				Sample 54			Sample 56			Sample 56B		
Mineral Name	Ilm	Ilm	Crd symp	Crd symp	Mag	Sil	Spl	Spl	Sil in Spl	Sil with Crd	Sil in Grt	Mag	Mag	Mag	Crd	Crd	Crd	Ilm	Ilm
No. oxygen	3	3	18	18	4	5	4	4	5	5	5	4	4	4	18	18	18	3	3
SiO_2	0.44	0.24	38.72	42.28	0.02	36.89	0.05	0.03	37.48	37.15	37.04	0.01	0.08	0.20	48.79	49.47	48.75	0.06	0.03
Al_2O_3	0.06	0.00	36.66	37.27	0.00	63.44	58.80	58.72	63.67	63.71	62.54	0.01	0.34	0.47	33.23	33.14	33.32	0.04	0.04
TiO_2	51.04	52.98	0.00	0.00	0.00	0.00	0.00	0.00	0.04	0.02	0.00	0.00	0.09	0.27	0.01	0.00	0.00	54.67	53.94
Cr_2O_3	0.00	0.00	0.00	0.02	0.00	0.14	0.64	0.57	0.26	0.00	0.11	0.01	0.05	0.08	0.01	0.00	0.00	0.04	0.00
FeO*	46.16	47.26	4.78	3.29	78.31	0.82	19.85	19.99	0.75	0.52	1.25	77.09	92.30	91.93	7.52	6.87	5.37	45.38	46.67
MnO	0.19	0.27	0.00	0.00	0.00	0.00	0.01	0.05	0.04	0.00	0.04	0.00	0.00	0.04	0.05	0.06	0.02	0.39	0.29
NiO			0.14	0.00	0.50	0.01	0.05	0.00	0.08	0.04	0.03				0.03	0.00	0.00		
MgO	0.71	0.14	4.80	3.45	0.00	0.00	5.61	5.68	0.00	0.00	0.04	0.05	0.01	0.00	9.18	9.43	10.22	0.33	0.42
CaO	0.01	0.01	0.73	0.94	0.00	0.02	0.00	0.00	0.02	0.02	0.02	0.00	0.00	0.00	0.00	0.01	0.02	0.00	0.00
Na_2O	0.00	0.02	0.25	0.31	0.02	0.01	1.21	1.34	0.02	0.00	0.01	0.00	0.00	0.01	0.10	0.09	0.10	0.05	0.00
K_2O	0.01	0.00	0.77	0.88	0.00	0.00	0.00	0.00	0.01	0.01	0.01	0.00	0.00	0.01	0.01	0.01	0.00	0.01	0.00
ZnO	0.09	0.00	0.03	0.02	0.02	0.00	15.15	15.55	0.52	0.26	0.07			0.06	0.04	0.01	0.09	0.09	0.00
Total	98.71	100.92	86.85	88.46	78.87	101.33	101.35	101.93	102.89	101.73	101.17	77.16	92.87	93.07	98.96	99.09	97.89	101.06	101.39
Si	0.011	0.006	4.496	4.750	0.001	0.987	0.001	0.001	0.991	0.990	0.996	0.000	0.004	0.010	4.976	5.017	4.977	0.001	0.001
Al	0.002	0.000	5.017	4.933	0.000	2.001	1.950	1.942	1.985	2.000	1.981	0.001	0.021	0.028	3.994	3.961	4.008	0.001	0.001
Ti	0.979	0.995	0.000	0.000	0.000	0.000	0.000	0.000	0.001	0.000	0.000	0.000	0.004	0.010	0.001	0.000	0.000	1.016	1.004
Cr	0.000	0.000	0.000	0.002	0.000	0.003	0.014	0.013	0.005	0.000	0.002	0.000	0.002	0.003	0.001	0.000	0.000	0.001	0.000
Fe^{3+}	0.000	0.000	0.000	0.000	0.000	0.000	0.000	0.000	0.000	0.000	0.000	0.000	0.000	0.000	0.000	0.000	0.000	0.000	0.000
Fe^{2+}	0.984	0.987	0.464	0.309	3.971	0.018	0.467	0.469	0.017	0.012	0.028	3.993	3.950	3.907	0.641	0.582	0.459	0.938	0.967
Mn	0.004	0.006	0.000	0.000	0.000	0.000	0.000	0.001	0.001	0.000	0.001	0.000	0.000	0.002	0.004	0.005	0.001	0.008	0.006
Ni	0.000	0.000	0.013	0.000	0.024	0.000	0.001	0.000	0.002	0.001	0.001	0.000	0.000	0.000	0.003	0.000	0.000	0.000	0.000
Mg	0.027	0.005	0.830	0.578	0.000	0.000	0.235	0.237	0.000	0.000	0.001	0.005	0.001	0.000	1.394	1.424	1.554	0.012	0.015
Ca	0.000	0.000	0.090	0.113	0.000	0.001	0.000	0.000	0.000	0.001	0.001	0.000	0.000	0.000	0.000	0.001	0.002	0.000	0.000
Na	0.000	0.001	0.055	0.066	0.003	0.001	0.066	0.073	0.001	0.000	0.001	0.000	0.000	0.001	0.020	0.018	0.020	0.002	0.000
K	0.000	0.000	0.113	0.125	0.000	0.000	0.000	0.000	0.000	0.000	0.000	0.000	0.000	0.001	0.001	0.002	0.000	0.000	0.000
Zn	0.002	0.000	0.002	0.001	0.001	0.000	0.315	0.322	0.010	0.005	0.001	0.000	0.000	0.002	0.003	0.001	0.007	0.002	0.000
Total	2.009	2.000	11.080	10.878	4.000	3.011	3.050	3.058	3.013	3.009	3.013	3.999	3.981	3.965	11.036	11.012	11.029	1.983	1.994
Mg/(Fe+Mg)	0.03	0.01	0.64	0.65	0.00	0.00	0.33	0.34	0.00	0.00	0.05	0.00	0.00	0.00	0.69	0.71	0.77	0.01	0.02
Na+K	0.00	0.00	0.17	0.19	0.00	0.00	0.07	0.07	0.00	0.00	0.00	0.00	0.00	0.00	0.02	0.02	0.02	0.00	0.00

FeO* as total Fe

Table 5-6. Optimal PT analysis of the Migmatitie gneiss (samples 53, 53b and 56)

Sample No.	avP	sd	avT	sd	cor	fit
53	7.4	0.9	893	59	0.867	0.95
53b	8	0.8	921	55	0.852	0.33
56	7.7	0.9	917	69	0.81	1.12
Average	7.70	0.87	910.33	61.00	0.84	0.80